EXPERIMENTAL STUDIES ON MAGNETIC CRYSTALS BELOW 1K

K.W. MESS

EXPERIMENTAL STUDIES ON MAGNETIC CRYSTALS BELOW 1K

PROEFSCHRIFT

TER VERKRIJGING VAN DE GRAAD VAN DOCTOR IN DE WISKUNDE EN NATUURWETENSCHAPPEN AAN DE RIJKSUNIVERSITEIT TE LEIDEN, OP GEZAG VAN DE RECTOR MAGNIFICUS DR J. GOSLINGS, HOOGLERAAR IN DE FACULTEIT DER GENEESKUNDE, TEN OVERSTAAN VAN EEN COMMISSIE UIT DE SENAAT TE VERDEDIGEN OP WOENSDAG 12 NOVEMBER 1969 TE KLOKKE 14.15 UUR

DOOR

KARL WILLI MESS

geboren te Rotterdam in 1942

1969
Drukkerij J. H. Pasmans - 's-Gravenhage

Promotor: Prof. dr C.J. Gorter

Dit proefschrift is tot stand gekomen
onder toezicht van dr W.J. Huiskamp

This investigation is part of the research program of the "Stichting voor Fundamenteel Onderzoek der Materie (F.O.M.)", which is financially supported by the "Organisatie voor Zuiver Wetenschappelijk Onderzoek (Z.W.O.)".

Aan mijn moeder.

Aan allen die mij in staat hebben gesteld
dit proefschrift te verwezenlijken.

Geloof niets, ongeacht waar men het leest of wie het gezegd heeft, zelfs niet als ik het gezegd heb, zo het niet overeenstemt met eigen rede en eigen gezond verstand.

[*Samengevat door H. Miller uit: Aṅguttara–Nikāya III, 65*]

STELLINGEN

I

De analyse welke Hamman geeft ten aanzien van exchange-interactie tussen derde en vierde naaste buren in $CoCs_3Cl_5$, naar aanleiding van de door hem met neutronendiffractie bepaalde magnetische struktuur, is onjuist.

J.Hamman, Physica 43(1969)277.
Dit proefschrift, hoofdstuk V.

II

De conclusie van Abeshouse e.a., getrokken op grond van de door hen verrichte metingen aan cerium magnesium nitraat, dat dit zout zich antiferromagnetisch ordent, is ondeugdelijk.

D.J. Abeshouse, G.O. Zimmerman, D.R. Kelland en E. Maxwell, Phys.Rev.Lett. 23(1969)308.
Dit proefschrift, hoofdstuk III.

III

Het is wenselijk elektronspin-resonantie en paramagnetische relaxatiemetingen te verrichten aan $Cu_3La_2(NO_3)_{12}.24H_2O$.

Dit proefschrift, hoofdstuk VI.

IV

De bewering van Friedberg en Schelleng dat de fasegrens tussen de antiferro- en paramagnetische toestand van een twee-subrooster uniaxiale antiferromagneet kán worden bepaald uit de buigpunten van isentropen in het H–T vlak, is niet algemeen geldig.

S.A. Friedberg en J.H. Schelleng, Proc.Int.Conf.Magn. Nottingham (1964)90.
Dit proefschrift, hoofdstuk V.

V

De bewering van Gluck en Luban dat de analyse van een meting van de soortelijke warmte met de funktie genoemd door Heller, zoals deze o.a. is toegepast bij EuS door Van der Hoeven,Jr., voor $|1-T/T_c| > 10^{-3}$ niet correct is, is in zijn algemeenheid onjuist.

P. Gluck en M. Luban, Phys.Lett. 28A(1969)607.
P. Heller, Repts.Progr.Phys. 30,dl.II(1967)789.
B.J.C. van der Hoeven,Jr., D.T. Teaney en V.L.Moruzzi, Phys.Rev.Lett. 20(1968)719.

VI

De bewering van Dixon en Rives, dat de bij de analyse van het kritische gedrag van de soortelijke warmte van $MnCl_2.4H_2O$ door hen ingevoerde coëfficiënt B_+ bij lage temperaturen ongeveer als T^{-2} moet variëren, is onjuist. Zelfs indien zij bedoelden „bij hoge temperaturen", is deze bewering nog onjuist.

G.S. Dixon en J.E. Rives, Phys.Rev. 177(1969)871.

VII

Abragam e.a. schrijven het door hen waargenomen minimum in de protonspin-roosterrelaxatietijd als funktie van de hoek die het veld maakt met de kristallografische c–as in lanthaan magnesium nitraat met 5% cerium toe aan het optreden van overgangen waarbij 8 protonspins en 1 elektronspin tegelijk betrokken zijn. Er is echter een veel eenvoudiger verklaring mogelijk.

A. Abragam, J. Combrisson, J.M. Delrieu en J. Ezratty,
Journal de Physique 27(1966)458.

VIII

Foner en McNiff Jr. beschrijven hun metingen van de magnetisatie van een Pd–Rh legering in sterke magneetvelden met een uitdrukking die op aanvechtbare wijze is verkregen. Het gebruikte model ligt bovendien niet het meest voor de hand voor dat systeem.

S. Foner en E.J. McNiff Jr., Phys.Lett. 29A(1969)28.

IX

Daar Watmough en Oliver de door de menselijke huid gereflecteerde straling buiten beschouwing laten, is de conclusie dat de thermografisch bepaalde emissiviteitsfaktor groter is dan 0.98 in het beschouwde golflengtegebied, onjuist.

D.J. Watmough en R. Oliver, Nature 218(1968)886.

X

Het gebruik van de term isotrope exchange-wisselwerking, zoals dit door Morrish wordt omschreven, kan aanleiding geven tot misverstanden.

A.H. Morrish, The Physical Principles of Magnetism, Wiley (1965)281.

XI

De storingstheoretische behandeling van de spin-baankoppeling voor toestanden met baan impulsmoment nul, zoals die in een aantal leerboeken over quantummechanika wordt gegeven, is onbevredigend.

XII

Voor het verkrijgen van korte insteltijden bij warmtegeleidingsexperimenten bij lage temperaturen is het wenselijk een kort preparaat te gebruiken.

XIII

In tegenstelling tot hetgeen aangegeven wordt door Müller e.a. bij de behandeling van botbreuken volgens de z.g. AO methode, verdient het aanbeveling om vóór het snijden van de schroefdraad eerst de lengte van de schroef te meten.

M.E. Müller, M. Allgöwer en H. Willenegger, Springer-Verlag (1965)44.

XIV

Het verdient aanbeveling het in een nieuw overhemd verwerkte aantal spelden op de verpakking aan te geven.

Stellingen behorende bij het proefschrift van K.W. Mess.

CONTENTS

CHAPTER I

GENERAL CONSIDERATIONS AND SURVEY OF THE MEASUREMENTS

1. Introduction 9
2. Magnetic ordering 10
3. Susceptibility 17
4. Magnetocaloric effect 20
5. Nuclear orientation 22
6. Spin-lattice relaxation 23
7. Summary of the measurements and their results 26
References 28

CHAPTER II

EXPERIMENTAL ARRANGEMENTS

1. Apparatus 30
2. Carbon resistance thermometry 32
2.1. Introduction 32
2.2. Experimental method 33
2.3. Temperature dependence 35
2.4. Reproducibility 36
2.5. Field dependence 37
2.6. Conclusion 38
References 38

CHAPTER III

THERMAL AND MAGNETIC PROPERTIES OF CERIUM MAGNESIUM NITRATE BELOW 1 K

1. Introduction 39
2. Experimental method 40
2.1. Susceptibility-entropy (χ–S) measurements 41
2.2. Entropy-heat content (S–Q) measurements 42
3. Results 43
3.1. χ–S measurements 43
3.2. S–Q measurements 46
3.3. χ measurements in low magnetic fields 50
3.3.1. Method 50
3.3.2. Results 52
4. Discussion 55
4.1. Susceptibility 55

4.2. Temperature scale 57
4.3. Value of b 59
4.4. Energy 62
5. Conclusions 65
References 65

CHAPTER IV

SPIN-LATTICE ENERGY TRANSFER BELOW 1 K IN $CuCs_2(SO_4)_2 \cdot 6H_2O$ AND IN $Ce_2Mg_3(NO_3)_{12} \cdot 24H_2O$

1. Introduction 67
2. Experimental method 69
3. Summary of the formulae 71
4. Experimental results 74
4.1. $CuCs_2(SO_4)_2 \cdot 6H_2O$, results and discussion 74
4.2. $Ce_2Mg_3(NO_3)_{12} \cdot 24H_2O$, results 77
4.2.1. Field dependence 77
4.2.2. Temperature dependence 79
4.2.3. Angular dependence 79
4.2.4. Concentration and thickness dependence 79
4.2.5. Effect of impurities 80
4.2.6. Very low temperature and low field data 82
4.3. Discussion of the CMN results 84
5. Conclusion 89
References 89

CHAPTER V

MAGNETIC PROPERTIES AND SPIN-LATTICE RELAXATION OF $CoCs_3Cl_5$ AND $CoCs_3Br_5$

1. Introduction 91
2. Experimental method 92
2.1. Susceptibility measurements 92
2.2. Specific-heat measurements 92
2.3. Magnetic field vs temperature diagram 92
2.4. Relaxation measurements 93
3. Susceptibility measurements 94
4. Phase boundary 101
4.1. $CoCs_3Cl_5$ 102
4.2. $CoCs_3Br_5$ 108
5. Spin-lattice relaxation 111
5.1. Internal field 111
5.2. Relaxation time 113
6. Conclusion 114
References 115

CHAPTER VI

MAGNETIC AND CALORIC STUDY OF THE PHASE TRANSITIONS OF COPPER, NICKEL, MANGANESE AND COBALT LANTHANUM DOUBLE NITRATE

1.	Introduction	116
2.	Experimental method	118
2.1	Specific-heat measurements	118
2.2.	Susceptibility measurements below 1 K	118
2.3.	Adiabatic field variations	118
2.4.	Nuclear orientation	119
2.5.	Susceptibility measurements above 1 K	119
2.6.	EPR and paramagnetic relaxation measurements	119
3.	Cu–La nitrate	120
3.1.	Heat capacity	120
3.2.	Susceptibility	123
3.3.	H–T diagram	124
4.	Ni–La nitrate	125
4.1.	Heat capacity	125
4.2.	Susceptibility above 1 K	128
4.3.	Susceptibility below 1 K	129
4.4.	Magnetization below T	130
4.5.	H–T diagram	131
4.6.	EPR and paramagnetic relaxation results	132
4.7.	Heat capacity of magnetically diluted Ni–La nitrate	135
4.8.	Heat capacity of Ni–Nd nitrate	137
4.9.	Heat capacity of mixed (Ni,Co)–La nitrate	138
5.	Mn–La nitrate	139
5.1.	Heat capacity	139
5.2.	Susceptibility above 1 K	141
5.3.	Susceptibility below 1 K	142
5.4.	H–T diagram	143
5.5.	Nuclear orientation experiments	144
6.	Co–La nitrate	147
6.1.	Heat capacity	147
6.2.	Susceptibility above 1 K	149
6.3.	Susceptibility below 1 K	151
6.4.	H–T diagram	152
7.	Discussion	153
	References	155

SAMENVATTING 157

Chapter I

GENERAL CONSIDERATIONS AND SURVEY OF THE MEASUREMENTS

1. Introduction

The temperature region below 1 K covers a most interesting field of research of magnetism in the solid state of matter. The experimentally acessible region goes down at least as far as approximately 10^{-3} K and comprises therefore three decades in the temperature, T.

Every substance in which permanent magnetic dipolar moments are present will undergo a transition from a state in which these dipolar moments are oriented at random, to a state which can be characterized by magnetic order, when the temperature is sufficiently lowered. Although such transitions may take place at temperatures appreciably above 1 K in many substances, the most detailed information about magnetic transitions is obtained at very low temperatures and in particular below about 1 K. For instance, heat-capacity measurements below 1 K often yield accurate information directly about the magnetic interactions, since the lattice heat capacity can be neglected. Magnetism in solids can arise from both the electronic spins and nuclear spins. Since the latter have magnetic moments which are roughly 10^3 times smaller than the electronic magnetic moments, ordering of nuclear magnetic moments through mutual interactions must be studied at very much lower temperatures ($\approx 10^{-6}$ K).

The use of very low temperatures makes it possible in many cases to consider only the lowest-lying energy levels of the magnetic ions studied. The influence of the electric crystalline field and the spin-orbit coupling usually results into a group of energy levels which is separated from the more numerous higher-lying energy levels by an amount of $\approx 10^2$ cm^{-1} (1 cm^{-1} $\hat{=}$ 1.44 K) in the rare-earth salts and by as much as $10^3 - 10^4$ cm^{-1} in the iron-group salts. Since at low temperatures, i.e. in the region around 1 K, only the lowest-lying energy levels are noticeably populated, the higher levels need not be taken into regard. This enables one to deal with a relatively simple magnetic system of, as is very often the case, effective spin ½. It also enables one to use a spin hamiltonian[1] which describes the energy levels of the magnetic ion with a relatively small number of parameters.

The temperature range below 1 K can easily be covered with the method of adiabatic demagnetization[2,3]. The use of a demagnetized cooling salt, in our case chrome potassium alum, permitted us to cool the samples down to temperatures of about 0.03 K. A limit to this indirect cooling of a specimen is set by the decreasing heat conduction of the connections (i.e. copper wires) of the samples to the demagnetized coaling salt. Also the limited amount of heat which can be absorbed by

the cooling salt determines the lowest temperature to which a sample may be cooled. As a second possibility to attain temperatures below 1 K, the use of liquid ^{3}He may be mentioned. The lowest temperature which can be obtained by reducing the vapor pressure above a ^{3}He liquid is however about 0.3 K. A recent development in the study of ^{3}He-^{4}He mixtures in the liquid state has led to the construction of a so-called dilution refrigerator[4]. With this technique temperatures of a few millidegrees have been obtained in several cases. The experiments described in this thesis have been performed by using the method of adiabatic demagnetization.

Generally speaking, ordering effects in a system of magnetic moments will occur when the magnetic interaction between the spins is of the same order of magnitude as the thermal energy i.e. when $\mu H \approx kT$; μ indicates the magnetic moment, H is the effective magnetic field to which the magnetic moments are exposed, k is the Boltzmann constant and T the absolute temperature. The temperature below which the magnetic system exhibits long-range order is called the critical temperature, T_c. When an electronic spin system orders, the internal molecular field is of the order of $H \approx kT_c/\mu = kT_c/g\beta s$, where g is the splitting factor, β the Bohr magneton and s the electronic spin. For $s = \frac{1}{2}$, $g = 2$ and $T_c = 1$ K, this field amounts to 10^4 Oe. When a magnetic field externally applied to an ordered sample is of the same order of magnitude as the molecular field in the specimen, the magnetic order is highly influenced. As a consequence of such an influence on the magnetic system many interesting features appear and in many cases valuable information about the internal magnetic forces in the sample may be obtained. As the molecular fields amount to approximately 10^4 Oe for samples which order in the temperature range of 1 K, these magnetic fields can easily be obtained with conventional laboratory equipment.

Application of a non-static magnetic field may disturb the magnetic system in such a way that the spin system is not in equilibrium with its surroundings. The characteristic time with which the magnetic spin system approaches thermal equilibrium with a surrounding bath of constant temperature after being disturbed by for instance a sufficiently fast change in the magnetic field, will be called the spin-lattice relaxation time.

2. Magnetic ordering

The ordering of a magnetic system at sufficiently low temperatures is often studied by measurements of the specific heat and the susceptibility as a function of the temperature. Other methods such as study of ferro- and antiferromagnetic resonance, nuclear resonance and the Mössbauer effect, are usually applied only when some knowledge about the magnetic behaviour of the compound is available from e.g. specific-heat measurements. In the temperature region in which a spin system becomes ordered, an extra contribution to the specific heat will be noticeable. If this region lies below 1 K, the extra specific heat will be predominant, as the lattice specific heat is much smaller. If interactions exist among the ions, long-

range order may occur even in the absence of an external field. Two types of such phenomena which can be most easily studied by performing specific-heat and susceptibility measurements are ferro- and antiferromagnetic phase transitions. Phase transitions may be characterized by discontinuities in the first or higher order derivatives of the Gibbs free energy, G, with respect to its independent variables e.g. the temperature[5,6,7]. A phase transition of the first order is found when the first derivative of G, such as $(\partial G/\partial T)_p$, changes discontinuously, as is the case in e.g. the vapour-liquid transition. Such a phase transition is also accompanied by a latent heat. In the magnetically ordered systems which are studied in this thesis no latent heat is involved; these phase transitions are of higher order.

A magnetic phase transition is accompanied by a sharp rise in the specific heat over a narrow temperature range. At the critical temperature, T_c, the specific heat attains a maximum value (it goes to infinity in several theoretical models). The long-range order, which occurs below a magnetic transition point is mostly due to exchange interactions between the ions. The general form of exchange interaction for a pair of spins (i,j) may be written as

$$H_{ij} = \sum_{\alpha,\beta} J_{ij}^{k,\alpha\beta} Q_{i\alpha}^{k} \quad Q_{j\beta}^{k} \qquad (\alpha,\beta = x,y,z) \tag{1}$$

where $J_{ij}^{k,\alpha\beta}$ is the exchange integral, and $Q_{i\alpha,\beta}^{k}$ are tensors of the rank k in the spin operators of the i^{th} and j^{th} ion respectively. Usually it is sufficient to consider only the first-rank tensors, whence

$$H_{ij} = \sum_{\alpha,\beta} J_{ij}^{\alpha\beta} s_{i\alpha} \; s_{j\beta} \tag{2}$$

This expression can be separated into scalar, antisymmetric tensor and symmetric tensor parts[8], which correspond to respectively the Heisenberg exchange interaction

$$J_{ij} \vec{s}_i . \vec{s}_j \, , \tag{3}$$

the Dzyaloshinsky-Moriya term[9,10]

$$\vec{d} . (\vec{s}_1 \times \vec{s}_2) \tag{4}$$

and to

$$D(3s_{zi} \, s_{zj} - \vec{s}_i . \vec{s}_j) + E(s_{xi} \, s_{xj} - s_{yi} \, s_{yj}). \tag{5}$$

In the case that the crystal structure shows inversion symmetry with respect to the center of mass of the two interacting ions (i,j), the $\vec{d}$ term is zero. For axial sym-

metry around the z axis also E = o and the sum of the Heisenberg term and the anisotropic D term can also be written as

$$H = -2J \sum_{i<j} [s_{zi}\, s_{zj} + \gamma(s_{xi} s_{xj} + s_{yi} s_{yj})]. \qquad (6)$$

In this relation J is the exchange integral, s_{xi}, s_{yi} and s_{zi} are the spin components of the i^{th} spin in a rectangular coordinate system the z axis of which is chosen to lie along the crystal's axis of symmetry, γ is a parameter which describes the anisotropy of the coupling between the ions and may take values of $0 \leq \gamma \leq 1$ for various salts. The exchange coupling is usually considered between nearest neighbours only, because of the fast decrease of J with increasing distance between the ions. The summation in (6) runs over all pairs of nearest neighbours in a sample. For γ=1 the exchange interaction is completely isotropic and the model obtained is called the Heisenberg model. For $\gamma = 0$ only the z components of the magnetic moments are taken into regard and this completely anisotropic coupling corresponds to the Ising model. The exchange interaction between two atomic electrons having free spin angular momenta is of the Heisenberg type, $-2J\vec{s}_1.\vec{s}_2$, i.e. classically speaking the exchange energy is independent of the orientation of the spin vectors $\vec{s}_1$, $\vec{s}_2$ with respect to the crystal axes and depends only on the mutual orientation of $\vec{s}_1$ and $\vec{s}_2$. However, considerably more complicated expressions may arise when spin-orbit coupling is taken into account and when the effective spin-hamiltonian formalism is introduced for describing the ground-state multiplet[11,12]. Taking, for instance, the case of Co ions in an orbitally non-degenerate ground state[11], the fourfold spin degeneracy (s = 3/2) may be removed by the combined effects of crystalline electric fields and spin-orbit coupling. This can to some extent be visualized as a preferred alignment of the effective orbital momentum along a crystal field axis (e.g. the z axis) and, by spin-orbit coupling, also of a preferred alignment of $\vec{s}$ along the z axis, resulting in a $s_z = \pm 3/2$ Kramers doublet ground state. When introducing the effective spin-hamiltonian formalism for this ground state doublet ($s' = ½$, $s_z' = \pm ½$) and considering interionic exchange as a small perturbation, then the exchange interaction will occur only among the z components of the spin angular momentum. This yields an extremely anisotropic exchange coupling of the type

$$H_{ij} = -2J s_{iz}' s_{jz}' \qquad (7)$$

which is equivalent to the Ising model. If, on the other hand, $s_z = \pm ½$ were lowest and if again effective spin $s' = ½$ is introduced, one finds that the exchange interaction would have the form

$$-2J[s_{iz}' s_{jz}' + 4(s_{ix}' s_{jx}' + s_{iy}' s_{jy}')]. \qquad (8)$$

When the term containing the z components can be completely neglected, one speaks of the XY model. The latter may be appropriate for describing interactions in e.g. cerium magnesium nitrate in which the Ce electronic angular momenta are practically exclusively aligned in a plane perpendicular to the crystalline c axis. In this connection it may be remarked that the interactions between the ions need not be all of the exchange type. The anisotropic "exchange" interaction may arise from dipole-dipole interactions. This can be seen from the expression for the dipole-dipole coupling between two magnetic moments, which takes the form

$$H_{d.d.} = \frac{\vec{\mu}_1 \cdot \vec{\mu}_2}{r^3} - \frac{3\mu_{1z}\mu_{2z}}{r^3}$$

if the z axis is chosen to lie along the line connecting the two dipoles.

The first theory which yielded some of the most relevant features of the experimentally observed ferromagnetic phase transitions is based on the well known molecular-field model introduced by Weiss[13]. In this phenomenological theory the strong interactions between the magnetic moments are assumed to be proportional to the magnetization $\vec{M}$. This interaction may be considered to be equivalent to some internal magnetic field, $\vec{H}_m$, which may be written as $\vec{H}_m = N_w \vec{M}$ in which N_w is the molecular-field or Weiss constant. A connection of this molecular-field constant with the exchange integral introduced in eq. (6) may be found by making the assumption that the isotropic exchange hamiltonian ($\gamma = 1$) can be replaced by the expression

$$H = -2z\, J \langle \vec{s}_i \rangle \sum_i \vec{s}_i \,. \tag{10}$$

In this relation $\langle \vec{s}_i \rangle$ is the time average of the spin value of the z nearest neighbours of spin i. As we have also the relation with the molecular field

$$H = -\sum_i \vec{\mu}_i \cdot \vec{H}_m \tag{11}$$

in which $\vec{\mu}$ is the magnetic moment of the ions and equals $g\beta\vec{s}$, we obtain from eqs. (10) and (11) the relation for the Weiss constant

$$N_w = \frac{2z\, J}{Ng^2\beta^2} \tag{12}$$

in which N is the total number of magnetic ions. Although the molecular-field model does predict several characteristics of magnetic phase transitions, there are, however, a number of important differences with the observed behaviour. Molecular-field theory predicts e.g. a discontinuity in the specific heat at the critical temperature

such that for $T < T_c$ the specific heat, c/R, where R denotes the gasconstant, is finite and for $T > T_c$, $c/R = 0$. At $T = T_c$ the discontinuity in c/R then amounts to $\Delta c/R = 5s\ (s + 1)/[s^2 + (s + 1)^2]$. In reality the specific heat is not discontinuous at T_c and there is a non-zero specific heat above the critical temperature which results from short-range ordering.

Various thermodynamic and thermal properties of different magnetic models, in particular the so-called critical parameters, such as for instance the entropy yield involved in magnetic ordering above and below T_c, or the quantity $3kT_c/2zJs\ (s+1)$, where z is the coordination number of a magnetic ion, can be found tabulated in the literature for the Heisenberg model as well as for the Ising model[6,14], for various values of the spin and for various crystal structures. The behaviour of a model is not primarily determined by the particular lattice structure within a given dimension, but rather by the dimensionality of the structure. For instance, a two-dimensional triangular lattice which has coordination number $z = 6$ has critical parameters which are much closer to those of a simple quadratic lattice which has $z = 4$, than to a simple cubic lattice which has $z = 6$.

In a temperature range where T is much larger than the temperature at which the maximum in the specific heat occurs, the magnetic interactions in a specimen lead to a specific heat, c/R, which is proportional to T^{-2}. Van Vleck[15] developed a general method for calculating magnetic interactions. It consists in the development of the partition function $Z = \mathrm{Tr}\ e^{-\beta H}$, where Tr means the trace taken over all diagonal matrix elements in a particular representation, while $\beta \equiv 1/kT$, in powers of 1/T in the high-temperature approximation. Four contributions to the magnetic specific heat may be mentioned, which are algebraically additive at sufficiently high temperatures.

a) Specific heat due to Stark splittings of the electronic energy levels. When the splitting of the energy levels under the influence of the electric crystalline field is described by the hamiltonian $H_{cr} = D\{s_z^2 - s(s+1)/3)\}$ in which D is a constant, the high-temperature specific heat amounts to

$$\frac{c}{R} = \frac{1}{45}\, s\,(s+1)(2s-1)(2s+3)\,\frac{D^2}{k^2T^2} \tag{13}$$

The specific heat due to crystalline-field splittings does not exhibit a sharply peaked curve as is found in cooperative phenomena, but is of a Schottky type. For a two-level energy scheme with splitting Δ, the Schottky specific heat per mole will be given by

$$\frac{c}{R} = \frac{\Delta^2}{k^2T^2}\ \frac{e^{-\Delta/kT}}{(1+e^{-\Delta/kT})^2}\,. \tag{14}$$

As can be seen from this formula the Schottky specific heat rises exponentially at

the lowest temperatures, passes through a maximum and it decreases at high temperatures with a T^{-2} dependence.

b) A contribution to the total specific heat may arise from interactions between electronic and nuclear magnetic moments (hyperfine interaction). When the interaction is isotropic it may be expressed as

$$H = A\vec{s}.\vec{I} \tag{15}$$

where A is called the hyperfine constant and $\vec{I}$ is the nuclear spin. The hyperfine interaction may be anisotropic, which is in general the case if the electronic g value is anisotropic. The hyperfine interaction can then be described by the hamiltonian

$$H = A_x s_x I_x + A_y s_y I_y + A_z s_z I_z \,. \tag{16}$$

The contribution to the specific heat due to h.f.s. interaction amounts in the high-temperature approximation to

$$\frac{c}{R} = \frac{1}{9k^2T^2}\; s(s+1)\, I\,(I+1)\,(A_x^2 + A_y^2 + A_z^2) \tag{17}$$

c) A high-temperature contribution due to electronic dipole-dipole interactions. For isotropic g factors and spin ½ this dipole-dipole specific heat amounts to[16)]

$$\frac{c}{R} = \frac{Q\tau^2}{6T^2} = \frac{g^4\beta^4 s^2(s+1)^2}{3k^2T^2} \sum_i r_{ii}^{-6} = \frac{3}{16}\frac{g^4\beta^4}{k^2T^2} \sum_i r_{ii}^{-6} \tag{18}$$

In this relation $Q = 2N^{-2} \sum r_{ii}^{-6}$ and $\tau = Ng^2\beta^2\, s(s+1)$; N is the total number of atoms per cm^3, r_{ij} is the distance between the magnetic ions. For anisotropic g values and an arbitrary crystal structure, assuming axial symmetry around the crystalline axis, the dipolar specific heat for $s = ½$ can be calculated according to the formula given by Daniels[17)]

$$\frac{c}{R} = \frac{\beta^4}{32\,k^2T^2}\,(g_{//}^4 + 5g_{\perp}^4) \sum_i \frac{1}{r_{ij}^{\,6}} - 6(g_{//}^2 - g_{\perp}^2)(g_{//}^2 - 2g_{\perp}^2) \sum_i \frac{z_{ij}^2}{r_{ij}^{\,8}} +$$

$$9(g_{//}^2 - g_{\perp}^2)^2 \sum_i \frac{z_{ij}^4}{r_{ij}^{\,10}}\,] \tag{19}$$

In this relation $g_{//}$ and $g_{\perp}$ are the splitting factors parallel and perpendicular to the crystalline axis.

The dipolar interactions will in addition give rise to a broadening of the spin-energy levels. To calculate these level broadenings similar formulae to (18) and (19) must be used. For a salt with an isotropic g value and spin ½ the dipolar broadening is expressed by [18]

$$\langle(\Delta\nu)^2\rangle = \frac{9}{16}\frac{g^4\beta^4}{h^2}\sum_i \left(\frac{1}{r_{ij}^6} - \frac{6z_{ij}^2}{r_{ij}^8} + \frac{9z_{ij}^4}{r_{ij}^{10}}\right) \tag{20}$$

$\langle(\Delta\nu)^2\rangle$ is the second moment of the spin resonance line, defined by

$$\int_{-\infty}^{+\infty} f(\nu)(\nu - \nu_o)^2 d\nu$$

in which ν_o is the resonance frequency at the center of the resonance line and $f(\nu)$ a normalized function which describes the shape of the line. For an anisotropic g tensor with axial symmetry a slightly different expression may be used, viz.[19]

$$\langle(\Delta\nu)^2\rangle = \frac{\beta^4}{16h^2}(g_{\perp}^2 + 2g_{//}^2)^2 \sum_i \left(\frac{1}{r_{ij}^6} - \frac{6z_{ij}^2}{r_{ij}^8} + \frac{9z_{ij}^4}{r_{ij}^{10}}\right) \tag{21}$$

which is only valid for the magnetic field along the axis of axial symmetry.

From relations (18) and (19) it can be seen that the high-temperature magnetic specific heat in zero magnetic field is proportional to T^{-2} and following Waller[16] and Van Vleck[15], it can be written as[20]

$$c_{H=0} = \frac{b}{T^2} \equiv \frac{CH_i^2}{2T^2} \tag{22}$$

in which C is the Curie constant, H_i^2 is the square of the so called internal magnetic field which characterizes to first approximation the magnetic interactions and is defined (in case of isotropic g values) by[15]

$$H_i^2 = 2\mu^2 \sum_i r_{ij}^{-6} \tag{23}$$

in which μ^2 is the average of the square of the magnetic moment of one ion. The quantity b/C can be obtained from specific-heat measurements in zero and non-zero magnetic fields at relatively high temperature, and from susceptibility measurements

by the relation

$$\frac{c_H}{c_{H=0}} = \frac{\chi_T}{\chi_S} = \frac{b + CH^2}{b} \tag{24}$$

For a simple cubic lattice with isotropic g values, Caspers[21] showed that for the second moment of the spin resonance line width, expressed by

$\langle(\Delta H)^2\rangle = \frac{h^2 \langle(\Delta\nu)^2\rangle}{g^2\beta^2}$, the relation $\langle(\Delta H)^2\rangle = 0.92\ b/C$ applies to a direction along a cubic axis. In many cases the second moment may be quite different from b/C due to the different dipolar sums involved in eqs. (18) and (20). It may be remarked, that the total resonance line width at half height, $(\Delta H)_{1/2}$, for a purely Gaussian shaped line amounts to $2.36\ \sqrt{\langle(\Delta H)^2\rangle}$. For e.g. cerium magnesium nitrate one obtains $b/C = 1725\ Oe^2$ using the dipolar sums of ref. 17 and $\langle(\Delta H)^2\rangle = 1770\ Oe^2$, using the formalism given in ref. 18. This result[22] was obtained in directions $15° < \theta \leq 90°$, θ being the angle with the crystallographic c axis. From ref. 19 one obtains $\langle(\Delta H)^2\rangle = 2625\ Oe^2$ along the c axis. Experimentally[23], in the direction $\theta = 90°$, $(\Delta H)_{1/2}$ amounts to 118 Oe which may be compared with 99 Oe, obtained from numerical evaluation of ref. 18, assuming a Gaussian shaped line.

d) A contribution to the total specific heat at high temperatures due to exchange interactions between the ions. This contribution amounts for the Heisenberg model to

$$\frac{c}{R} = \frac{2\ s^2(s+1)^2 z\ J^2}{3k^2\ T^2} \tag{25}$$

Several theoretical models have been developed to predict the behaviour of the specific heat as a function of T for various magnetic structures. Thus far only for the two-dimensional Ising model in zero magnetic field an exact solution has been obtained[24]. For the more complicated systems various approximate theories have been developed. For temperatures well above T_c the series-expansion method[25] is applied which consists of expanding the quantum mechanical partition function into a power series of e.g. J/kT. At the lowest temperatures i.e. for $T < T_c/2$ a good approximation for the calculation of the various quantities of ferromagnets is obtained by using spin-wave theory[26,27]. To illustrate the qualitative behaviour of the specific heat for the various approximations, some examples are shown in fig. 1.

3. Susceptibility

Much information on magnetic phase transitions can be obtained by measuring

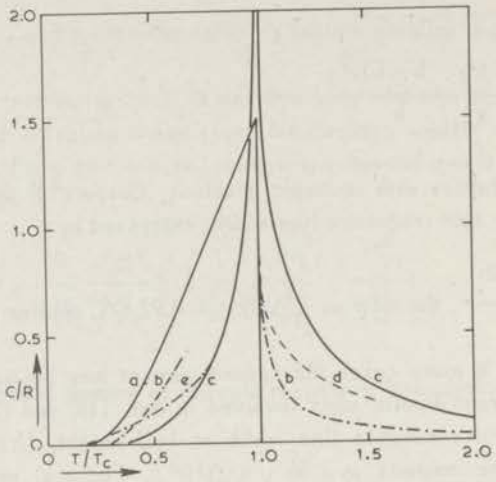

Fig. 1. Some examples of the specific heat, c/R, for a spin ½ system in various approximations.

a: molecular-field model
b: b.c.c. Ising, series expansion
c: simple quadratic lattice, exact (Onsager)
d: b.c.c. Heisenberg, high T expansion
e: b.c.c. spin-wave theory.

the susceptibility, χ, of the specimen as a function of temperature. The susceptibility defined as the ratio M/H, is called the static susceptibility. Very often χ is measured by a dynamical method i.e. variation of H with time and then one defines $\chi = (\partial M/\partial H)$. The dynamical susceptibility can be determined either at constant temperature, i.e. the isothermal susceptibility, χ_T, or at constant entropy, i.e. the adiabatic susceptibility, χ_S. The isothermal susceptibility χ_T equals the static susceptibility as long as the magnetization is proportional to the magnetic field. The functional dependence of M on the temperature and magnetic field in an ideal paramagnet is described by the relation

$$M(T,H) = Ng\beta sB_s(x), \text{ with } x = \frac{g\beta sH}{kT}. \tag{26}$$

$B_s(x)$ is called the Brillouin function. For values of $x << 1$ the Brillouin function can be replaced by the approximation $B_s(x) \approx (s + 1)x/3s$ and relation (26) can be written as

$$M(T,H) = N\frac{g^2\beta^2 s(s+1)H}{3kT} \equiv C\frac{H}{T} \tag{27}$$

C is called the Curie constant. From relation (27) it is seen that in this approxima-

tion the static susceptibility, M/H, is identical with the dynamical susceptibility $(\partial M/\partial H)_T$ and is equal to $\chi = C/T$; this relation is called the Curie law.

It is, however, found that most paramagnetic substances follow a Curie-Weiss law $\chi = C/(T - \theta)$, where θ is called the Curie-Weiss constant. The occurrence of a Curie-Weiss constant may have three causes.

a) When the magnetic ions are not mutually independent but exert mutual exchange forces of the form of eq. (1), a deviation from Curie's law will occur. According to molecular-field theory a Curie-Weiss constant of $\theta = 2\ s\ (s + 1)z\ J/3k$ will occur when the exchange interactions are isotropic and occur among nearest neighbours only. In the case of the strongly anisotropic Ising exchange interaction

$$H = -\frac{J'}{s^2} \sum_{i<j} s_z^i\ s_z^j \tag{28}$$

with $s = \frac{1}{2}$, the Curie-Weiss constant amounts to $\theta = zJ'/k$ if the susceptibility is measured along the z axis.

A more elaborate way to calculate the Curie-Weiss constant is to form the partition function Z. The susceptibility is then given by the relation

$$\chi = \lim_{H \to 0} \frac{kT}{H} \frac{\partial}{\partial H} \ln Z \tag{29}$$

In the above relation $Z = \mathrm{Tr}\ e^{-\beta H}$, in which the hamiltonian H includes a Zeeman term due to the presence of an external magnetic field. If the partition function is developed into a high-temperature expansion, one obtains the susceptibility in powers of 1/T. The first term in this sequence is proportional to T^{-1}, the second to T^{-2} and from the ratio of these proportionality constants the value for θ can be obtained. In molecular-field theory the Curie-Weiss θ is equal to the transition temperature, T_c. In the case that no exchange interactions are present and only dipolar interactions occur, the Curie-Weiss constant is determined by the shape-dependent dipolar sum

$$\frac{\theta}{C} = -\frac{1}{N} \sum_i (1 - 3\cos^2\theta_{ij})/r_{ij}^3 \tag{30}$$

where C is the Curie constant per cm^3. This relation has been shown[28] to be valid not only in the molecular field approximation, but to hold rigorously.

b) When the ground-state levels of a magnetic ion are split under the influence of the electric crystalline field, deviations from Curie's law will occur. The susceptibility will follow to first approximation a Curie-Weiss law at temperatures high compared to the ground-state energy splittings. For a crystalline-field of axial symmetry a Curie-Weiss constant of

$$\theta = a\,(\frac{D}{k})\,(2\,s - 1)\,(2s + 3) \tag{31}$$

will occur in which $a = -\frac{1}{15}$ for H parallel to the crystalline axis and $a = +\frac{1}{30}$ for H perpendicular to that axis.

c) A deviation from Curie's law may also occur due to the difference between the local field, H_{loc}, which acts on the magnetic ions and the externally applied field H_{ext}. This difference is caused by the occurrence of demagnetizing effects. The demagnetizing field amounts to $-NM$ where N is the geometrical demagnetizing factor of the sample and M is the magnetization per unit volume. In the Lorentz approximation the local field in a cubic lattice equals

$$H_{loc} = H_{ext} + (\frac{4\pi}{3} - N)M \tag{32}$$

As we have $\chi = M/H_{loc} = C/T$ in the paramagnetic region where Curie's law is obeyed, and if we define $\chi_{exp} = M/H_{ext} \equiv C/T^*$, where T^* is called the magnetic temperature, the relation

$$T = T^* + (\frac{4\pi}{3} - N)C = T^* + \theta \tag{33}$$

is obtained. It is seen from this relation that the Curie-Weiss constant is shape dependent. In the Lorentz approximation it equals zero for a spherical sample and in that case the magnetic temperature equals the absolute temperature in the region where the susceptibility follows Curie's law. The Curie-Weiss constant due to demagnetizing effects may, however, be quite different for various samples. For an infinitely long cylinder ($N = 0$) of $Ce_2Mg_3(NO_3)_{12}.24H_2O$ it amounts to $\theta = 0.00366$ K. For a magnetically concentrated salt with a large spin value, e.g. for EuO, θ amounts to 0.204 K for such a shaped sample.

4. Magnetocaloric effect

As we have shown, measurements of the specific heat and the susceptibility yield information about the magnetic interactions in a specimen and they are equally useful for the study of ferro- and antiferromagnetic ordering. Supplementary information can be obtained from the so called magnetocaloric effect when an antiferromagnetically ordered system is studied. From the thermodynamic Maxwell relation

$$(\frac{\partial M}{\partial T})_H = (\frac{\partial S}{\partial H})_T \tag{34}$$

and by considering the entropy as a function of T and H, hence

$$T\,dS = T\left(\frac{\partial S}{\partial T}\right)_H dT + T\left(\frac{\partial S}{\partial H}\right)_T dH \tag{35}$$

one may obtain the relation for an adiabatic process

$$dT = -\frac{T}{c_H}\left(\frac{\partial M}{\partial T}\right)_H dH \tag{36}$$

where c_H is the magnetic specific heat in a constant magnetic field. Since for a paramagnetic and ferromagnetic salt $(\partial M/\partial T)_H$ is negative, an increase in magnetic field produces a temperature rise. However, for an antiferromagnet $(\partial M/\partial T)_H$ is positive and a decrease in temperature will occur when the applied magnetic field is increased adiabatically. As is well known, a simple antiferromagnet exhibits a critical curve in the H–T plane, the phase boundary. Inside this curve the magnetic moments are aligned antiparallel, outside the phase boundary the moments are oriented with respect to the magnetic field like in a normal paramagnet, and the magnetization follows a Brillouin curve. The neighbourhood of the transition from the antiferromagnetic to the paramagnetic region is characterized by a change in sign of the quantity $(\partial M/\partial T)_H$, i.e. on varying the magnetic field adiabatically the initially observed temperature decrease will change into a temperature increase. Although it is not in general the case, the temperature at which the change in sign of $(\partial M/\partial T)_H$ occurs will represent the critical temperature in the applied field. This field will then be approximately equal to the internal exchange field in the specimen. By measuring the temperature variation when a magnetic field is applied adiabatically, as a function of temperature in zero field, a phase boundary may be obtained under certain conditions. The form of this critical curve may yield information on the magnetic model under consideration. In the low-field region the phase boundary of an antiferromagnet may be established more precisely. This may be accomplished by measuring the specific heat in the presence of a constant magnetic field, since application of a field shifts the critical temperature, T_N, to a lower value. Estimates for the magnitude of such a shift can be obtained e.g. from molecular-field theory. In the molecular-field approximation the magnetization of the sublattices is described by a Brillouin function. By expanding the Brillouin function into powers of its argument it can be shown that the Néel temperature $T_N(H)$ in a field H applied along the direction of spin alignment is given by

$$\frac{T_N(H) - T_N(0)}{T_N(0)} = \left(\frac{3s}{s+1}\right)^3 \frac{B_s'''(0)}{2(Ng\beta s)^2}\,\chi_\perp^2\,H^2 \tag{37}$$

where $B_s'''(0) = -(s+1)[(s+1)^2 + s^2]/90\ s^3$ and $\chi_\perp$ is the susceptibility perpendicular to the direction of spin alignment. Rigorous calculations have been performed on the basis of the Ising model by Bienenstock[29]. The result of his computer calculations, using Padé approximants, can be numerically expressed by

$$\frac{T_N(H)}{T_N(0)} = [1 - (\frac{H}{H_c})^2]^b \qquad (38)$$

with b = 0.87 and 0.35 for the square and simple cubic lattice, respectively. In this relation $H_c = -zJ'/g\beta s$.

The crystalline anisotropy which determines the direction of spin alignment can be represented by a magnetic field H_A. In the Heisenberg model $H_A \ll H_E$, where $H_E = 2zJs/g\beta$ is the effective exchange field at zero temperature. For an Ising system $H_A \gg H_E$. When we have $H_A \leq H_E$ application of a magnetic field parallel to the axis of spin alignment in an antiferromagnet may result in a phenomenon sometimes called spin flopping[30]. This occurs when on increasing the magnetic field the orientation of the magnetic moments changes from parallel into perpendicular to the magnetic field direction.

5. Nuclear orientation

As was already remarked, ordering effects in a magnetic system will occur under conditions of magnetic field and temperature such that $\mu H \approx kT$. The summary of several magnetic and caloric phenomena given above deals with the electronic magnetic moments. Similar phenomena may occur for a system of nuclear magnetic moments. The temperatures at which notable nuclear orientation occurs are much lower than those at which the ionic moments become ordered because of the much smaller nuclear magnetic moments. If a magnetic ion has a nucleus with non-zero magnetic moment, there will be an additional splitting of the ionic levels, the hyperfine splitting, due to the mutual interaction of the nuclear and electronic moments. Depopulation of the upper hyperfine levels with decreasing temperature will give rise to an orientation of the nuclear spins and to a Schottky-type nuclear specific heat. If the interaction between the electronic and nuclear moment is isotropic, it can be represented by eq.(15). If the hyperfine magnetic fields are oriented along the same axis for all ions, the preferential population of the nuclei on lowering the temperature corresponds to orientation of the nuclei parallel to the spatially determined axis of electron spin alignment. Such an axis of orientation can be obtained by polarizing the electronic moments in a magnetic field at low temperatures. In an antiferromagnet the axis of electron spin alignment is generally determined by crystalline anisotropy. Nuclear orientation may be studied by inserting in the sample relatively few radioactive nuclei and observing the directional γ-ray intensity distri-

bution. As an assembly of oriented nuclei has anisotropic properties, the γ-ray emission is no longer spatially isotropic. Quite generally the directional distribution of γ radiation from oriented nuclei is given by the relation

$$W(\theta) = \sum_{k=o}^{\min(i_i, L)} a_{2k} N_{2k} f_{2k} P_{2k}(\cos\theta) \qquad (39)$$

in which θ is the angle with the axis of orientation, a_{2k} is a numerical constant, depending on the radioactive decay characteristics, while k is related to the multipolarity of the gamma radiation, N_{2k} depends on the nuclear spin, f_{2k} is called an orientation parameter and depends on the temperature, and $P_{2k}(\cos\theta)$ is the Legendre polynomial of the $2k^{th}$ degree. $W(\theta)$ is normalized such that $\int_{\text{sphere}} W(\theta)d\Omega = 4\pi$. For e.g. dipole radiation in which the angular momentum L of the gamma radiation equals $i_i - i_f = L = 1$, where i_i and i_f are the initial and final spin momenta of the nucleus respectively, eq.(39) yields

$$W(\theta) = 1 + \frac{3}{2} N_2 f_2 P_2(\cos\theta) \qquad (40)$$

Nuclear orientation can be obtained in an axial two-sublattice antiferromagnet simply by cooling a single crystal to a temperature both sufficiently below its Néel temperature and below roughly the temperature given by A/k. The nuclei will then become oriented either parallel or antiparallel (depending on the sign of A) to the directions of spontaneous magnetization of the two sub-lattices. Antiferromagnetic substances in which nuclear orientation is studied must be cooled by an indirect method. Nuclear orientation is, however, quite often restricted because the nuclear spin-lattice relaxation time below 1 K may be so long that the nuclei cannot be cooled in the time available for an experiment. Generally speaking, the higher the Néel temperature, the longer the relaxation time at temperatures where nuclear orientation occurs.

6. Spin-lattice relaxation

Suppose a magnetic system in a constant magnetic field, H, and in equilibrium with the lattice. When the magnetic field is suddenly changed to a value $H + \Delta H$, the magnetization of the sample does not follow the change in magnetic field instantaneously. It takes a finite time, τ, for the magnetization to reach a new state of equilibrium during which time energy is exchanged between the spin system and the lattice (spin-lattice relaxation). Alternatively, spin-lattice relaxation may occur if, in addition to the constant magnetic field, an alternating field of frequency ω is

applied. If the angular frequency of the applied field is much smaller than $2\pi/\tau$, the magnetic moments can easily follow the field variations and the dynamic susceptibility will be the same as the static susceptibility, provided no saturation effects are present. With increasing frequency of the magnetic field variation, the orientation of the ions will get out of phase with that of the field. The susceptibility can then be considered as a complex quantity of the form $\chi = \chi' - i\chi''$ in which χ' is the real and χ'' the imaginary part of the susceptibility. Both χ' and χ'' will be frequency dependent; the variation of χ' with ω is called paramagnetic dispersion; χ'' is proportional to the energy absorbed by the magnetic substance. The real and imaginary part of the susceptibility are given by the relations

$$\chi' = \chi_S + \frac{\chi_T - \chi_S}{1+\omega^2\tau^2} \qquad \text{and} \qquad \chi'' = \frac{(\chi_T - \chi_S)\omega\tau}{1+\omega^2\tau^2} \tag{41}$$

Macroscopically, the spin-lattice relaxation time is the time needed for the magnetization along the z axis, M_z, to reach its equilibrium value M_o. This process can be described phenomenologically by the relation[31]

$$\frac{\partial M_z}{\partial t} = \frac{M_o - M_z}{\tau} \tag{42}$$

Microscopically, spin-lattice relaxation can be pictured as a redistribution of the populations of the energy levels of a paramagnetic substance. Hyperfine splitting does not essentially alter this picture. When for simplicity a two-level energy scheme is considered ($s = \frac{1}{2}$) as is often the case at low temperatures in many substances, we may denote the equilibrium populations of upper and lower energy level by N_1 and N_2, where $N_1 + N_2 = N$ is the total number of spins. When we denote the probability for a single transition per second from level 1 to level 2 with P_{12}, we have in equilibrium $N_1 P_{12} = N_2 P_{21}$. When we further define $\tau_{12} = 1/P_{12}$ and $\tau_{21} = 1/P_{21}$ as the time for a transition, we obtain the relation $N_2/N_1 = \tau_{21}/\tau_{12} = e^{g\beta H/kT}$. If after some disturbance the spin system relaxes to its equilibrium state we may write, assuming that the transition probability is independent of the level populations, $\frac{dN_2}{dt} = -\frac{dN_1}{dt} = \frac{N_1}{\tau_1} - \frac{N_2}{\tau_2}$. After some simple algebraic manipulations the relation $\frac{dM_z}{dt} = \left(\frac{1}{\tau_{12}} + \frac{1}{\tau_{21}}\right)(M_o - M_z)$ is obtained from which it is seen that the inverse of the spin-lattice relaxation time τ, defined in eq.(42) is equal to $1/\tau = (1/\tau_{12} + 1/\tau_{21})$.

Spin-lattice relaxation has its origin in the variations of the crystalline electric field which arise from the thermal vibrations of the ions[32,33]. The lattice vibrations can formally be replaced by a system of harmonic oscillators; the quantized lattice

vibrations are called phonons. The lattice vibrations can act on the electronic orbits and the changes in orbital motion will interact with the spins via the spin-orbit coupling. This mechanism of spin-lattice interaction yields in many cases a reasonable estimate of the experimentally determined relaxation times, especially in the rare-earth double nitrates and ethyl sulphates. The effect of the lattice vibrations on the dipole-dipole interaction, viz. varying the distance between the magnetic dipoles, may also cause spin-lattice relaxation[34,35]. This mechanism is, however, in general insufficient to explain the observed relaxation times.

Theoretically there are three main types of spin-lattice relaxation in solids. At relatively high temperatures i.e. $T > 1$ K, the Raman and Orbach process may occur. In the Raman process a phonon of one energy is absorbed, combined with the emission of a phonon having a different energy. The difference in energy of these phonons equals the energy of the spin transition. In contrast to the Raman process, in the Orbach process the absorbed phonon must have the energy required to lift a spin to a higher electronic energy level. The energy of the emitted phonon then corresponds to the transition of the spin to the ground state. These two-phonon processes display a steep temperature dependence and are usually operative at temperatures well above 1 K. Below 1 K the direct process relaxation is dominant. Experimentally the predicted field and temperature dependence of the spin-lattice relaxation time for the above mentioned processes may be observed in dilute samples. In concentrated samples very often deviations from the mentioned theoretical predictions are observed. In the direct process the spin system reduces its energy by emitting a phonon with an energy equal to the spin transition. When we have a two-level system and they form a non-Kramers doublet, i.e. the magnetic properties arise from an even number of unpaired electrons, the direct relaxation time, τ_d, is found to vary as a function of magnetic field and temperature as $\tau_d \propto H^{-2}T^{-1}$. If the two levels form a Kramers doublet, which occurs in ions with an odd number of unpaired electrons, τ_d varies proportional to $H^{-4}T^{-1}$.

When the direct process below 1 K is sufficiently fast, a complication in the spin-lattice relaxation may arise. The band of lattice oscillators with which the spin system can interact, the so called phonons on speaking terms, have a relatively small thermal contact with the helium bath to which the spin energy is delivered. As these phonons on speaking terms may not be able to exchange their energy with the other lattice oscillators or with the helium bath rapidly enough, and as they have a heat capacity small compared to that of the spin system, they are heated and the effective temperature of these phonons may approximate the spin temperature. This is called the phonon bottleneck. The time constant t_{ph}, characterizing the exchange of energy between the band of phonons and the bath may be estimated to be of the order of d/v_o where d is the linear dimension of the sample and v_o the velocity of sound. A phonon bottleneck will arise if the maximum energy flow from the spins to the phonons on speaking terms i.e. E_{spins}/τ_d, is much larger than the energy flow

from the phonons to the helium bath i.e. E_{ph}/t_{ph}. The energy flow from the spin system to the bath will then be determined by an observed spin-bath relaxation time, τ_b, which equals $\tau_b = E_{spins} t_{ph}/E_{ph}$. Since in the high-temperature approximation E_{spins} is proportional to $1/T$ and E_{ph} to T, τ_b will be proportional to T^{-2}.

Spin-lattice relaxation data are usually obtained by observing the recovery of the spin system as it approaches equilibrium with a surrounding helium bath at constant temperature. In our experiments the sample is completely isolated from its surroundings and the heat capacity is determined only by the spin system, as below 1 K the phonon heat capacity is very small compared to the heat capacity of the spin system. According to Kittel[36] the time, t_o, to establish approximate equilibrium between the electron spins and the phonon system may be written as

$$t_o = \tau_d \left(\frac{c_{ph}}{c_{spins}}\right) \tag{43}$$

in which relation c_{spins} is the heat capacity of the spin system and c_{ph} that of the phonon system. As $(c_{ph}/c_{spins}) \ll 1$ below 1 K, t_o may be orders of magnitude smaller than the intrinsic spin-lattice relaxation time. As will be outlined in chapter IV, in our experiments a thermal bath is artificially created by producing a heat flow from the phonons into the spin system and measuring the temperature difference when a stationary situation is obtained. In the case of $CuCs_2(SO_4)_2.6H_2O$ on which relaxation data are reported, a spin-bath relaxation time of about 10^2 s is found at $T = 0.1$ K and $H = 4000$ Oe, while a stationary temperature difference between the lattice and spin system was obtained in less than 20 s.

7. Summary of the measurements and their results

The experimental equipment is shortly described in chapter II. The method of temperature measurement by using a carbon resistor is discussed in some detail. As a result of our measurements it appears that a carbon resistor is most useful as a thermometer at very low temperatures especially in experiments in which an externally applied magnetic field is used.

Magnetic and caloric measurements on $Ce_2Mg_3(NO_3)_{12}.24H_2O$ at very low temperatures, i.e. $T < 0.01$ K are presented in chapter III. Susceptibility versus entropy measurements were performed on a spherically and an ellipsoidally shaped single crystal. The results show that for entropies below 0.38 R the susceptibility reaches a constant and maximum value of $1/N$ for both samples, where N is the demagnetizing factor. From heat content versus entropy measurements a temperature scale, i.e. a relation between the absolute temperature, T, and the magnetic temperature of a spherical sample, $T^{\circledast}$, was established. From the entropy versus absolute temperature relation a specific-heat curve was obtained, displaying a maximum at

$T_c = 1.9\ (\pm\ 0.1)$mK. From these results and measurements of the magnetization of the spherical sample at constant entropy a ferromagnetic transition at T_c was concluded. Below T_c the sample splits up into domains. Additional measurements of the susceptibility in small longitudinal and tranverse magnetic fields are presented.

Chapter IV discusses the spin-lattice heat contact of two paramagnetic salts $CuCs_2(SO_4)_2.6H_2O$ and $Ce_2Mg_3(NO_3)_{12}.24H_2O$. These two salts were chosen because of their well-defined Zeeman energy level system. The magnetic interactions between the ions are relatively weak and are almost exclusively due to dipole-dipole interaction. Both salts remain paramagnetic down to very low temperatures, i.e. to $T << 0.1$ K. From these measurements it appeared that below 1 K the spin-bath heat transfer is not determined by the direct process but by phonon-bottleneck effects. In the copper salt a thickness dependence of the energy flow between the lattice and the spin system is found, which seems to be absent in the cerium salt. The effect of some impurities on the relaxation in cerium magnesium nitrate is studied as well as the effect of diluting the cerium spin system with diamagnetic lanthanum. From the observed angular and field dependence of the heat transfer in cerium magnesium nitrate the onset of the direct process in small magnetic fields making a small angle with the crystallographic c axis may be concluded.

Chapter V presents magnetic, caloric and relaxation data for the three-dimensional Ising salt $CoCs_3Cl_5$ and the apparently two-dimensional Ising salt $CoCs_3Br_5$. From susceptibility measurements performed on single crystals it is concluded that these salts order antiferromagnetically below the critical temperature. These critical temperatures amount to $T_N = 0.527$ K and $T_N = 0.282$ K for the chloride and bromide respectively. Measurements of the shift of the position $T_N(H)$ of the heat-capacity anomaly under the influence of an external magnetic field agree with theoretical predictions on a three-dimensional simple cubic and a two-dimensional simple quadratic Ising antiferromagnet for the chloride and bromide respectively. For both salts a phase diagram in the H–T plane was obtained by measuring the temperature change upon applying a magnetic field adiabatically. The spin-lattice relaxation time, τ, was found to obey approximately $\tau \propto T^{-7}$ and to be practically field independent at temperatures $T > T_N$.

In chapter VI heat-capacity measurements on four double nitrates of composition $X_3La_2(NO_3)_{12}.24H_2O$, where X stands for Cu, Ni, Mn and Co respectively, are discussed. These salts show anomalies in the heat capacity at 0.089 K, 0.393 K, 0.230 K and 0.189 K respectively. Below these temperatures the Cu, Mn, and Co compounds show antiferromagnetic behaviour while the Ni compound shows ferromagnetic features. On basis of the crystal structure and particularly on basis of the experimental results obtained for the copper salt, a model is proposed in which 2/3 of the divalent ions at crystallographic X sites are coupled in pairs antiferromagnetically according to an exchange coupling $H = -2J\vec{s}_1.\vec{s}_2$. On the basis of this model an exchange constant $J/k = -0.23$ K for the Cu-ion pairs was deduced from the specific-heat data.

This was done by fitting a Schottky anomaly above T_N to the observed Schottky-type high-temperature specific heat, assuming a singlet-triplet energy level scheme resulting from the isotropic exchange coupling. Isentropes in the H–T plane were seen to yield a cooling for all specimens, the strongest cooling being observed in the Ni salt. Nuclear orientation of ^{54}Mn in the manganese salt was studied under various conditions of magnetic field and temperature. These data indicate a short nuclear spin-lattice relaxation time in contrast to results on other antiferromagnetic or paramagnetic Mn^{++} compounds.

The experiments described in this thesis do not form a closed and very detailed field of research. Except $CoCs_3Cl_5$ and $CoCs_3Br_5$, the magnetic systems studied are not examples of simple models on which theoretical predictions can be made. However, the results given do present a variety of interesting and new features of magnetic and caloric properties of some magnetic systems below 1 K. An aspect that is common to all experiments is the use of an externally applied magnetic field at very low temperatures. As the application of a magnetic field may provide serious difficulties if the susceptibility of a paramagnetic salt is used as a thermometer, carbon thermometry was applied in all experiments.

References

1) Abragam, A. and Pryce, M.H.L., Proc.Roy.Soc. A205 (1951)135.
2) Debije, P., Ann.Phys. 81 (1926) 1154.
3) Giauque, W.F., J.Am.Chem.Soc. 49 (1927) 1864, 1870.
4) Wheatley, J.C., Vilches, O.E. and Abel, W.R., Physics 4 (1968) 1.
5) Ehrenfest, P., Commun.Kamerlingh Onnes Lab., Leiden, Suppl. No. 75b; Proc. Roy.Acad., Amsterdam 36(1933)153.
6) Fisher, M.E., Reports on Progr. in Phys. XXX(1967)615.
7) Gorter, C.J., Commun. Kamerlingh Onnes Lab., Leiden, Suppl. No. 124c; Physica 34(1967)220.
8) Erdös, P., J. Phys.Chem.Solids 27(1966)1705.
9) Moriya, T., Phys.Rev. 120(1960)91.
10) Dzyaloshinsky, I., Soviet Physics JETP 6(1958)1130; J.Phys.Chem.Solids 4 (1958)241.
11) Varret, F. and Hartmann-Boutron, F., Ann.Phys. 3(1968)157.
12) Elliot, R.J. and Thorpe, M.F., J.Appl.Phys. 39(1968)802.
13) Weiss, P., J. de Phys. 6(1907)667.
14) Domb, C. and Miedema, A.R., Progr. Low Temp. Phys. IV(1964)296.
15) Van Vleck, J.H., J.Chem.Phys. 5(1937)320.
16) Waller, I., Z.Phys. 104(1937)132.
17) Daniels, J.M., Proc.Phys.Soc. 66(1953)673.

18) Pryce, M.H.L. and Stevens, K.W.H., Proc.Phys.Soc. 63(1950)37.
19) Koloskova, N.G. and Kopvillem, U.Kh., Soviet Phys.Sol.State 2(1960)1243.
20) Gorter, C.J., Paramagnetic Relaxation, Elsevier 1947.
21) Caspers, W.J., Commun. Kamerlingh Onnes Lab., Leiden, Suppl. No. 118b; Physica 26(1960)798.
22) De Boo, N., private communication.
23) Zimmerman, N.J., private communication.
24) Onsager, L., Phys.Rev. 65(1944)117.
25) Opechowski, W., Physica 4(1937)181.
26) Bloch, F., Z.Physik 61(1930)206.
27) Dyson, F.J., Phys.Rev. 102(1956)1217,1230.
28) Levy, P.M., Phys.Rev. 170(1968)595.
29) Bienenstock, A., J.Appl.Phys. 37(1966)1459.
30) Gorter, C.J., Rev.Mod.Phys. 25(1953)277,332.
31) Bloch, F., Phys.Rev. 70(1946)460.
32) Kronig, R. de L., Physica 6(1939)33.
33) Van Vleck, J.H., Phys.Rev. 57(1940)426. 59(1941)724.
34) Waller, I., Z.Physik 79(1932)370.
35) Al'tshuler, S.A., Izv.Akad.Nauk. SSSR, 20(1956)1207.
36) Kittel, C., Phys.Rev. 104(1956)1807.

Chapter II

EXPERIMENTAL ARRANGEMENTS

1. Apparatus

The apparatus which was used for the measurements reported in this thesis is a standard device in the adiabatic demagnetization group in the laboratory and has already been described several times[1,2,3]). Only the relevant parts will be presented. In fig. 1 the all-glass apparatus is shown schematically. The arrangement shown was in particular used for the magnetic and caloric measurements on cerium magnesium nitrate (see chapter III). In the figure the susceptibility coils which were located around the sample (C) on the outer glass tube, which is immersed in liquid helium, are not shown. The susceptibility, χ, of the sample was measured, using a

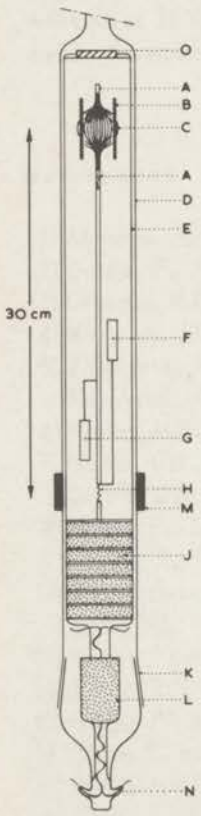

Fig. 1. The apparatus.

A: copper bundle.
B: perspex plates.
C: CeMgN sphere.
D: high vacuum glass tube.
E: glass thermal shield.
F: heater.
G: carbon resistor.
H: thermal switch.
J: cooling salt.
K: glass ground joint.
L: guard cylinder.
M: superconducting coil.
N: Pt-glass seals.
O: capacitor of 120 pF.

Not shown in the figure are the susceptibility coils at the sample (C).

Hartshorn mutual inductance bridge. The real part, χ', and the imaginary part, χ'', were measured as a function of temperature at a frequency of 260 Hz. When χ'' was considerable such as for instance at the approaching of the magnetic transition point of a sample, the static susceptibility was measured ballistically, using a galvanometer. The glass ground joint (K) was high-vacuum tight using a silicone grease between the ground surfaces. At the lowest part of the apparatus four Pt-to-glass seals (N) were made, providing electrical leads into the inner apparatus. The leads from the Pt seals going into the inner apparatus were made of manganin wire of 0.1 mm diameter in order to minimize the heat leak from the helium bath to the inner system. The manganin wires were spiraled through the guard salt (L) in order to further suppress the heat leak. The cooling salt (J) consisted of circular slabs of Cr-K-alum single crystal of 5 mm thickness which were rigidly clamped between brass plates with Apiezon N grease and were tightly screwed on a copper rod. The lower end of this copper rod was thermally connected to coil foils on the glass thermal shield (E), which could be kept at a temperature of approximately 0.15 K, reducing the totally observed "natural" heat leak to approximately 0.2 erg/s typically. The upper end of the rod was connected to a thermal switch (H) through which the sample and metal system could be cooled down to temperatures of about 0.02 K. The thermal switch consisted of a few (usually 3) threads of pure lead or tin of 0.15 mm diameter and 1 cm length. The heat switch could be brought in the normal, heat conducting state by a magnetic field of about 800 and 300 Oe for a lead and tin switch respectively. These fields were supplied by a small superconducting coil of niobium wire with a diameter of 0.05 mm (M). The coil was mounted on the high vacuum glass tube; the maximum coil current required for activating a Pb switch was about 2.5 A. This current was led through a string of four copper wires of 0.2 mm diameter, causing a negligible loss of liquid helium by forced evaporation due to Joule heating in the leads. The choice of a Pb or Sn heat switch depends on the measurements one wants to make in a certain temperature range. A specific-heat measurement at relatively high temperatures, i.e. $T > 0.3$ K, requires a Pb switch. The heat conduction to the demagnetized cooling salt of Pb in the superconducting state is smaller than for Sn in the high-temperature range, resulting in a smaller negative heat leak. A measurement in which the sample has to be cooled down to the lowest possible temperature requires a tin switch, because the magnetic field required to disturb the superconductivity is lower than for Pb. This is favourable when switching off the niobium coil, causing less heat input in the thermally isolated measuring system of sample, heater, thermometer plus metal connections.

The samples consisted in most cases of single crystals shaped into flat plates, varying in weight between approximately 0.5 and 3 g. The crystals were mounted between brass plates with Apiezon N grease in order to establish thermal contact and were mounted in the inner apparatus by means of thin cotton threads which could be firmly attached to the glass thermal shield (E). Copper rods of 1.5 mm diameter

were silver-soldered to these brass plates and connected the sample to the heater, thermometer and to the thermal switch. Interchanging the samples required disconnection of only three soft-soldered joints while leaving the sample between the brass plates. Care was taken to prevent soft soldered joints from being very near to the susceptibility coils. Otherwise anomalies were observed in the susceptibility versus temperature relation due to the superconducting transitions in the soft solder between approximately 4.2 and 2 K.

Heat could be applied electrically to the sample with the aid of two of the leads through the ground joint. The heater consisted of a wire of Pt-W alloy with a diameter of 0.025 mm, wound on a copper rod of 1.5 mm diameter. The resistance of the heater amounted to 1865 Ω at liquid-helium temperatures, which was very high compared to the resistance of the manganin leads to the heater which was about 20 Ω.

Apart from the sample plus metal plates, heater and connections, the standard set-up of the inner apparatus included a carbon resistor serving as a thermometer through its known resistance versus temperature relation (section 2 of this chapter). The total heat capacity of the metal system above the thermal switch amounted to approximately 1500 T erg/K. This value appeared to be a negligible quantity in most cases, compared to the heat capacity of the samples at temperatures below about 0.7 K.

2. Carbon resistance thermometry

2.1. Introduction

As a thermometer below 1 K the susceptibility of a paramagnetic salt is widely used. The most suitable substance for this purpose appears to be $Ce_2Mg_3(NO_3)_{12}\cdot 24H_2O$ which follows Curie's law, $\chi = C/T$, down to about 6 mK[4,5] when the appropriate demagnetizing correction to the magnetic temperature is applied (see chapter III). However, when a magnetic field is applied to the sample, as was done in most of the measurements described in this thesis, the susceptibility readings of the cerium magnesium nitrate thermometer are highly influenced by such a magnetic field. Often large and uncertain corrections to the magnetic temperature are required in order to obtain the thermodynamic temperature. Therefore a carbon resistor was used as a thermometer since the temperature versus resistance relation is only slightly field dependent (see section 2.5). Because the resistor was mounted approximately 25 cm below the sample (fig. 1) and the center of the magnetic field, the field at the resistor amounted to about 10% of the maximum field value. Hence no corrections to the temperatures obtained from the resistor were required.

Carbon resistors are favourable for use as low-temperature thermometers also because of their high thermometric sensitivity, small physical size, low heat capacity and their fast response to temperature changes. Carbon film resistors and Allen-Bradley radio resistors are very useful down to 1 K but become less useful at much

lower temperatures because their high resistance prevents accurate measurements. Dupré et al.[6] have been able to use carbon film resistors down to 0.2 K. Clement et al.[7] have shown that the Allen-Bradley resistors have 0.2% irreproducibility at liquid-helium temperatures after warming to room temperature. Nicol and Soller[8] showed that Speer resistors could be utilized down to 0.1 K. Black et al.[9] found that these resistors can be used down to 0.02 K and measured the field dependence down to 0.3 K. Symko[10] reported the use of a Speer 220Ω carbon resistor to a temperature of approximately 6×10^{-3} K, below which the thermometer was loosing thermal contact. So Speer resistors are usable down to very low temperatures and neither their resistance, R, nor dR/dT becomes prohibitively large. In order to get experience with carbon resistors, we carried out a number of auxiliary experiments in which the problem of providing thermal contact between thermometer and sample was adequately solved. In order to determine the properties of Speer resistors we have examined the reproducibility of the R–T curves after warming to room temperatures. Also the magnetic field dependence down to approximately 0.1 K in fields up to 6 kOe was examined.

2.2. Experimental method

In all the experiments described in the following chapters, a Speer carbon resistor of nominally 220 ohms, ½ watt was used as a thermometer. Speer denotes the standard grade of the resistors used, by the number 1002. From the resistors we used, the outer insulating layer was ground off, however, the carbon kernel was not affected. The resistor was tightly bound in the middle of a bundle of 250 copper wires of 0.07 mm diameter, running parallel to the resistor's axis. Apiezon N grease was used to improve thermal contact. The top of this bundle of wires was soldered to a copper wire of 1.0 mm diameter which connected the resistor to the sample. Once the bundle with the resistor was mounted it was not removed or remounted before recalibration, in order to preserve the reproducibility of the resistor. Heating of the resistor while soldering the copper wire to the brass plates between which the sample was mounted could change the resistance by sometimes as much as 20% at 0.1 K. The resistance of the carbon thermometer was measured by a Wheatstone bridge. Alternating current of 675 Hz was used in order to prevent the occurrence of thermovoltages and to minimize the recorded noise. In fig. 2 the measuring circuit is shown schematically. The output from the 675 Hz oscillator is led via an attenuator to the Wheatstone bridge. The signal from the bridge is amplified by selective amplifiers (quality factor of 35 and 35, 150, 500 respectively) and the signal is displayed on an oscilloscope and via a phase-sensitive detector on a recorder. Fig. 3 shows the scheme of the Wheatstone bridge. For the variable, known resistance, R_{var}, an E.S.I. five decade Dekabox was chosen (accuracy $1 : 10^4$). A set of variable capacitors, C_{var}, shunted this dekabox in order to compensate for the parasitic capacity

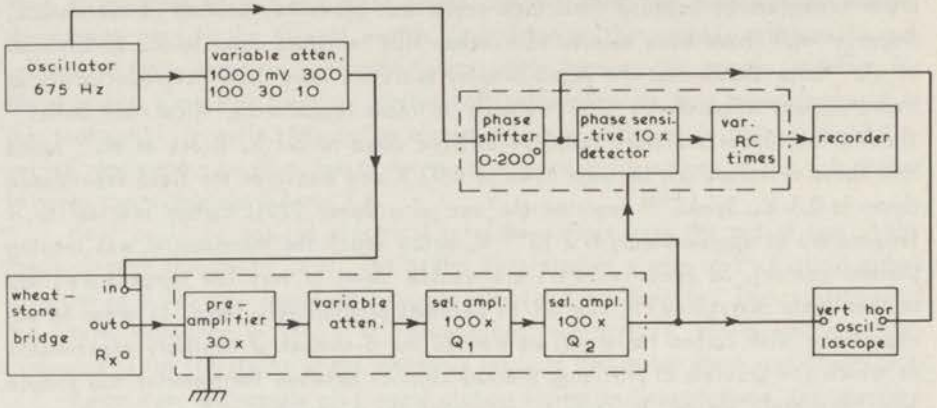

Fig. 2. Block diagram of the measuring circuit of the Wheatstone bridge. The quality factors Q_1 and Q_2 have values of respectively 35 and 35, 150, 500.

of the leads to the carbon resistor. The two resistances of 10 kΩ were bifilar wound metal Bobin resistors. The output of the oscillator was decoupled from the Wheatstone bridge by a 40 : 1 transformer. It followed from our measurements that special precautions had to be taken with regard to rf stray fields. In order to minimize the pick-up of such stray fields, the carbon resistor was shunted by a 120 pF ceramic capacitor which was mounted at the top of the inner apparatus (see fig. 1 (0)). The leads from the Wheatstone bridge to the Pt-glass seals in the liquid helium were coaxial. The pick-up in the remaining length of about 50 cm to the carbon resistor inside the high-vacuum space was minimized by twisting the leads. Below a temperature of approximately 0.2 K the bridge power level was maintained below 3×10^{-11} watt even although heating effects were not seen until 3×10^{-10} watt was applied. From the unbalanced bridge signal as displayed on a recorder, we calculated the resistance of the carbon thermometer using a calibrated relation between a change in the vari-

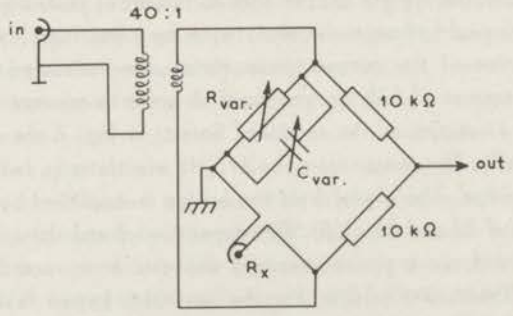

Fig. 3. Scheme of the Wheatstone bridge to measure the resistance of the carbon resistor, R_x. The maximum value of C_{var} amounted to 4000 pF.

able resistance, ΔR, and the change in unbalanced bridge voltage, ΔV. A definite change in the variable resistance yields, however, a strongly temperature (i.e. resistance) dependent unbalanced bridge voltage as can easily be calculated using the scheme of fig. 3. Therefore every measuring point was started and concluded with a ΔR versus ΔV calibration and the average was taken to calculate the relevant temperatures of the experimental point.

2.3. Temperature dependence

The temperature versus resistance relation of the carbon resistor was established using the susceptibility of cerium magnesium nitrate which salt follows Curie's law down to about 6 mK. The accuracy of the temperature determination is mainly limited by the accuracy with which the susceptibility versus absolute temperature relation can be established in the liquid-helium temperature region. In our experiments this error amounted to approximately 1%. At relatively high temperatures, i.e. $T > 0.1$ K, the R versus T relation can be obtained more accurately by using as a thermometer $CoCs_2(SO_4)_2.6H_2O$ which salt exhibits a Curie constant of about ten times that of cerium magnesium nitrate in the crystallographic K_3 direction. The susceptibility of the cobalt salt follows a Curie-Weiss law, $\chi/C = 1/(T - 0.03)$. A representative R versus T relation for a Speer carbon resistor of 220 ohm at room temperature is shown in fig. 4. We did not try to obtain a temperature calibration much below 25 mK ($1\ mK = 10^{-3}$ K) because all measurements were performed at higher temperatures. It is seen in fig. 4 that the ln R versus ln T curve does not significantly level off at the lowest temperatures. The occasional observation of such a leveling off which we found particularly when the investigations of carbon thermometry were

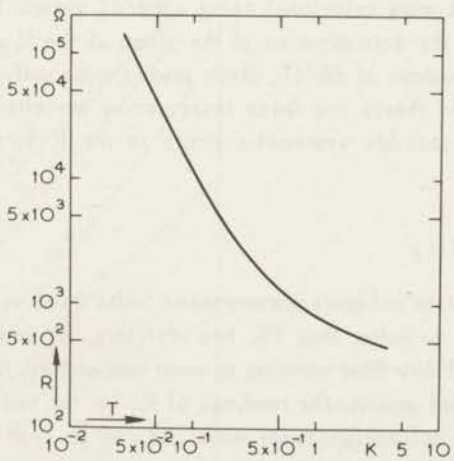

Fig. 4. Temperature calibration for a Speer carbon resistor of nominally 220 ohm, ½ watt, mounted as described in section 2.2.

started (see also ref. 11) must be ascribed to stray rf heating which warms up the resistor. This yields a lower resistance value than corresponds to the temperature of the specimen to which it is attached. The R versus T relation shown in fig. 4 was used during one year covering 50 cyclings to room temperature. Regularly the carbon resistor was recalibrated against the susceptibility of cerium magnesium nitrate, but these measurements yielded the same R versus T curve within the experimental error. Under favourable conditions, i.e. when the measuring system is well isolated thermally and the noise level is relatively low, the fractional temperature resolution of a Speer carbon resistor of 220 ohm nominally amounts to approximately 1×10^{-4} at relatively high temperatures and to 3×10^{-4} at $T = 0.1$ K. This is to be compared with the fractional temperature resolution of 5×10^{-4} for a cerium magnesium nitrate thermometer of 12 grams[3] mounted in susceptibility coils which are comparable with the coils of our apparatus (fig. 1). A higher fractional temperature resolution can be obtained by using a carbon resistor with a steeper dependence of R on T.

Carbon resistors are extremely useful to perform measurements on a relative temperature scale such as the determination of the shape of a specific-heat anomaly in the region of the critical temperature or the shift of the critical temperature when a magnetic field is applied to an antiferromagnetically ordered sample. Below about 0.1 K the use of a carbon resistor is also favourable especially when a magnetic field is applied. However, the R versus T calibration below 0.1 K is very sensitive to stray rf fields. Also the measured heat leak to the sample appeared to be about two times larger (i.e. ≈ 0.2 erg/s), at least in our apparatus, compared to an identical apparatus in which no carbon resistor was used.

All temperatures were deduced graphically from the measured resistances; small temperature differences were calculated using a dR/dT versus T relation. Although graphical methods for the determination of the slope of the R versus T curve lead to relative inaccurate values of dR/dT, these proved to be sufficient for the experiments described in this thesis and these inaccuracies are often small compared to the above mentioned possible systematic errors in the R versus T determination itself.

2.4. Reproducibility

As it is difficult to calibrate paramagnetic salts used as a thermometer in a small sized apparatus to better than 1%, two resistors, R_1 and R_2, were compared to check the reproducibility after warming to room temperature. In fig. 5 the quantity $(R_2 - R_1)/R_2$ is plotted against the readings of R_2 for the two successive days in which the temperature calibrations were made. As can be seen from this figure the greatest departures of the measured values from a smooth curve are approximately 5×10^{-3} over the whole measured temperature region from about 0.075 to 4.2 K, which departures may partly be due to lack of thermal equilibrium. From fig. 5 it

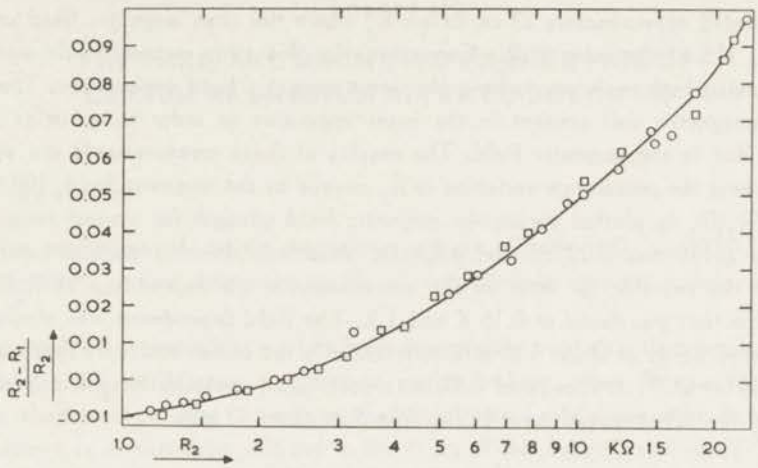

Fig. 5. Plot of the fractional difference $(R_2 - R_1)/R_2$ versus R_2 for two successive days.

seems reasonable to assert that the temperature characteristics are reproducible to within 0.3% in spite of repeatedly warming up to room temperature.

2.5. Field dependence

The field dependence of one of the two resistors, R_2, was measured by comparing its value in various magnetic fields with that of the second resistor, R_1, which

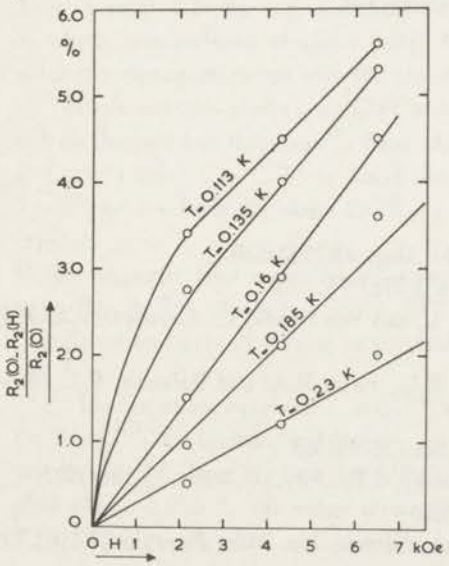

Fig. 6. Percentage decrease in R_2 as a function of the applied magnetic field for several temperatures. The quantity $R_2(H)$ is the value of R_2 measured in a field H.

was mounted approximately 23 cm below R_2 where the stray magnetic field amounted to about 11% of the value at R_2. Corrections for this stray magnetic field were made by assuming both resistors to have the same magnetic field dependence. There was no paramagnetic salt present in the inner apparatus in order to minimize heating effects due to the magnetic field. The results of these measurements are shown in fig. 6 where the percentage variation in R_2 caused by the magnetic field, $100\,(R_2(0) - R_2(H))/R_2(0)$, is plotted versus the magnetic field strength for several temperatures between 0.113 and 0.23 K. The magnetic field was directed perpendicular to the axis of the resistor for most of the measurements; no dependence of $R_2(H)$ upon field direction was found at 0.16 K and 1 K. The field dependence was also measured in large fields at about 1 K with substantially the same results as those obtained by Black et al.[9]. A change of 0.9% was seen when applying a field of 9 kOe. The slope of the ΔR versus H curve is flat from 9 to about 13 kOe.

2.6. Conclusion

The temperature characteristics of Speer carbon resistors have been found to be reproducible down to approximately 0.075 K after temperature cycling to room temperature to within 0.3%. This would cause an error of 5×10^{-4} K at 0.3 K and 2.5×10^{-4} K at 0.1 K. Below 0.075 K reproducibility was found within about 1% by comparing the carbon resistor with the susceptibility of CMN. When using a carbon resistor in order to obtain absolute temperatures care must be taken to prevent heating when soldering the carbon resistor to the connections with a sample; also the influence of stray rf fields can drastically change the R versus T relation, especially what the temperature region below 0.1 K is concerned.

References

1) De Klerk, D., thesis Leiden 1948.
2) Lubbers, J., thesis Leiden 1967.
3) Wielinga, R.F., thesis Leiden 1968.
4) Daniels, J.M. and Robinson, F.N.H., Phil.Mag. 44(1953)630.
5) Hudson, R.P. and Kaeser, R.S., Physics 3(1967)95.
6) Dupré, A., Van Itterbeek, A., Michiels, L. and Van Neste, L., Cryogenics 4(1964) 354.
7) Clement, J.R., Quinnell, E.H., Steele, M.C., Hein, R.A. and Dolecek, R.L., Rev. sci.Instr. 24(1953)545.
8) Nicol, J. and Soller, T., Bull.Am.phys.Soc. 2(1957)63.
9) Black, Jr., W.C., Roach, W.R. and Wheatley, J.C., Rev.sci.Instr. 35(1964)587.
10) Symko, O.G., Phys.Letters 25A (1967)385.
11) Edelstein, A.S. and Mess, K.W., Commun. Leiden, No. 344c; Physica 31(1965)1707.

Chapter III

THERMAL AND MAGNETIC PROPERTIES OF CERIUM MAGNESIUM NITRATE BELOW 1K

1. Introduction

The properties of cerium magnesium nitrate, $Ce_2Mg_3(NO_3)_{12}.24H_2O$ (called CMN hereafter) at low temperatures are of considerable interest mainly for three reasons:

a) its magnetic susceptibility, χ, has been extensively used as a thermometer in the centidegree and millidegree temperature region, where other thermometers have serious shortcomings. The assumption that χ follows Curie's law down to very low temperatures is in particular utilized in the study of the properties of liquid ^3He and is related to the assertion that ^3He is a Fermi liquid[1].

b) the magnetic interactions of the cerium ions are almost exclusively, if not entirely, due to magnetic dipolar coupling[2]. The question whether such a dipolar system exhibits a magnetic phase transition was raised many years ago[3]. Experimentally there are few ionic compounds in which dipolar interactions predominate strongly and which are also sufficiently simple. CMN is a favourable example since all Ce ions are magnetically equivalent and have a simple g tensor, while further the Ce ions are arranged in a simple Bravais lattice[4].

c) CMN was the first compound in which strong polarization of radioactive atomic nuclei (inserted as impurity ions at the Mg site in the crystal) was achieved[5,6,7,8]. This is related to the circumstance that CMN is magnetically a very dilute crystal in which temperatures of about 0.003 K can easily be obtained by straightforward adiabatic demagnetization with the aid of a moderate external magnetic field.

Experimental studies on CMN have been started by Cooke, Duffus and Wolf[2] and by Daniels and Robinson[9]. They showed for instance, that:

a) Curie's law, $\chi = C/T$, is valid above 0.006 K, which may be also stated as $T = T^{\circledast}$ for $T > 0.006$ K, where $C/T^{\circledast} \equiv \chi$ is the susceptibility of a spherically shaped crystal.

b) the magnetic heat capacity, c, at relatively high temperatures, can be expressed as $c/R = b/T^2$, where $b = 7.5 \times 10^{-6}$ K^2. This may be compared with the value calculated on basis of dipolar interactions, which amounts to $b = 6.8 \times 10^{-6}$ K^2, see ref. 2.

The relation between T and $T^{\circledast}$ has been studied later more extensively by De Klerk[10], by Carboni and Sapp[7], by Frankel, Shirley and Stone[8] and by Hudson and Kaeser[11]. They all find that CMN can be demagnetized to a temperature appreciably below 0.003 K, the value originally found by Daniels and Robinson, but their $T - T^{\circledast}$ relations show considerable differences. Further, susceptibility and heat-

capacity measurements of Wheatley et al.[1,12] on powders of CMN single crystals, pressed into a pill of cylindrical shape, gave a deviation from the $c/R = b/T^2$ relation and showed the approximate validity of Curie's law down to 0.002 K. Recent investigations on the specific heat of powdered CMN by Abraham and Eckstein[13], however, gave rise to some doubt on the temperature scale of such a cylindrically shaped powder sample.

The above mentioned experiments did not show the occurrence of a phase transition in spite of the fact that at the lowest temperatures obtained, a considerable fraction (62.5%) of the available entropy of R ln 2 per gramion CMN had been removed from the crystal.

It was the purpose of the present investigation to obtain still lower values of the entropy, hence of the temperature, in order to establish whether a phase transition occurs or whether this dipolar system looses practically all its entropy in short-range ordering. The method of obtaining lower temperatures simply consists of demagnetizing a CMN single crystal from a lower initial temperature. The detection of a phase transition is based on the measurement of a maximum in the susceptibility versus temperature and of a maximum in the heat-capacity versus temperature curve. Our experimental results indicate that CMN becomes ferromagnetic at $T_c = 0.0019$ (± 0.0001) K.

2. Experimental method

The experiments were performed on two specimens of CMN viz. a spherically shaped sample (weight 3.24 g, demagnetizing factor $N = 4\pi/3 = 4.19$) and an ellipsoidal sample (weight 0.50 g, demagnetizing factor $N = 0.54 \pm 0.03$).

The spherical sample consisted of a stack of four flat single crystals glued together with araldite and ground into a sphere of 14.5 mm diameter. The ellipsoid was ground from a single crystal. The demagnetizing factor of the ellipsoid was calculated from its geometry, the ratio of the short principal axis b, and the long principal axis, a, being $b/a = 0.159$. The apparatus used in these experiments is shown schematically in fig. 1 of chapter II. The most important difference of our experiments with those reported by Daniels and Robinson and by Hudson and Kaeser, is the use of a demagnetized Cr-K-alum cooling salt, which permitted us to demagnetize the CMN sample from a lower initial temperature, thus from a lower initial entropy. Most of the experiments were performed on the spherically shaped sample. The sphere was rigidly clamped between two perspex plates having circular holes and held with the aid of cotton threads. The CMN sphere was wrapped in a bundle of 100 copper wires and greased with Apiezon N in order to provide thermal contact with the Cr-K-alum cooling salt via the heat switch, which consisted of three Sn wires of 1 cm length and 0.15 mm diameter. Just above the heat switch the heater was connected to the copper bundle. Ten wires from the copper bundle were connect-

ed thermally to a Speer carbon resistor. All soldered joints were made of pure tin. For the experiments on the CMN ellipsoid the same apparatus as for the sphere was used. The samples were mounted with the crystallographic c axis horizontal. The precise orientation of the c axis in the horizontal plane ($g_{\perp} = 1.84$, $g_{//} \approx 0.025$) could be determined at about 0.1 K in a magnetic field of about 1000 Oe, by measuring the susceptibility as a function of the direction of the magnetic field. The susceptibility shows a pronounced maximum when the magnetic field is parallel to the c axis. The position of the c axis could be established with an accuracy of 0.5°.

2.1. Susceptibility-entropy(χ-S) measurements

Susceptibility measurements were performed on the CMN sphere and ellipsoid as a function of the entropy. The susceptibility was measured with a Hartshorn mutual inductance bridge, operated at a measuring frequency of 260 Hz. The signal of the bridge was displayed on a recorder by means of a lock-in detector. The sample was cooled in a magnetic field of 2795 Oe (applied perpendicular to the c axis) via the heat-conducting tin switch by the demagnetized cooling salt to the desired initial temperature T_i. After the heat switch was made superconducting, this temperature was measured with the carbon resistor. The CMN sample was adiabatically demagnetized from the known initial magnetic field H_i and temperature T_i. From H_i and T_i the initial entropy S_i/R could be calculated. The susceptibility in zero external field was recorded within five seconds after demagnetization, and immediately thereafter the field was returned to its initial value H_i, whereupon the final temperature, T_f, was measured. From this procedure, i.e. completing the magnetic field cycle, an irreversible entropy gain, $\Delta S/R$, occurred, i.e. $S_f/R > S_i/R$ where S_f/R can be calculated from H_i and T_f. In analyzing the χ-S measurements, the susceptibility was plotted versus the initial entropy, which was corrected for this entropy gain. This correction was assumed to be approximately half the above mentioned entropy gain $\Delta S/R = S_f/R - S_i/R$. At the lowest initial entropy of $S_i/R = 0.02$, the correction is relatively large, namely $\Delta S/2R = 0.04$, but it decreases rapidly to 0.006 at $S_i/R = 0.6$. In fig. 1 $\Delta S/R$ for the CMN sphere is plotted versus the initial entropy S_i/R. With the aid of the measured S–T relation, the above mentioned entropy corrections can be transformed into amounts of heat with the relation $\Delta Q = T\Delta S$. At $S_i/R = 0.1$ one can calculate $\Delta Q = 33$ ergs and at $S_i/R = 0.4$, $\Delta Q = 16$ ergs, which value stays rather constant above this entropy. The calculated values of ΔQ refer to the lowest temperature obtained in demagnetization, i.e. the true ΔQ, involved in covering an appreciable temperature variation may be even larger. The heat capacity of the metal system was measured in a separate experiment and amounted to $c_{met} = \alpha T$ erg/K, where $\alpha = 1600$ erg/K^2 ($c_{met}/R = 0.46 \times 10^{-3}$ T). During the demagnetization of the sample, the temperature of the metal system as observed from the resistor, at first decreased with the temperature of the CMN, but it did not fall below 0.04 K. At low

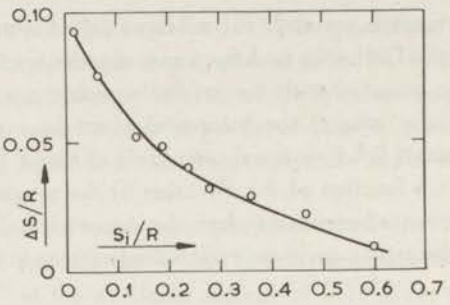

Fig. 1. The irreversible entropy gain, $\Delta S/R$, plotted vs. the initial entropy, S_i/R, as measured for the CMN sphere.

fields the temperature increased and reached a temperature of about 0.08 K, this temperature being almost independent of S_i/R as was observed from various demagnetizations. In zero field the temperature of the metal decreased rapidly, until H was increased again to H_i. From the known specific heat of the metal system, an electronic heat content of about 5.1 ergs at T = 0.08 K was calculated. Comparison of this relatively small heat content to the above calculated large ΔQ, which follows from the observed irreversible entropy gain, shows that the latter cannot be accounted for by the heat capacity of the metal system in thermal contact with the demagnetized CMN. We therefore assume that the observed irreversible entropy gain is largely due to joule heating in the metal system and to transitions in the soldered joints from the normal to the superconducting state and vice versa. In order to determine the χ-S curve for entropies higher than S/R = 0.5, the sample was demagnetized from a transversal magnetic field of 255 Oe. Using a field of 2800 Oe for this entropy region gave a high initial temperature, resulting in a considerable heat leak and a considerable energy content of the metal system.

2.2. Entropy-heat content (S-Q) measurements

After demagnetization from known initial conditions of magnetic field, H_i, and temperature T_i (hence from known initial entropy S_i/R) a known heat current, dQ/dt, was applied to the sample by the heater and the time required to warm up to a fixed temperature, T_{ref} ($\approx$ 0.04 K), was measured. Heating periods ranged from 100 to 32 seconds. The S–Q curve was measured in an entropy range of $S_i/R = 0.016$ to $S_i/R = 0.64$. The entropy of the lattice, S_l, was neglected ($S_l = 0.2 \times 10^{-3}$ R at T = 1 K[14]). In order to check whether a reference temperature of about 0.04 K was high enough to guarantee a uniform temperature of the sample, our results of the S–Q measurements were verified for a reference temperature of about 0.09 K. It appeared that when using the same heating rate, the results of all heat content measurements were augmented with approximately the same amount of heat; so the choice of a higher reference temperature did not affect our S–T relation, as can easily be understood.

3. Results

3.1. χ-S measurements

The results of the susceptibility versus entropy measurements on the CMN sphere are presented in fig. 2. The measured susceptibility divided by the Curie constant, $\chi/C \equiv 1/T^{\Theta}$, is plotted versus the corrected entropy $\bar{S}/R \equiv (S_i + S_f)/2R$. As can be seen from fig. 2 the real part of the a.c. susceptibility, χ', reaches a maximum value of $1/T^{\Theta} = 276\ K^{-1}$ at $\bar{S}/R = 0.38$ and decreases slightly for lower entropies, while the imaginary part, χ'', increases. This is a familiar phenomenon at magnetic phase transitions and is usually related to relaxation effects e.g. due to domain switching. Hence we measured some susceptibility points ballistically, two of which are indicated in fig. 2. The results show that for $\bar{S}/R < 0.1$ the d.c. susceptibility $1/T^{\Theta}_{d.c.}$ equals the maximum in the a.c. susceptibility viz. $1/T^{\Theta}_{d.c.} = 276\ K^{-1}$. From this we conclude that the susceptibility reaches a maximum value

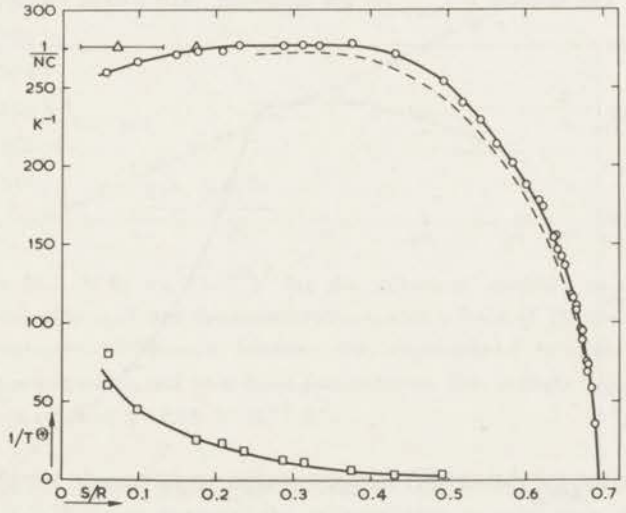

Fig. 2. Susceptibility of the CMN sphere, plotted as $1/T^{\Theta} = \chi/C$ vs. mean entropy $\bar{S}/R = (S_i + S_f)/2R$.

O: a.c. results, χ'.

Δ: d.c. results. Only two measured points are given. The entropy gain is indicated for one point.

□: a.c. results, $10\chi''$.

- - - - : results of Hudson and Kaeser.

The maximum susceptibility of a ferromagnetic spherical sample, magnetized in domains, $(\chi/C)_{max} = 1/NC$, is indicated on the vertical scale.

$1/T^{\circledast} = 276\ K^{-1}$, which is constant within the measuring accuracy for entropies below $\bar{S}/R = 0.38$. The experimental error in the susceptibility data is about 2% which is determined by the uncertainty in the calibration of χ against the helium vapour pressure between 4.2 and 0.9 K. Similar measurements were performed on the CMN ellipsoid, the results of which are shown in fig. 3. The dashed part of fig. 3 is drawn such as to give the best fit to the Curie-Weiss law (see fig. 11) at temperatures above 6 mK; (1mK $\equiv 10^{-3}$ K). For the ellipsoidal specimen $1/T^{*} \equiv \chi/C$ reaches a maximum value of $2170\ K^{-1}$ at an entropy of $\bar{S}/R \approx 0.38$. As can be seen from fig. 3 the irreversible entropy gain is larger than for the sphere, which is due to the smaller mass of the ellipsoid. The maximum susceptibility, χ_{max}, may be compared for both specimens to the value $1/N$, where N is the demagnetizing factor. On the basis of the calculated Curie constant per cm^3 ($= 8.73 \times 10^{-4}$ e.m.u/cm^3), using Zalkin's[4] value of 2.10 g/cm^3 for the density of CMN, we then find $1/T^{\circledast}_{max} = 1/NC = 274\ K^{-1}$ for the sphere and $1/T^{*}_{max} = 1/NC = (2122 \pm 100)\ K^{-1}$ for the ellipsoid, which agrees nicely with the experimental results of $276\ K^{-1}$ and $2170\ K^{-1}$ respectively. The error in $1/T^{*}_{max}$ for the ellipsoid, indicated in fig. 3, is determined

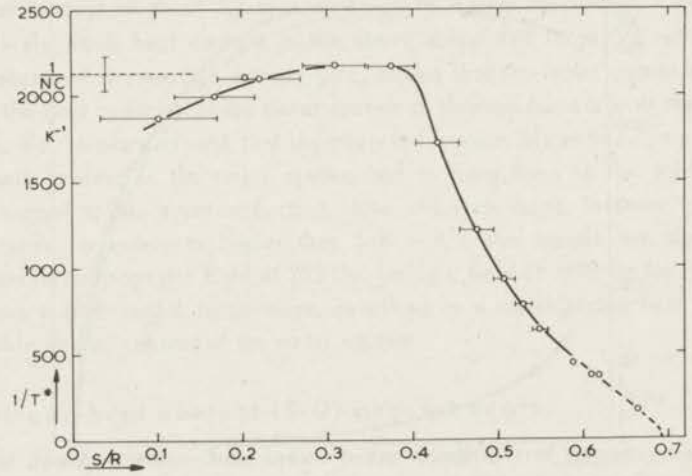

Fig. 3. $1/T^{*}$ for the ellipsoidal sample as a function of $\bar{S}/R$. The uncertainties in the entropy are indicated by horizontal bars.
I : uncertainty in 1/NC, due to a possible error in N.

by the error in the demagnetizing factor. This behaviour of the susceptibility of both samples is that of a ferromagnetic substance magnetized in domains, in which the magnetization of the specimen will be such that within the specimen the applied and demagnetizing fields cancel; so the above mentioned experimental results strongly suggest that CMN orders in ferromagnetic domains below an entropy of $S/R = 0.38$. No accurate χ data at high entropy, viz. $S/R > 0.67$, could be obtained because of a relatively large negative heat leak through the heat switch to the cooling salt. In

fig. 2 also the results of Hudson and Kaeser[11] have been plotted and compared to our results of the CMN sphere. As can be seen from this figure, our results differ systematically from their data. Our results obtained for the CMN ellipsoid are less reliable than those for the sphere because of the relatively larger entropy gain during the magnetic field variations.

At relatively high temperatures, viz. $T > 0.006$ K, where the relation $T = T^{\circledast}$ approximately holds, the temperature dependence of the entropy is described by the formula $\ln 2 - S/R = b/2T^2$. In fig. 4 we plotted the results of the low-field magnetizations and demagnetizations of the sphere ($H = 255$ Oe) as $\ln 2 - S/R$ versus $(1/T^{\circledast})^2$. The result is straight line with a slope of $b/2 = 2.37 \times 10^{-6}$ K^2.

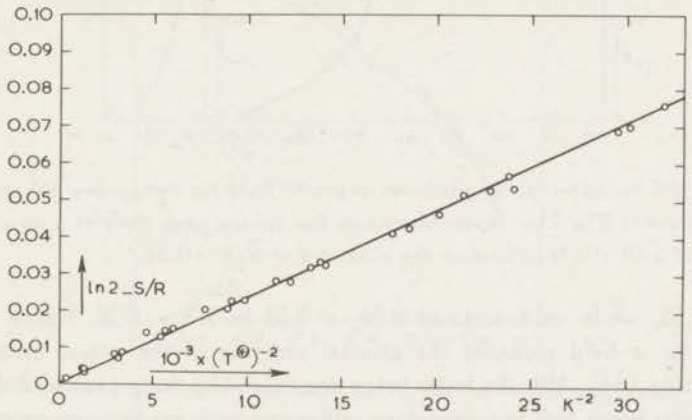

Fig. 4. $(\ln 2 - S/R)$ vs. $(1/T^{\circledast})^2$ for the spherical sample as obtained from magnetizations and demagnetizations with a field of 255 Oe. There is no systematic difference between the experimental data, obtained from magnetizations and from demagnetizations. The straight line corresponds to a value of $b = 4.75 \times 10^{-6}$ K^2.

As a further support of the assumption that CMN orders ferromagnetically below an entropy of 0.38 R, we measured the susceptibility as a function of a longitudinal external magnetic field. The results obtained for the sphere and the ellipsoid are presented in fig. 5. The measurements on the sphere were performed at an entropy of $\bar{S}/R = 0.14$ and on the ellipsoid at an entropy of $\bar{S}/R = 0.36$. Below $\bar{S}/R = 0.38$ the volume susceptibility remains initially at the constant value of $1/N$ as a function of the parallel field. When the field is further increased it is found that χ decreases, which corresponds to the approach of the saturation magnetization. By integrating χ versus the magnetic field one can calculate the magnetization. We find for the CMN sphere $M/M_o = 0.88$, where M_o is the saturation magnetization at zero temperature. This can be compared with the value $M/M_o = 0.92$, calculated for an ideal paramagnet at an entropy of $S/R = 0.14$. The measurements on the ellipsoid yield

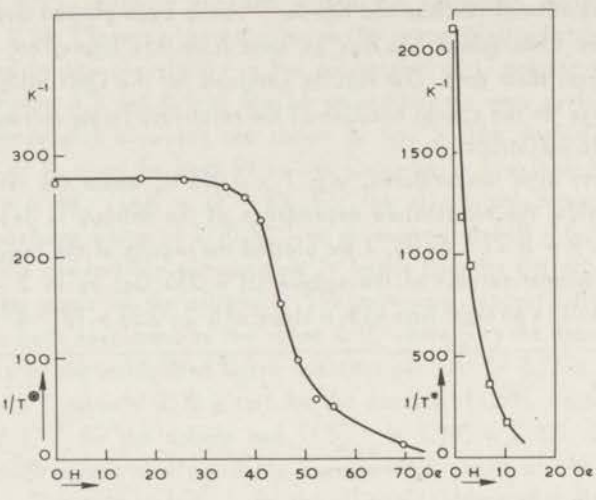

Fig. 5. χ/C vs. external longitudinal magnetic field for the sphere (○) and the ellipsoid (□). The measurements on the sphere were done at a mean entropy of $\bar{S}/R = 0.14$; those on the ellipsoid at $\bar{S}/R = 0.36$.

$M/M_o = 0.53$, while we calculated $M/M_o = 0.54$ at $S/R = 0.36$. Hence there is no evidence for a field opposing the parallel ordering of the spins, other than the demagnetizing field $-NM$, the latter being determined by the geometry of the sample. These results agree with ferromagnetism rather than with antiferromagnetism.

3.2. S-Q measurements

The relation between entropy and heat content was measured on the CMN sphere only. From a known initial magnetic field H_i of 2795 Oe and initial temperature T_i, hence from a known initial entropy S_i/R, the CMN sphere was demagnetized.

On the measured heat content two corrections were applied:

1. the "natural" heat leak of about 0.25 erg/s, due to radiation, vibrations and heat conduction through the leads with which the sample was mounted. This heat leak was measured regularly during a measuring day by comparing the drift in susceptibility, $1/T^*$, due to the "natural" heat leak with the drift due to a known applied heat flow plus the "natural" heat leak. The "natural" heat leak was found to be constant within 10% during a day.
2. the heat leak from the cooling salt through the tin switch. After each measured point of the S–Q curve the temperature of the cooling salt was measured and with the known measured heat conduction of the heat switch, the heat leak from the cooling salt could be calculated. In heating the sample to the reference temperature a heat flow of 7.5 erg/s was used, which was approximately 30 times the natural heat

leak. The results of the S–Q measurements are given in fig. 6. When the initial entropy values are corrected for irreversible heating (as discussed above) according to fig. 1, the dash-dotted curve in fig. 6 is obtained. However, when measuring the S–Q curve, unlike in the χ-S experiments the magnetic field is only reduced to zero and not returned to H_i. Therefore the applied correction to the initial entropy will be an overestimate of the "true" entropy gain during demagnetization.

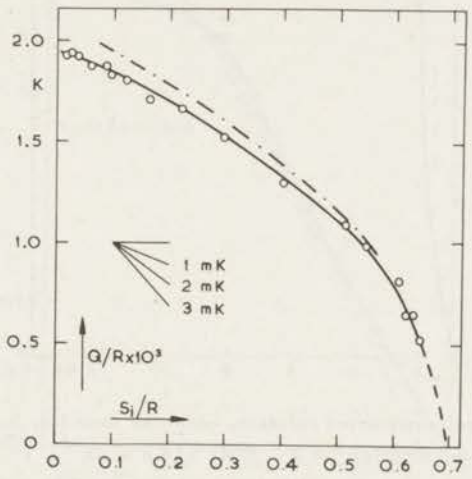

Fig. 6. The measured heat content per mole, Q/R, vs. the initial entropy S_i/R, for the CMN sphere. The dash-dotted curve corresponds to the maximum possible correction of S_i/R for irreversible entropy gain, according to fig. 1. The corresponding absolute temperatures are indicated in the figure.

Finally, differentiation of the curves in fig. 6 gives the relation between the absolute temperature, $T = -(\Delta Q/\Delta S)$, and the entropy S. The result of this differentiation is given in fig. 7. The curve shown is an average curve and the end points of the error bars in temperature, indicated in fig. 7 at low entropies, are obtained from the two curves in fig. 6 and therefore represent limiting values for the absolute temperature. Temperatures up to 8 mK could be obtained from the S–Q curve. Above this temperature we could not reliably establish an S–Q relation because of the negative heat leak through the tin switch. From fig. 7 the lowest temperature we reached after demagnetization appears to be $T_{min} = (1.0 \pm 0.3)$ mK. The descent in the entropy as a function of the absolute temperature is steepest below an entropy of $S/R \approx 0.4$, corresponding to a maximum in the specific heat. In fig. 7 the results of Hudson and Kaeser are also presented. Although their measurements give an S–T curve roughly analogous to our results, there is clearly a distinct difference over the whole measured temperature range. From this figure it can also be seen that at high temperatures the experimental points obtained from our S–Q curve, can smoothly

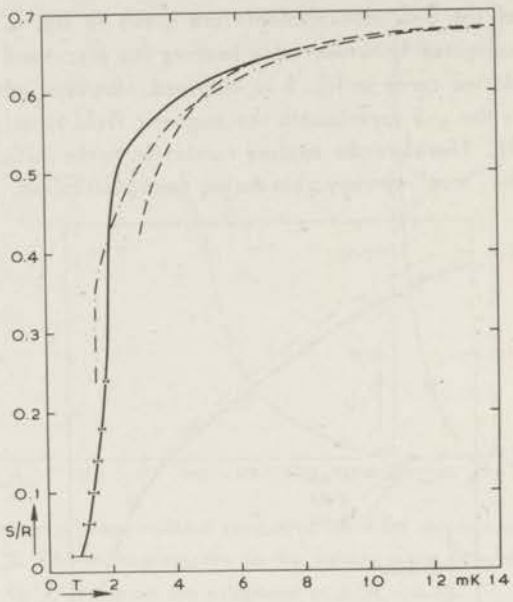

Fig. 7. Entropy-absolute temperature relation, obtained from fig. 6. The dashed curve corresponds to the relation $(\ln 2 - S/R) = (4.8 \times 10^{-6})/T^2$. The dash-dotted curve represents the results of Hudson and Kaeser. The indicated errors in the temperature at low entropies correspond to the two curves, shown in fig. 6.

be jointed to the relation $\ln 2 - S/R = b/2T^2$, where $b = 4.8 \times 10^{-6}$ K^2. From fig. 7 one can derive, by differentiating to the temperature, the specific heat versus temperature curve, according to the relation $c/R = T\, d(S/R)/dT$. The result of this differentiation is shown in fig. 8. As can be seen from this figure there is a distinct maximum at a temperature of $T = (1.9 \pm 0.1)$mK, corresponding to an entropy of about 0.38 R, which may be related to the ferromagnetic transition point T_c of CMN. It must be emphasized, however, that at the lowest temperatures the curve for c/R is rather inaccurate since the double differentiation of the S–Q relation introduces a considerable uncertainty.

The specific heat of the sample was also measured in the conventional calorimetric way, i.e. by applying a known amount of heat to the sample and determining the corresponding temperature difference by observing the temperature drift before and after heating. These measurements were performed on the CMN sphere at temperatures higher than $T^{\Theta} = 6$ mK, where we made the assumption that $T^{\Theta} = T$. The result of these "high" temperature measurements are also shown in fig. 8. It may be noticed that there is a deviation from a T^{-2} law at temperatures higher than 0.02 K, which qualitatively agrees with the results of Hudson and Kaeser[11]. In the temperature range from 8 to 20 mK the specific heat can be described by the relation $c/R = b/T^2$

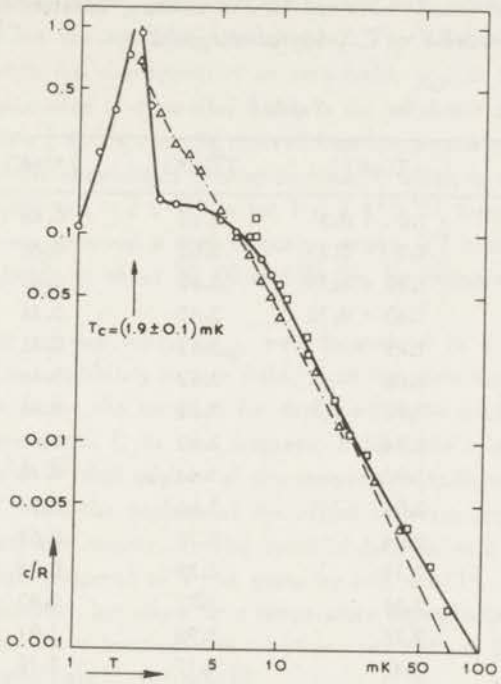

Fig. 8. Specific heat, divided by R, vs. temperature of the CMN sphere.
○: obtained by differentiation from fig. 7
□: directly measured specific heat data
Δ: results, reported by Wheatley et al.
The dashed curve represents a T^{-2} relation.

where $b = 5.2 \times 10^{-6}$ K^2. Integration of the c versus T curve yields the energy, involved in magnetic ordering in CMN. This energy yield amounts to $E/R = -2.2$mK. From fig. 6 an energy gain of −1.9 mK below 0.04 K can directly be obtained. Augmenting this value with about −0.2 mK for the energy content above 0.04 K yields practically the same E/R value as obtained from the specific heat curve. In fig. 8 results of Wheatley et al.[1,12] on the specific heat of powdered CMN are also shown. From the latter measurements a value for b of 4.2×10^{-6} K^2 is obtained, which is more than 25% lower than the value reported by Hudson and Kaeser[11]. Similar experiments were performed on the CMN ellipsoid. After having applied a demagnetizing correction of 3.18 mK to the ellipsoid's magnetic temperature, the results of the specific-heat measurements were in reasonable agreement with those obtained for the sphere. The coefficient of the specific heat in the T^{-2} range was $b = 5.8 \times 10^{-6}$ K^2, the experimental error being ± 10%.

Table I gives the results obtained for the entropy, absolute temperature, and $T^{\circledast} \equiv C/\chi$ for the sphere and $T^{*} \equiv C/\chi$ for the ellipsoid.

Table I

S/R	T(mK)	$T^{\circledast}$(mK)	T*(mK)
0.02	1.0 ± 0.3	3.62	0.46
0.05	1.2 ± 0.2	3.62	0.46
0.10	1.42 ± 0.15	3.62	0.46
0.15	1.60 ± 0.10	3.62	0.46
0.20	1.75	3.62	0.46
0.25	1.86	3.62	0.46
0.30	1.92	3.62	0.46
0.35	1.94	3.62	0.46
0.40	1.97	3.64	0.48
0.42	2.00	3.66	0.54
0.44	2.05	3.71	0.63
0.46	2.11	3.79	0.74
0.48	2.16	3.87	0.82
0.50	2.25	3.98	1.01
0.52	2.45	4.17	1.19
0.54	2.75	4.35	1.39
0.56	3.20	4.61	1.64
0.58	3.75	4.93	1.92
0.60	4.40	5.32	2.31
0.61	4.80	5.58	2.56
0.62	5.30	5.88	2.84
0.63	6.00	6.21	(3.12)
0.64	6.75	6.76	(3.60)
0.65	7.50	7.47	(4.31)

3.3. χ measurements in low magnetic fields

3.3.1. Method

In order to determine a more accurate value of b, defined by $b = cT^2/R$, where c is the heat capacity in zero magnetic field, the following experiments were carried out.

a. Adiabatic magnetizations and demagnetizations with a magnetic field perpendicular to the direction of the susceptibility measurement. The susceptibility in the presence of a transversal field, χ_H, was compared with the susceptibility in zero field, χ_O, at the same entropy.

b. Adiabatic magnetizations and demagnetizations with a magnetic field parallel to the direction of the susceptibility measurement. The adiabatic susceptibility, χ_{ad}, was compared with the susceptibility in zero field, χ_O, at the same entropy. The susceptibility, measured in a parallel field, is the adiabatic susceptibility, χ_{ad}, for temperatures below 2 K. This can be derived from our measuring frequency $\nu = 260$ Hz and the value of the spin-lattice relaxation time, τ, which in a small magnetic field (< 100 Oe) amounts to $\tau > 2 \times 10^{-3}$ s for $T < 2$ K[15,16], hence $\omega\tau > 3$. In agreement with this value we observed a step in our χ versus 1/T plot, measured in longitudinal magnetic fields of about 30, 60 and 90 Oe, for temperatures between 1.9 and 2.2 K.

c. The adiabatic susceptibility, χ_{ad}, was determined in a longitudinal field and compared to the susceptibility in zero field, χ_O at the same temperature.

In order to derive the formulae for analyzing these experiments, the following assumptions were made: 1. In zero magnetic field Curie's law is valid, $\chi = C/T$. It can be shown[17,18] that neglect of the temperature independent susceptibility of $\chi/C = 0.07\ K^{-1}$ and the neglect of the effect of paramagnetic saturation do not appreciably affect our results. 2. The specific heat in zero magnetic field and at temperatures, high compared to T_c is given by $c/R = b/T^2$, in which we assume b to be field independent, but allow for a temperature dependence. From thermodynamic reasoning and the above mentioned assumptions one obtains for the specific heat in a constant magnetic field H, see ref. 19

$$c_H = \frac{b' + CH^2}{T^2}$$

where $b' = bR$. The entropy of the spin ½ system in a magnetic field H and at temperature T is given by

$$S = R \ln 2 - \int_T^\infty \frac{b'}{T^3}\, dT - \tfrac{1}{2}\frac{CH^2}{T^2}. \qquad (1)$$

For an adiabatic demagnetization from a field H and temperature T_H to zero field and temperature T_O, we find

$$\int_{T_O}^{T_H} \frac{b'}{T^3}\, dT = \tfrac{1}{2}\frac{CH^2}{T_H^2}. \qquad (2)$$

When b is temperature independent, we derive from eq. (2)

$$\frac{T_O^2}{T_H^2} = \frac{b'}{b' + CH^2}\ . \qquad (3)$$

Since magnetic saturation may be neglected, the susceptibility is not influenced by a perpendicular magnetic field, hence $T_H = C/\chi_H$ and $T_O = C/\chi_O$. So, with the aid of relation (3) we derive for the experiments mentioned at a) the formula

$$\frac{b'}{C} = H^2 \frac{\chi_H^2}{\chi_O^2 - \chi_H^2} \quad . \tag{4}$$

When b' is temperature dependent, it can be seen from eq. (2) that the b' value, derived from eq. (4) is an average over the temperature interval T_O to T_H.

The adiabatic susceptibility χ_{ad}, in a parallel field H at a temperature T_H is given by

$$\chi_{ad} = \frac{C}{T_H} \cdot \frac{b'}{b' + CH^2} \quad . \tag{5}$$

In experiment b) T_H can be derived from relation (3) and $T_O = C/\chi_O$ which yields in combination with (5)

$$\chi_{ad} = \chi_O \left(\frac{b'}{b' + CH^2}\right)^{3/2} \tag{6}$$

from which one derives

$$\frac{b'}{C} = H^2 \frac{\chi_{ad}^{2/3}}{\chi_O^{2/3} - \chi_{ad}^{2/3}} \quad . \tag{7}$$

Finally, in experiment c) T_H can be derived from the susceptibility in zero magnetic field viz. $T_H = C/\chi_O$ and hence from eq. (5)

$$\frac{b'}{C} = H^2 \frac{\chi_{ad}}{\chi_O - \chi_{ad}} \quad . \tag{8}$$

For the ellipsoid similar relations hold, however, one has to use a Curie-Weiss law for the isothermal susceptibility, $\chi_O = C/(T - \theta)$, where θ is the demagnetizing correction. In formula (3) H is replaced by $H \cdot T_H/(T_H - \theta_\perp)$ in which $\theta_\perp$ is the demagnetizing correction in the direction of the field ($\theta_\perp \neq \theta$).

3.3.2. Results

ad.a). Demagnetizations were performed from transversal magnetic fields of 35.7, 71.4 and 255 Oe for the CMN sphere as well as for the ellipsoid. Fig. 9 gives χ_O/χ_H

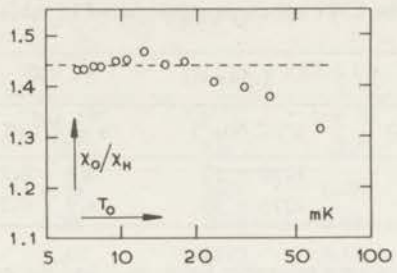

Fig. 9. χ_o/χ_H vs. the temperature in zero field, T_o, as obtained for the CMN sphere from demagnetizations and magnetizations in a transversal magnetic field of 35.7 Oe. Above about 30 mK the experimental error exceeds 10%.

as a function of the temperature T_O for demagnetizations and magnetizations performed on the CMN sphere, in a magnetic field of 35.7 Oe. As can be seen from this figure, χ_O/χ_H is rather constant in the temperature range of 20 mK to the lowest temperatures obtained i.e. about 6 mK. Towards higher temperatures χ_O/χ_H decreases which corresponds to an increasing value of b'/C. The results obtained for the sphere and the ellipsoid, averaged over the temperature range from 6 to about 20 mK, are given in table II.

Table II

$H_\perp$ (Oe)	Sphere		Ellipsoid	
	b'/C (Oe^2)	b x 10^6 (K^2)	b'/C (Oe^2)	b x 10^6 (K^2)
35.7	1200 ± 50	4.6 ± 0.2	1150 ± 50	4.4 ± 0.2
71.4	1200 ± 50	4.6 ± 0.2	1270 ± 50	4.9 ± 0.2
255	1320 ± 50	5.05 ± 0.2	1325 ± 50	5.1 ± 0.2

The value of b derived from demagnetizations from 255 Oe is somewhat higher than the values obtained from the demagnetizations with lower fields. This may be due to the relatively high temperatures, T_H, measured in the presence of a magnetic field, as compared to T_O. If b depends on the temperature, as is suggested by the deviation from the T^{-2} behaviour of the specific heat above $T \approx 20$ mK, then according to eq. (2) an average b value is found, which lies between $b(T_O)$ and $b(T_H)$. At temperatures higher than 30 mK the experimental error becomes rather large (> 10%) so at higher temperatures this method is not useful to obtain b values.

ad.b). Demagnetizations and magnetizations were performed in longitudinal magnetic fields of 34.8 and 69.6 Oe. As in the transversal magnetizations, $(\chi_O)_{T_O}/(\chi_{ad})_{T_H}$ as a function of T_O is rather constant. Towards higher temperatures (T_O > 20 mK) this ratio decreases, corresponding to an increasing b'/C. At temperatures higher than about 30 mK the experimental error becomes too large to determine b'/C values.

The results obtained for the CMN sphere are presented in table III.

Table III

$H_{//}$ (Oe)	b'/C (Oe^2)	$b \times 10^6$ (K^2)
34.8	1250 ± 50	4.8 ± 0.2
69.6	1275 ± 50	4.9 ± 0.2

ad.c). The susceptibility in zero magnetic field, χ_O, and the adiabatic susceptibility, χ_{ad}, in longitudinal fields of 30.8, 61.5 and 92.3 Oe were measured from liquid-helium temperatures down to about 0.03 K. In a magnetic field the temperature of the sample was measured by the carbon resistor. Comparison of χ_O and χ_{ad} at the same temperature yields in combination with eq. (8) values of b'/C in the temperature range mentioned above. In fig. 10 the result of these measurements, performed on the CMN sphere, is shown. As can be seen from this figure χ_{ad} deviates from a 1/T dependence below a temperature of 0.15 K, corresponding to a decreasing b'/C value. Table IV summarizes b'/C as a function of the temperature, calculated according to eq. (8).

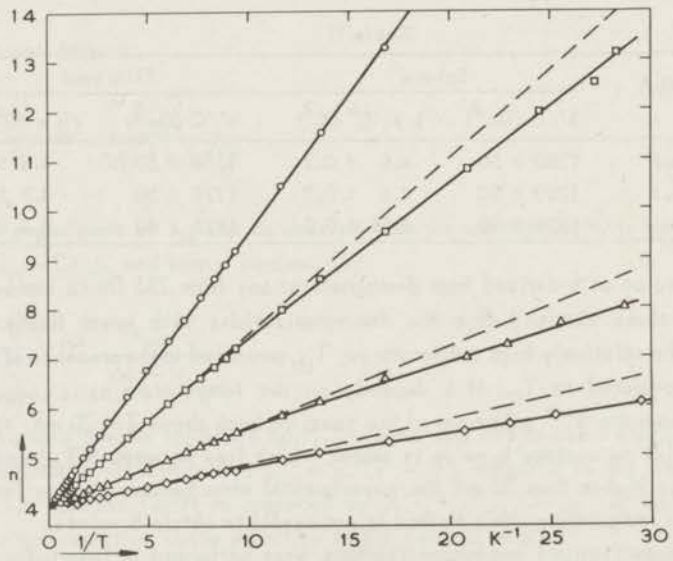

Fig. 10. Susceptibility in arbitrary units (bridge turns) vs. 1/T, for the sphere in zero field and in longitudinal magnetic fields.

○: H = 0 Oe
□: H = 30.8 Oe
△: H = 61.5 Oe
◇: H = 92.3 Oe

Table IV

$1/T(K^{-1})$	$H_{//} = 30.8$ Oe		$H_{//} = 61.5$ Oe		$H_{//} = 92.3$ Oe	
	b'/C (Oe^2)	$b \times 10^6$ (K^2)	b'/C (Oe^2)	$b \times 10^6$ (K^2)	b'/C (Oe^2)	$b \times 10^6$ (K^2)
< 6	1659	6.34	1609	6.16	1600	6.12
10	1538	5.88	1538	5.88	1522	5.82
15	1433	5.48	1472	5.63	1457	5.58
20	1385	5.30	1409	5.39	1351	5.18
25	1305	5.00	1320	5.05	1275	4.88
30	1281	4.90	1261	4.83	1261	4.83

4. Discussion

4.1. Susceptibility

In fig. 11 the relation is shown between the absolute temperature T, obtained by differentiation of the S–Q curve and the magnetic temperature $T^* \equiv C/\chi$ for the sphere as well as for the ellipsoid. These data are also summarized in table I. Although we did not reliably establish the validity of Curie's law in CMN (temper-

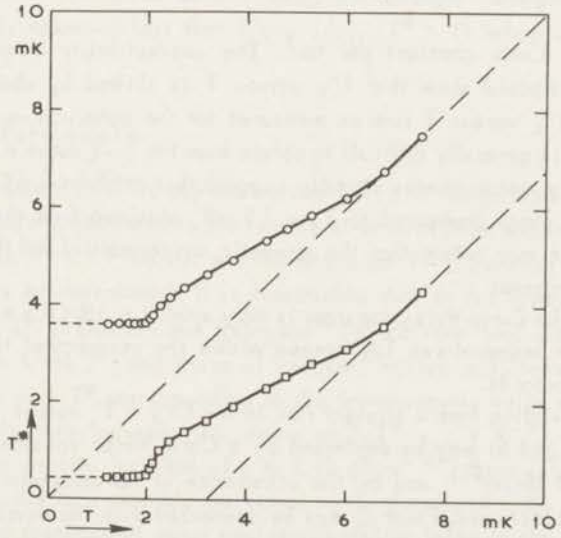

Fig. 11. $T^* \equiv C/\chi$ vs. absolute temperature for the sphere (○), and the ellipsoid (□) The dashed lines correspond to Curie's law for the sphere, and a Curie-Weiss law $\chi = C/(T - \theta)$, where $\theta = 3.18$ mK, for the ellipsoid. The points in the figure are not experimental points, but refer to the smoothed values, given in table I.

atures only to T = 8 mK have been obtained) several experiments reported in the literature[9,11] show that CMN follows Curie's law down to 6 mK. From fig. 11 it can be seen that the susceptibility approaches the constant value of 1/N at a temperature of about 2 mK. This temperature is practically equal to the temperature at which the specific heat, obtained from the T–S diagram, exhibits a maximum. For the ellipsoidal sample we could not reliably establish a temperature-entropy scale, so we used the temperature scale obtained for the sphere. The qualitative behaviour of the susceptibility of the ellipsoid is, however, similar to that of the sphere when we use this temperature scale. Other experiments[8,11] at higher temperatures, do not suggest a shape-dependent T–S relation, as might have been anticipated in the paramagnetic region. Recently, Griffiths[20] showed that in the thermodynamic limit, for a spin system with dipole-dipole interactions the sample posesses a well-defined bulk free energy, which is independent of sample shape, provided there is no magnetic field.

The susceptibility of the ellipsoid can be reduced to a spherically shaped specimen by applying the shape-dependent demagnetizing correction, θ, to the magnetic temperature T*. This correction, calculated with the demagnetizing factor of N = 0.54, amounts to

$$\theta = (\frac{4\pi}{3} - N)C = 3.18 \text{ mK},$$

where C is the Curie constant per cm^3. The susceptibility measurements above 6 mK for the ellipsoid show that $1/\chi$ versus T is shifted by about 3.18 mK with respect to the $1/\chi$ versus T line as measured for the spherical specimen (see fig. 11). Although it is generally difficult to obtain from the χ–T curve a transition point, our susceptibility measurements strongly suggest that at about 2 mK a ferromagnetic transition takes place (compared to T_c = 1.9 mK, obtained from the specific heat). From fig. 11 one may notice that the magnetic susceptibility for the sphere shows three distinct features:

a) the value of the Curie-Weiss constant is very small i.e. $|\theta| < 0.5$ mK.

b) at the lowest temperatures $1/\chi$ agrees within the accuracy of the data with the demagnetizing factor N.

c) there is a deviation from a straight line in the $C/\chi \equiv T^*$ versus T plot above T_c.

Points a) and b) may be explained by a Curie-Weiss constant, θ, calculation of Peverley and Meyer[21], and by the occurrence of ferromagnetic domains at low temperatures respectively. Point c) may be connected with the deviations from molecular-field theory close to T_c. The expansion of the susceptibility χ in powers of 1/T is carried out to T^{-2} terms in the Onsager approximation, for which Brout and Thomas[22] have recently given additional theoretical justification. The Onsager formula, as modified by Van Vleck[23], is given by

$$\frac{C}{T^{\circledast}} = \frac{M}{H} = \chi_O \left[1 + \left(\frac{4\pi}{3} - N\right)\chi_O + \left(\frac{4\pi}{3} - N\right)^2 \chi_O^2 - \right.$$

$$\left. - \left(1 + \frac{3}{8s(s+1)}\right) Q \chi_O^2 + \ldots\right] \qquad (9)$$

where

$$Q = \frac{2}{(N/V)^2} \sum_i r_{ij}^{-6} \qquad \text{and} \qquad \chi_O = \frac{C}{T};$$

r_{ij} is the distance between the cerium ions. Eq. (9) should hold for cubic lattices and for isotropic g values and hence is not directly applicable to CMN. The reason for discussing this formula is that CMN has for most practical purposes a negligible Curie-Weiss constant and in this respect resembles a cubic substance with dipolar interactions only. In that case, namely for a sphere having $N = 4\pi/3$, the first-order term in χ_O between brackets vanishes, and only the second-order term, containing Q, accounts for the deviation from Curie's law. For CMN a calculation of Daniels[24] yields $Q = 18.3$ and equation (9) predicts for instance at $T = 5$ mK, that $T^{\circledast} = 3T$. This gives at least an order of magnitude estimate of the temperature where interactions between magnetic ions strongly influence the susceptibility, even when the Curie-Weiss constant vanishes. Qualitatively, the Onsager correction accounts for the experimentally observed fact that $1/\chi > 1/\chi_O$ ($T^{\circledast} > T$) below 6 mK (as can be seen from fig. 11).

4.2. Temperature scale

In fig. 12, where $1/T^{\circledast}$ is plotted versus $1/T$, the temperature scale obtained from our experiments is compared to the results of several other experiments, mentioned in the literature[8,9,11]. From our measurements the $T-T^{\circledast}$ relation above $T = 6$ mK could not reliably be determined. It is remarkable that at the lowest temperatures, the results for $1/T^{\circledast}$ of Daniels and Robinson[9] (which have been discussed and reinterpreted by De Klerk[10]) and those of Frankel, Shirley and Stone[8] considerably exceed the value of $1/T^{\circledast}$ corresponding to the ferromagnetic value of a spherically shaped sample. In this ferromagnetic value of $1/T^{\circledast} = 274$ K^{-1}, which has been calculated from a density for CMN of $\rho = 2.10$ g/cm^3 [4], there is an experimental error of about 5%, due to a possible correction to the density of CMN. This correction may be due to the presence of water enclosures and/or holes in the single crystals; this would effectively lower the specimen density to for instance $\rho = 2.0$ g/cm^3, a value which is mostly adopted for the density of CMN[10,25]. The ferromagnetic susceptibility for a sphere will be in that case $1/T^{\circledast} = 288$ K^{-1}. The curvature of $1/T^{\circledast}$ versus $1/T$ to the ferromagnetic value at $1/T = 460$ K^{-1} does not occur in the results

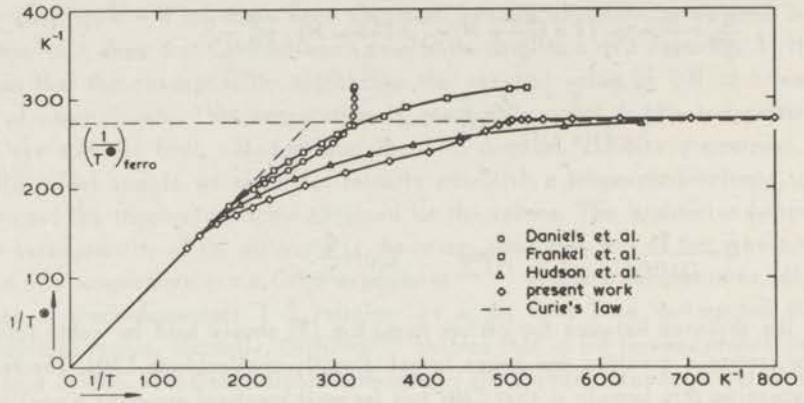

Fig. 12. Temperature scale for the spherical sample compared to the results of various other experimentalists. The maximum value of χ/C for a ferromagnetic sphere, splitted up into domains, is indicated in the figure $((1/T^{*})_{ferro})$.

of Hudson and Kaeser, as can be seen from fig. 12. However, the number of their experimental points is rather small in this temperature range, so a precise behaviour of $1/T^{*}$ versus $1/T$ is not obtainable. The maximum value of $1/T^{*}$, which is found by Hudson and Kaeser, is in good agreement with the calculated value of 274 K^{-1}. Below a temperature of 2 mK our experimental susceptibility stays constant within the experimental error, down to the lowest temperatures measured. From this figure one can conclude that CMN is useful as a thermometer above temperatures of T = 2 mK, although by two-stage demagnetization still lower temperatures with this substance can be obtained, namely $T \leq 1.25$ mK. Although we did not establish a temperature scale for the ellipsoid, it may be argued from our results and those of several other experimentalists[8,11] that there is no shape dependence of the temperature scale. It also appears from our measurements that for both CMN samples the susceptibility reaches 1/N at the same entropy of about S/R = 0.38. On basis of molecular-field theory one expects a ferromagnetic transition temperature $T_c = 4\pi C/3$, where C is the Curie constant per cm^3, if the substance is magnetized in long and thin ferromagnetic domains. However, deviations from molecular-field theory occur at the lowest temperatures, as can be concluded from our measurements, which result in a lower transition temperature of 1.9 mK which is also shape independent. In this connection one may consider the measurements on the specific heat of powdered, cylindrically shaped CMN samples which were done by Wheatley et al.[1,12]. They derived from various other experiments that for such a sample $T^{*} = T$, which relation holds to an absolute temperature of about 2 mK. They measured the highest susceptibility at a temperature of $T^{*} = 1.8$ mK, which temperature was almost inde-

pendent of the grain size of the powder. This temperature may be compared to our results on the transition temperature of CMN.

4.3. Value of b

From our measurements on the specific heat of the CMN sphere, a coefficient of $b = 5.2 \times 10^{-6}\ K^2$ in the T^{-2} range is deduced, while from our demagnetizing experiments we derive $b = 4.8 \times 10^{-6}\ K^2$. Recent calculations on the lattice sum of CMN, done by Peverley and Meyer[21] show, that a Curie-Weiss constant of $\theta = -0.273$ mK has to be expected in a direction perpendicular to the c axis. If we apply this correction to the temperature scale of the directly measured specific heat data above $T^{\circledast} = 6$ mK, the coefficient b is reduced to a value of $b = 5.0 \times 10^{-6}\ K^2$. Although the results of our specific heat measurements are not very precise, they show that in the temperature range of 8 to about 20 mK the specific heat of CMN can be described by the formula $c/R = b/T^2$. Wheatley[12] concludes from his specific-heat data, that it is not clear whether the specific heat obeys a T^{-2} or $T^{-1.7}$ law. However, from our determinations of b as a function of T (see fig. 13) it follows that

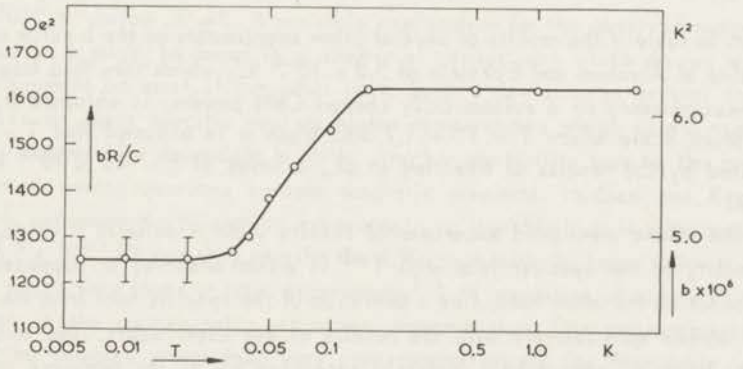

Fig. 13. Temperature dependence of b, also given as bR/C. Below 20 mK the results obtained from low field demagnetizations are shown; the experimental error in these results is indicated by vertical bars.

between 8 and 20 mK the specific heat obeys the relation $c/R = b/T^n$, where $n = 2.0 \pm 0.1$. Above about 20 mK the specific heat deviates from the T^{-2} law and the description of the magnetic system with a constant b value looses its meaning. In fig. 13 the results obtained for the b value from the experiments, mentioned in section 3.3, are plotted versus temperature on a semi-logarithmic scale. As can be seen from this figure b has a constant value of $6.2 \times 10^{-6}\ K^2$ above a temperature of about 0.15 K, and reaches another constant value of $(4.8 \pm 0.2) \times 10^{-6}\ K^2$ below about 20 mK. Between these two temperature regions b is obviously temperature de-

Table V

Experimentalists	Method	$b \times 10^6$ (K^2)
Cooke, Duffus and Wolf[2]	dipolar sum	6.75
	a.c. adiab. susc.	7.5
Daniels and Robinson[9]	adiab. demagnetization	6.4
Daniels[24]	dipolar sum	6.6
Hudson and Kaeser[15]	a.c. adiab. susc.	6.3
	adiab. demagnetization	5.5
	adiab. demagnetization	5.9
Hudson and Kaeser[11]	adiab. demagnetization	5.76
Abel, Anderson, Black and Wheatley[1,12]	specific heat	4.2
Abraham and Eckstein[13]	specific heat	5.8
		(4.2)
This research: $T > 0.15$ K	a.c. adiab. susc.	6.2
$T < 0.02$ K	adiab. demagnetization	4.8 ± 0.2

pendent. In table V the results of several other experiments on the b value are given. The value of Abraham and Eckstein of 5.8×10^{-6} K^2, which they find from specific heat measurements on a cylindrically shaped CMN powder, is obtained by using a temperature scale where $T = T^* + 1.7$ mK. When it is assumed that $T = T^*$, as is suggested by the results of Wheatley et al., a value of $b = 4.2 \times 10^{-6}$ K^2 can be derived.

The above mentioned experimental results yield a definite b value, i.e. proportionality of the specific heat with T^{-2} is either observed or supposed. Hudson and Kaeser on the other hand, find a deviation of the specific heat from the T^{-2} law, which agrees qualitatively with the results of our experiments. The observed deviation, however, cannot be completely accounted for by the measured temperature dependent b value, as can be derived from the measurements of the susceptibility in a magnetic field and in zero field. At 0.1 K, for instance, the specific heat, calculated according to the relation $c/R = b/T^2$, would amount to $c/R = 5.9 \times 10^{-4}$ while the experimental results yield a value of 9.6×10^{-4}. Apart from a deviation from a T^{-2} law, which may be expressed by a temperature dependence of b, in addition there seems to be an unknown, anomalous heat capacity at temperatures higher than 20 mK, as already has been stated by Hudson and Kaeser[11,15]. This anomalous heat capacity does not show up in the susceptibility measurements. It may therefore be of non-magnetic origin and is supposed to be in poor thermal contact with the magnetic spin system[11]. It may be remarked that our specific-heat measurements are not very accurate in the higher temperature range ($T > 50$ mK) because of the increased heat capacity of the calorimeter. The b value of 4.8×10^{-6} K^2, obtained

from our demagnetization experiments is remarkably low in comparison to the value, which follows from the measurements of Hudson and Kaeser, namely $b = 5.76 \times 10^{-6}\ K^2$. A possible explanation for this discrepancy might be found in the fact that all values of the entropies which are used in the discussion of their experiments are initial entropies; so a possible irreversible entropy gain at demagnetization is not accounted for. A correction to the entropy due to a similar entropy gain would yield a lower value for b. As a second possibility to explain the relatively high value of Hudson and Kaeser, it may be mentioned that they demagnetize the CMN sample from a temperature of about 1 K. At this relatively high temperature the specific heat is higher than can be calculated on basis of the relation $c/R = b/T^2$, where b is the coefficient in the low temperature range (8 to 20 mK), because of the deviation to higher temperatures from the T^{-2} behaviour. For adiabatic demagnetization relation (2) holds. From this formula one may calculate an average b value in the temperature range T_O to T_H. If c is higher than calculated with the relation $c/R = b/T^2$, which is valid at the lowest temperatures, then a higher b value is obtained from demagnetization experiments. From our measurements it appears that b is a gradually varying function of the temperature and it decreases from $6.2 \times 10^{-6}\ K^2$ at $T > 0.15$ K to $4.8 \times 10^{-6}\ K^2$ below 20 mK. A possible explanation for the observed temperature dependence of b might be found in a number of cerium ions which do not have the same environment as most of the other ions. Such a deviation in crystal structure might cause an extra specific heat at higher temperatures which gives rise to an effectively temperature dependent b value. Another possibility may be the presence of impurities having non-zero nuclear magnetic moments. Hudson and Kaeser[15] report from paramagnetic relaxation experiments at liquid-helium temperatures a b value of $6.3 \times 10^{-3}\ K^2$ and they ascribe the difference with the lower value of $5.76 \times 10^{-6}\ K^2$, which they found in later experiments[11], to impurities of mostly Pr and to imprecision in the paramagnetic relaxation determination. Our measurements were performed on samples grown from very pure cerium nitrate (no detectable impurity present, i.e. $< 10^{-6}$) and from magnesium nitrate which is commonly used in chemical analysis and might have contained some impurities.

Recently, Wong, Dembinsky and Opechowski[26] have calculated the T^{-3} term in the specific heat of spin ½ systems, having dipolar interactions and anisotropic g values. By numerical computation of their formulae for the case of CMN they find, using $g_\perp = 1.84$ and lattice constants taken from ref. 24:

$$\frac{c}{R} = 6.80 \times 10^{-6}\ T^{-2} - 0.023 \times 10^{-6}\ T^{-3}. \qquad (10)$$

This result shows that cT^2/R is expected to be practically constant (variation less than 4%) only for temperatures above 0.1 K, which is much higher than usually assumed. This is in agreement with some experimental results on some other compounds having predominantly dipolar interaction[27,28]. Equation (10) would also

yield an effectively temperature dependent value of $b \equiv cT^2/R$ towards low temperatures. However as appeared from our measurements b has a constant value below 20 mK, which does not follow from relation (10). Such an effectively T^{-2} region in the specific heat might be found when still higher-order terms in 1/T are included in eq. (10). Somewhat better agreement with our experimental results is obtained when including an isotropic exchange interaction with $J/k \approx 1.3 \times 10^{-4}$ K. Such an exchange interaction would result in a high-temperature contribution to the specific heat of less than 1%, compared to the dipolar specific heat. The experimental values of b are however substantially lower than the T^{-2} coefficient in eq. (10). It may therefore be concluded that the precise behaviour of the specific heat of CMN is not established and that more results, both experimental and theoretical, are required. Therefore, the b values quoted in this chapter should be considered as strictly experimental data, from which the magnitude of c/R can be derived in a limited temperature interval, but which should not be directly compared with the coefficient of the first term in the above equation.

4.4. Energy

Magnetic structure predictions, based on energy calculations at zero temperature, were made by Daniels and Felsteiner[29]. They applied the method of Luttinger and Tisza[30] for minimizing the dipolar energy of eight magnetic sublattices, generated by the eight lattice points of the rhombohedral unit cell, the spins of any two ions separated by two lattice spacings being parallel. They concluded from their calculations that the lowest energy is obtained for an antiferromagnetic spin configuration and amounts to $E/R = -1.85$ mK. The configuration with the next higher energy gave $E/R = -0.55$ mK, hence this method of calculation definitely favours antiferromagnetism. The predicted value, although its absolute magnitude is very probably overestimated in this molecular-field approach, is higher than the experimental result based on the heat-capacity data and its extrapolations, namely $E/R = -2.2$ mK. It may be argued that larger magnetic structure unit cells should be taken into consideration and may yield lower energies than found by Daniels et al. More seriously, however, the susceptibility measurements suggest that CMN becomes ferromagnetic at the transition point, while Daniels et al. give $E = 0$ for a ferromagnetic configuration. The latter is related to the group-theoretical requirement that ferromagnetic alignment in a trigonal crystal in zero external field only occurs along the trigonal axis, but in that direction CMN has g value zero. Since our susceptibility measurements clearly indicate that at low temperatures χ is restricted by the demagnetizing factor, we assume that the formation of ferromagnetic domains plays an important role, not only in the susceptibility but also in the energy value. In an external magnetic field, as applied in the susceptibility measurements, the magnetization may be oriented in any direction in the $g_\perp$ plane. For that case Peverley and Meijer[21]

have calculated the quantity

$$\Delta_{\perp} = \frac{g_{\perp}^2 \beta^2 s^2}{k} \Sigma \frac{3x^2 - r^2}{r^5} .$$

The summation over all ions in a sphere yielded $\Delta_{\perp} = -0.273$ mK, which is the Curie-Weiss constant in the molecular-field approximation and which is closely related to the local field of a ferromagnetically ordered single crystal. The local field at zero temperature in a spherically shaped single domain, magnetized in the $g_{\perp}$ direction, is given by

$$H_{loc} = g_{\perp} \beta s \, \Sigma \frac{r^2 - 3x^2}{r^5} = \frac{0.273\ k}{g_{\perp} \beta s} \times 10^{-3} .$$

This corresponds to an energy gain in the molecular-field approximation for $R/k = 6.03 \times 10^{23}$ dipoles of

$$E/R = -\tfrac{1}{2} M \cdot H_{loc} = -\tfrac{1}{2} g_{\perp} \beta s \cdot \frac{(-0.273)}{g_{\perp} \beta s} = 0.14 \text{ mK}.$$

However, when subdividing the crystal in needle shaped ferromagnetic domains, then one may estimate how much energy is gained with respect to that of the single domain spherical crystal. This energy gain equals $-\frac{1}{2}(4\pi/3)M^2$ per unit volume, where $4\pi/3$ is the demagnetizing factor for a sphere and M is the saturation magnetization ($\approx$ 14.1 ergs/oersted cm^3), hence $E/R = -1.83 + 0.14$ mK $= -1.69$ mK. Although the above calculated absolute magnitude is smaller than the experimental value, the assumption of the occurrence of ferromagnetic domains would otherwise give a reasonable explanation for the experimental results:
a) the maximum of the susceptibility is determined by the demagnetizing factor,
b) the absence of a significant Curie-Weiss constant in the $1/\chi$ versus T data ($|\theta| < 0.5$ mK).

In this connection it may be mentioned that ferromagnetism is found in another compound having practically exclusively dipolar coupling, namely dysprosium ethyl sulphate[31]. Similarly as in CMN, short-range ordering accounts for most of the energy yield, while the energy yield below the transition point has not yet been precisely determined. The heat-capacity data of dysprosium ethyl sulphate, extrapolated to low temperatures ($T_c = 0.115$ K), lead to $E/R = -0.14$ K. The Curie-Weiss constant of $\theta = +0.12$ K may be deduced from the susceptibility data and closely agrees with the dipolar sum calculation of Daniels[24], which yields $\theta = 0.122$ K. From the latter one deduces $E/R = -0.061$ K for the energy yield of a single domain ferromagnetic sphere at zero temperature. When the sphere breaks up into needle shaped domains,

an additional energy of $-\frac{1}{2}NM^2/R = -0.083$ K is obtained. The sum of the two calculated energies is therefore $E/R = -0.144$ K, in excellent agreement with the observed value.

For an ellipsoidal CMN specimen (demagnetizing factor N) the above given energy derivation has to be slightly modified, but yields the same result as can be seen from the following:

a) the Curie-Weiss constant is changed into

$$\Delta_\perp = -0.273 \times 10^{-3} - (N - \frac{4\pi}{3}) \frac{g_\perp^2 \beta^2 s^2}{k}$$

and hence the local field in a single domain sample is given by

$$H_{loc} = \frac{0.273\ k}{g_\perp \beta s} \times 10^{-3} + (N - \frac{4\pi}{3})\ g_\perp \beta s$$

which corresponds to an energy of

$$E/R = \frac{1}{2} \{0.273 \times 10^{-3} + (N - \frac{4\pi}{3})\ M^2\}.$$

b) the energy due to subdivision into needle-shaped domains is $-\frac{1}{2}NM^2$. The changes in energy due to a) and b) cancel and hence the total energy gain is again

$$E/R = 0.14 - \frac{4\pi}{3} \cdot \frac{M^2}{2} = -1.69 \text{ mK}.$$

Therefore the energy gain for a crystal, subdivided in domains, is independent of external shape. From this one can conclude that the transition temperature T_c does not depend on the geometry of the sample.

All the above given considerations are classical, but a theoretical justification has recently been given by Levy[32]. We notice that a considerable fraction of the energy is removed in short-range ordering above the transition temperature (T_c = 1.9 mK) which to some extent invalidates the molecular-field approximation, particularly in the case of the antiferromagnetic ground state considered by Daniels. For the ferromagnetic case the classical dipolar sum may give a satisfactory approximation to the energy, but the value of the demagnetizing energy may be overestimated, since it represents an upper limit for needle shaped domains. In this connection it may be remarked that in the $g_\perp$ plane no anisotropy energy is expected (g is isotropic in the $g_\parallel$ plane), hence the domain size is not determined by anisotropy constants and wall effects. Hence, if the domains were extremely small, there would

be not much difference between ferromagnetism in conjunction with needle-shaped domains and antiferromagnetism. In this connection it may also be remarked that Griffiths and Arrot[33] have argued that the lowest energy state of a ferromagnetic system is not a state of uniform magnetization. Furthermore, due to non uniformity of the magnetization, the local field may vary over the sample and hence the critical temperature may not be sharp and will also depend on the strength of an externally applied magnetic field.

5. Conclusions

1. CMN shows ferromagnetic ordering in domains below $T_c = 1.9$ mK which shows that purely dipolar substances sustain long-range order. This experimental result may be considered in the context that

a) the effective spin ½ is constrained to the $g_\perp$ plane, but that there is no anisotropy in that plane;

b) the Curie-Weiss θ is very small compared to T_c and negative, hence ferromagnetic ordering cannot be explained by molecular-field theory.

2. The $T-T^{\circledast}$ relation for a single crystal is appreciably different from that of a loose packed, cylindrically shaped powder (see section 4.2).

3. The heat capacity above T_c is not easily explained in terms of $b \equiv cT^2/R$ being constant and equal to the theoretically calculated dipolar heat capacity. There are indications for an anomalous heat capacity above 20 mK, but this does not affect the conclusion that short-range ordering accounts for a substantial fraction of the total entropy gain of R ln 2.

References

1) Abel, W.R., Anderson, A.C., Black, W.C. and Wheatley, J.C., Physics 1(1965)337; Phys.Rev. 147(1966)111.
2) Cooke, A.H., Duffus, H.J. and Wolf, W.P., Phil. Mag. 44(1953)623.
3) Keffer, F., Handbuch der Physik XVII/2 (1966) 93, and earlier references mentioned.
4) Zalkin, A., Forrester, J.D. and Templeton, D.H., J.chem.Phys. 39(1963)2881.
5) Grace, M.A., Johnson, C.E., Kurti, N., Lemmer, H.R. and Robinson, F.N.H., Phil. Mag. 45(1954)1192.
6) Levi, M.W., Sapp, R.C. and Culvahouse, J.W., Phys.Rev. 121(1961)538.
7) Carboni, F. and Sapp, R.C., Ann. Phys. (N.Y.) 1(1965)77.
8) Frankel, R.B., Shirley, D.A. and Stone, N.J., Phys.Rev. 140(1965)1020.
9) Daniels, J.M. and Robinson, F.N.H., Phil.Mag. 44(1953)630.
10) De Klerk, D., Handbuch der Physik XV(1956)119.
11) Hudson, R.P. and Kaeser, R.S., Physics 3(1967)95.

12) Wheatley, J.C., Ann.Acad.Sci. Fennicae. A210(1966)15.
13) Abraham, B.M. and Eckstein, Y., Phys. Rev. Letters 20(1968)649.
14) Bailey, C.A., Proc.Phys.Soc. 83(1964)369.
15) Hudson, R.P., Kaeser, R.S. and Radford, H.E., VII int. Conf. on low Temp. Phys., Toronto 1960, pg. 100.
16) Hudson, R.P. and Mangum, B.W., Nuovo Cimento 23(1962)1133.
17) Hudson, R.P. and Hosler, W.R., Phys. Rev. 122(1961)1417.
18) Leask, M.J.M., Orbach, R., Powell, M.J.D. and Wolf, W.P., Proc.Roy.Soc. A272 (1963)371.
19) Gorter, C.J., Paramagnetic Relaxation (Elsevier 1947).
20) Griffiths, R.B., Phys.Rev. 176(1968)655.
21) Peverley, J.R. and Meyer, P.H.E., Phys.Stat.Sol. 23(1967)353.
22) Brout, R. and Thomas, H., Physics 3(1967)317.
23) Casimir, H.B.G., Magnetism and Very Low Temperatures (Dover) 1961, pg. 67.
24) Daniels, J.M., Proc.Phys.Soc. 66(1953)673.
25) Bailey, C.A., Phil.Mag. 4(1959)833.
26) Wong, S., Dembinsky, S.I. and Opechowski, W., Physica 42(1969)565.
27) Wielinga, R.F., Lubbers, J. and Huiskamp, W.J., Commun. Leiden, No. 361b; Physica 37(1967)375.
28) Rayl, M., Vilches, O.E. and Wheatley, J.C., Phys. Rev. 165(1968)698.
29) Daniels, J.M. and Felsteiner, J., Canad. J. Phys. 42(1964)1469.
30) Luttinger, J.M. and Tisza, L., Phys. Rev. 70(1946)954.
31) Wielinga, R.F. et al., to be published; Huiskamp, W.J., Ann.Acad.Sci.Fennicae A210(1966)180.
32) Levy, P.M., Phys.Rev. 170(1968)595.
33) Arrot, A., Phys.Rev.Letters 20(1968)1029.

Chapter IV

SPIN-LATTICE ENERGY TRANSFER BELOW 1K IN $CuCs_2(SO_4)_2.6H_2O$ AND IN $Ce_2Mg_3(NO_3)_{12}.24H_2O$.

1. Introduction

In the past few years many experiments on spin-lattice relaxation at low temperatures have been reported[1-7]). The mechanism of spin-lattice energy transfer seems to be reasonably well understood especially in so far as the rare-earth double nitrates[1,2,4,7] and ethyl sulphates[1,5,8,9] are concerned. At the lowest temperatures the one-phonon relaxation process, the direct process, is dominant while at higher temperatures ($T > 1$ K) the two-phonon processes, i.e. the Raman and the Orbach process become important. In the direct process the spin system can interact with a surrounding bath of constant temperature (e.g. the liquid-helium bath) via a band of lattice oscillators (phonons on speaking terms). If it can be assumed that this band of lattice oscillators has good thermal contact with the other lattice oscillators of different frequency, or with the helium bath, the average phonon-excitation number, N_δ, is given by its thermal equilibrium value, $1/(e^{\delta/kT_B} - 1)$, where T_B is the bath temperature. However, it may occur that if the relaxation time of the direct process, τ_d, is sufficiently short, the phonons on speaking terms are unable to transport the energy flow from the spin system rapidly enough. The energy-rate determining process is then situated in the phonon system in stead of in the spin system itself. In that case the experimentally observed spin-bath relaxation time, τ_b, is significantly larger than the intrinsic spin-lattice relaxation time. As the heat capacity of the band of lattice modes with which the spin system interacts is very much smaller than the heat capacity of the spin system at liquid-helium temperatures, phonon heating effects can occur in which the effective temperature of the phonons on speaking terms rises to approximately the temperature of the spin system. This phenomenon has become known as the phonon bottleneck[1,10-18]. A detailed formula for the heat flow per cm^3, $\dot{Q}$, between the lattice and a two-energy level spin system in the case of a phonon bottleneck and which is equivalent to the formula for the spin-bath relaxation time, given by Scott and Jeffries[1]), is

$$\dot{Q} = \frac{1}{t_{ph}} \rho(\nu)\Delta\nu \left[\frac{\delta}{e^{\delta/kT_{L-1}}} - \frac{\delta}{e^{\delta/kT_{s-1}}}\right] = \frac{1}{t_{ph}} \left(\frac{12\pi\nu^2 k\Delta\nu}{v_o^3}\right) (T_L' - T_s') \qquad (1)$$

where

$$T_L' = \frac{\delta/k}{e^{\delta/kT_{L-1}}} \quad \text{and} \quad T_s' = \frac{\delta/k}{e^{\delta/kT_{s-1}}} .$$

In eq. (1) $\rho(\nu)$ is the density of lattice oscillators per unit band width and equals $12\pi\nu^2 v_o^{-3}$, t_{ph} is the lifetime of hot phonons of the frequencies concerned, $\Delta\nu$ is the phonon band width, v_o is the velocity of sound, δ is the average Zeeman energy splitting of the spin system, T_L is the lattice temperature and T_s is the spin temperature.

At first sight, transfer of energy between lattice oscillators of different frequencies can take place only in case of anharmonic terms of the lattice potential energy. At very low temperatures this process may become very ineffective as can be concluded from data on thermal conductivity of crystals[19] and especially from investigations on the propagation of ultrasonic waves[20,21,22]. The latter clearly show that ultrasonic waves can propagate over appreciable distances through a crystal without sharing their energy with other oscillators. Any inelastic phonon scattering process would result in a temperature dependent value of t_{ph} unless it occurs at lattice imperfections or crystal boundaries. The experiments of Nash[23,24] on copper tutton salts, of Scott and Jeffries[1] and of Ruby, Benoit and Jeffries[2] on dilute rare-earth double nitrates indicated that the hot phonon lifetime, t_{ph} was dependent on crystal size. In those experimental results t_{ph} appeared to be approximately equal to the time required to traverse half the crystal thickness d, i.e. $t_{ph} \approx d/2v_o$. More generally it can be stated that $t_{ph} = \eta d/2v_o$, where η is a transmission factor and equals the number of times that the phonons on speaking terms traverse half the crystal thickness, before they are inelastically scattered.

The spin-bath energy transfer can in general take place in two different ways[15,16]. Firstly, the spin-bath relaxation time may be determined by a diffusion process in which the hot phonons are absorbed and re-emitted many times by the spin system before reaching the crystal boundaries or cracks inside the crystal, where they are inelastically scattered and as such disappear. The mean free path of the phonons will then be much smaller than the crystal dimensions d. For such a diffusion process, which can be expected to occur in a salt in which the paramagnetic resonance line is inhomogeneously broadened, an apparent spin-bath relaxation time, τ_b, will occur. According to Giordmaine and Nash[16] τ_b is then proportional to $N^2 d^2 \tau_d^{-1} \Delta\nu_s^{-2} T_B^{-4}$, where N is the number of spins per cm^3, τ_d the direct spin-lattice relaxation time, $\Delta\nu_s$ is the width of a rectangularly shaped spin-resonance line and T_B is the bath temperature. Experimentally, the occurrence of a spin-bath relaxation time determined by an inelastic phonon diffusion process, is found by Schedewie[25] in neodymium ethyl sulphate. For a homogeneously broadened resonance line the spin-bath contact is primarily determined by the energy transfer of the phonons on speaking terms with frequencies which lie in the wings of the resonance line. Such phonons have a mean free path of the order of the crystal dimensions. For a Gaussian shaped resonance line Giordmaine and Nash predicted a spin-bath relaxation time being proportional to $Nd\Delta\nu_s^{-1} T_B^{-2}$. From the results obtained on the copper tutton salts[24] and on dilute rare-earth double nitrates[1,2] which yield a spin-bath relaxation time $\tau_b \propto d T_B^{-2}$,

it can be concluded that in these salts the bottlenecked spin-bath energy transfer is determined by the phonons on speaking terms with a mean free path of the order of the crystal dimensions.

The experiments mentioned in this chapter, studied the spin-lattice heat transfer in concentrated $CuCs_2(SO_4)_2.6H_2O$ and $Ce_2Mg_3(NO_3)_{12}.24H_2O$ (CMN), for which it will further be shown that the energy transport is determined by the phonon bottleneck. The measurements on $CuCs_2(SO_4)_2.6H_2O$ have already been published[14] so only a short summary and some additional results concerning the thickness dependence of the spin-lattice energy flow will be given. Measurements on dilute cerium-lanthanum magnesium nitrate have already been reported by Ruby et al.[2], Larson and Jeffries[4] and by Brya and Wagner[6,17,26]. The measurements on CMN discussed in the present chapter, were performed on concentrated and 10% diluted single crystals. From the field dependence of $\dot{Q}/(T_L' - T_s')$ ($\propto H^2$ because of the ν^2 factor of the phonon density in eq. (1)), the presence of a phonon bottleneck is concluded.

2. Experimental method

The experimental arrangement used in the apparatus which is described in chapter II, is shown schematically in fig. 1. The spin-lattice heat transfer measurements on $CuCs_2(SO_4)_2.6H_2O$ could be performed with a CMN susceptibility thermometer as well as with a carbon resistor. The heat flow to the sample was supplied

Fig. 1. Schematic diagram of the essential parts of the apparatus.
A: sample.
B: heater.
C: carbon resistor thermometer.
D: thermal switch (Pb).
E: cooling salt.

electrically by the Pt-W alloy heater. In the experiments described in this chapter a Pb switch was used. In the superconducting state the heat conduction of this switch could be described approximately by the relation $\dot{Q} = \lambda T^4$, where T is the temperature of the metal system. It was found that λ amounted to 50 erg/K^4s typically. This experimental arrangement allowed us to measure the spin-lattice contact to temperatures up to about 0.5 K, the heat leak through the switch to the cool-

ing salt exceeding acceptable limits (about 4 erg/s) at higher temperatures. The heat leak due to radiation, vibrations and conduction through the leads, amounted to approximately 0.25 erg/s. The electrically applied heat flow to the sample varied between 10 and 30 erg/s typically. The CMN samples consisted of flat single crystals with thickness varying between 1 and 4 mm and weights varying between 1 and 3 grams. The samples were mounted between brass plates with Apiezon N grease, the crystallographic c axis being horizontal. By measuring the susceptibility perpendicular to a horizontal magnetic field of about 1000 Oe as a function of the direction of this field, the orientation of the c axis could be determined with an accuracy of 0.5°.

The experimental procedure of obtaining the spin-lattice relaxation data was as follows. After the sample was cooled down to the desired temperature range through the thermal switch, the contact with the cooling salt was broken (heat switch superconducting) and after some time an isolated system (consisting of sample, heater, thermometer plus metal plates) being in thermal equilibrium, was obtained. The temperature of this system was registered continuously by the carbon resistor, being displayed on a recorder. When the isolated system is in internal equilibrium, i.e. no heat is applied by the heater, the temperature of the carbon resistor, which is essentially the lattice temperature, T_L, equals the temperature of the spin system, T_s. At the time t_1 (fig. 2) heating is started and the sample warms up slowly, T_L

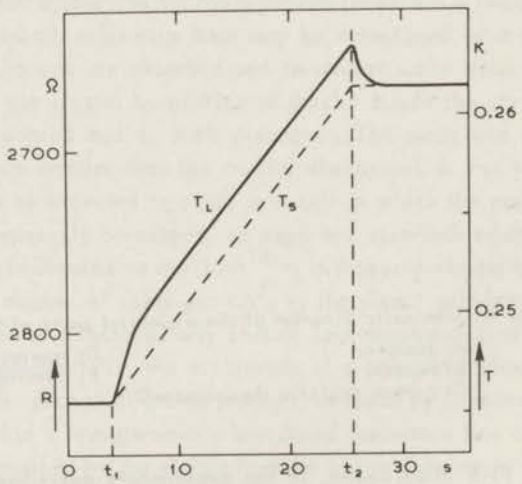

Fig. 2. Temperature, T_L, and resistance of the carbon resistor as a function of time for a concentrated CMN sample with a thickness of 1.6 mm, in a field of 3.96 kOe perpendicular to the c axis. The applied heat flow amounted to $\dot{Q}$ = 29.6 erg/s. At t_1 the heating is started, at t_2 it is stopped. T_s is the interpolated spin temperature.

being higher than T_s. After some time (10-30 s) a stationary difference between T_L and T_s is obtained. At time t_2 the heating is stopped and the lattice temperature drops to T_s, assuming the lattice plus metal heat capacity to be negligible compared to the heat capacity of the spin system. After a few seconds the whole system is in temperature equilibrium again and T_L equals T_s. A typical pattern for a CMN sample on the recorder is shown in fig. 2. By extrapolating back the linear part for $t > t_2$ in fig. 2 to the time t_2, we both know $\dot{Q}$, T_L and T_s, from which the spin-lattice heat contact can be derived.

As to the applicability of the above-given procedure in obtaining relaxation data, some remarks must be made.

a) The temperature difference, $T_L - T_s$, as registered by the carbon resistor represents the "true" temperature difference between lattice and spin system only if the heat capacity of the metal plus lattice can be neglected compared to the heat capacity of the magnetic system. In a separate experiment the heat capacity of the metal system was determined to be $c_{met} = 1500\ T$ erg/K. The lattice specific heat for CMN can be estimated[27,28] to be $c_{lat}/R = 6 \times 10^{-4}\ T^3$. So, at $T = 0.25$ K, a temperature at which most of the relaxation data were taken, we obtain for the heat capacity of the metal system 375 erg/K. The magnetic heat capacity of a typical sample of 1 g CMN at 0.25 K in a magnetic field of 800 Oe perpendicular to the c axis can be estimated to be about 4000 erg/K (see also chapter III). The lattice heat capacity amounts approximately to 1 erg/K and can be neglected. In lower magnetic fields the heat capacity of the metal becomes relatively more important; no relaxation data were taken for magnetic fields lower than 880 Oe.

b) In order to measure the correct temperature difference $T_L - T_s$, at one side of the crystal while the heat input occurs at the other side, the thermal conductivity of the lattice should be good compared to the spin-lattice heat contact. Experimentally the presence of a substantial drop in lattice temperature may be noticed from a small rise in T_L for $t > t_2$, under which condition T_L has decreased to T_s. This rise in T_L may be due to a homogenizing effect of the lattice temperature. Such an effect was observed in CMN samples having a thickness of about 5 mm or more. In order to avoid a similar drop in T_L across the sample, most of the measurements on CMN were performed on a 1.6 mm thick single crystal, in which such a homogenizing effect was not observed. The measurements on $CuCs_2(SO_4)_2.6H_2O$ did not show such an effect, probably because of a better lattice heat conduction and a weaker spin-lattice contact as compared to CMN.

3. Summary of the formulae

In the following considerations a magnetic spin system in which only two energy levels are significantly populated, will be taken into account. Suppose the energetic distance between the lower level $|a\rangle$ with a spin population number N_a,

and the upper level $|b>$ with population number N_b, amounts to $\delta = g\beta H$, where g is the splitting factor and H the appied magnetic field. The following relations hold for N_a and N_b:

$$N_a + N_b = N \tag{2a}$$

$$\frac{N_b}{N_a} = e^{-g\beta H/kT_s} \tag{2b}$$

$$N_a - N_b \equiv n = N \tanh\left(\frac{g\beta H}{2kT_s}\right). \tag{2c}$$

N is the total number of spins. When the sample is in internal equilibrium, T_s equals T_L and we have $n \equiv n_o$. At liquid-helium temperatures it has been observed[1] that the difference in spin population number recovers exponentially towards thermal equilibrium (after e.g. a saturating microwave pulse) describable by a single time constant τ_b, the observed spin-bath relaxation time. Then, for the population difference of a two-level spin system, the relation holds

$$\frac{dn}{dt} = -\frac{n - n_o}{\tau_b}. \tag{3}$$

In the direct process the spin system can only exchange energy with its surroundings through a narrow band of lattice modes, the phonons on speaking terms, near the electron-spin resonance frequency. If this band of phonons can exchange its energy rapidly to a bath of constant temperature, the observed spin-bath relaxation time will be equal to the relaxation time of the direct process, τ_d. (Only for $T \gg 1$ K higher-order relaxation processes should be taken into account). However, if the direct relaxation process is sufficiently fast, the band of phonons will not be able to transfer energy to the bath sufficiently rapidly and the temperature of these phonons will rise to approximately the spin temperature. The observed spin-bath relaxation time will then be governed by the lifetime of the hot phonons, t_{ph}. As a result of a phonon bottleneck τ_b will be larger than τ_d. For the heat flow, $\dot{Q}$, from the spin system to the bath, one can write with eq. (3),

$$\dot{Q} = -\frac{\dot{n}}{2}\delta = \frac{n_o - n}{2\tau_b}\delta. \tag{4}$$

With the aid of the following relation, which is obtained after some simple algebra,

$$(n - n_o) = 2 \tanh\left(\frac{\delta}{2kT_L}\right) \{(N_\delta + 1)\, N_b - N_\delta\, N_a\} \tag{5}$$

where N_δ is the average phonon excitation number and equals $1/(e^{\delta/kT_L} - 1)$, eq. (4) can be written as

$$\dot{Q} = \frac{N}{\tau_b} \tanh^2\left(\frac{\delta}{2kT_L}\right) \cdot \left(\frac{\delta}{e^{\delta/kT_{s-1}}} - \frac{\delta}{e^{\delta/kT_{L-1}}}\right) \tag{6}$$

or alternatively, with the definitions of eq. (1)

$$\frac{\dot{Q}}{(T_s' - T_L')} = \frac{Nk}{\tau_b} \tanh^2\left(\frac{\delta}{2kT_L}\right) \tag{7}$$

From the coupled spin-phonon rate equations[1], Scott and Jeffries derived for the apparent spin-bath relaxation time near thermal equilibrium

$$\tau_b = \sigma \tau_d + \tau_d \,. \tag{8}$$

In this relation the quantity σ is called the bottleneck parameter and it equals

$$\sigma = \frac{\text{energy of the spin system}/\tau_d}{\text{energy of the phonons on speaking terms}/t_{ph}} = \frac{N}{\rho(\nu)\Delta\nu} \tanh^2\left(\frac{\delta}{2kT_L}\right) . \frac{\tau_d}{t_{ph}} \tag{9}$$

From eq. (8) one may notice that for $\sigma \ll 1$ the apparent spin-bath relaxation time will be equal to the direct-process relaxation time. For $\sigma \gg 1$ the energy flow from the spins to the bath is bottlenecked and the relaxation time τ_b equals approximately $\sigma\tau_d$. For the direct process one derives[7], if the states $|a\rangle$ and $|b\rangle$ form a Kramers doublet,

$$\frac{1}{\tau_d} = a g^3 \sin^2\theta \; H^5 \coth\left(\frac{\delta}{2kT_L}\right). \tag{10}$$

In this relation a is a constant and θ is the angle between H and the c axis. When we use the relation

$$g^2 = g_{//}^2 \cos^2\theta + g_\perp^2 \sin^2\theta \tag{11}$$

where $g_\perp = 1.84$ and $g_{//} \approx 0$ for CMN, we obtain for the angular dependence of τ_d in a

constant magnetic field

$$\frac{1}{\tau_d} = b \sin^5\theta \coth\left(\frac{\delta}{2kT_L}\right) \tag{12}$$

in which b is a constant. From this relation it can be seen that $1/\tau_d$ is proportional to $\sin^4\theta$ if $\delta \ll kT_L$. In the case of a severe phonon bottleneck (i.e. $\sigma \gg 1$), one can derive[1)]

$$\frac{1}{\tau_b} = \frac{1}{\sigma\tau_d} = \frac{12\pi\nu^2\Delta\nu}{t_{ph}v_o^3 c} \coth^2\left(\frac{\delta}{2kT_L}\right) \tag{13}$$

where $c = N/V$ is the number of spins per unit volume. Eq. (13) yields in combination with eq. (7) the relation for the heat flow between the lattice and the spin system in case of a phonon bottleneck (viz. eq. (1)) i.e.

$$\frac{\dot{Q}}{(T_L' - T_s')} = A\, t_{ph}^{-1} H^2 \Delta H \tag{14}$$

where we have used the relation $\nu = g\beta H/h$ and $\Delta\nu = g\beta\Delta H/h$. From eq. (10) it can be seen that the direct-process relaxation time is field and temperature dependent i.e. $\propto H^{-4}\ T^{-1}$ for $\delta \ll kT_L$, while the bottlenecked spin-bath relaxation time depends on the temperature as $\tau_b \propto T^{-2}$ for $\delta \ll kT_L$ (eq. (13)), but also depends on the concentration of the spins and the crystal thickness. The thickness dependence enters through the relation $t_{ph} = \eta d/2v_o$.

4. Experimental results

Most of the data reported in this section for CMN have been obtained on a concentrated single crystal of 1.6 mm thickness. The $CuCs_2(SO_4)_2.6H_2O$ samples had a thickness varying between 10 and 2.2 mm. As we have outlined in section 2, the spin-lattice contact was studied for $T_L > T_s$. As has been reported previously[14)] no difference was found in the relaxation data for $(T_L - T_s)$ being positive or negative, within 10%, which uncertainty may be regarded as the experimental error of the measuring points.

4.1. $CuCs_2(SO_4)_2.6H_2O$, results and discussion

$CuCs_2(SO_4)_2.6H_2O$ is a tutton salt which has a monoclinic crystal structure. The crystallographic b axis is normal to the plane, containing the a and c axis which

make an angle of 105° with each other. The unit cell contains two types of copper ions. The crystalline field of both ions have approximately tetragonal symmetry. Two of the principal axes of the susceptibility ellipsoid lie in the ac plane, one (K_1 axis) being the bisector of the tetragonal axes, the other (K_2 axis) being perpendicular to the K_1 axis[29]. The third principal axis (K_3 axis) coincides with the b axis. The ground state is a Kramers doublet and is separated from the next higher-lying orbital levels by 10^4 cm^{-1}. The paramagnetic resonance line consists of four lines due to the nuclear spin 3/2 of the copper nuclei and which are coalesced into a single line at relatively high temperatures with a line width at half height of approximately 400 Oe. $CuCs_2(SO_4)_2.6H_2O$ remains paramagnetic down to very low temperatures ($\simeq$ 0.01 K) and no transition point has been reported thus far. The spin-bath energy transfer measurements were performed with the field along the K_2 axis in which direction the two copper ions behave identically. The results of the spin-lattice heat transfer in the copper salt, as obtained with the method described in section 2, are presented in fig. 3. In this figure $\dot{Q}/(T_L' - T_s')$ is plotted versus H on a logarithmic scale and it can be seen that the curves tend to a H^2 dependence at the high-field side, in agreement with eq. (14). The measurements have been performed on three samples having different thickness (10.0, 5.0 and 2.2 mm). The

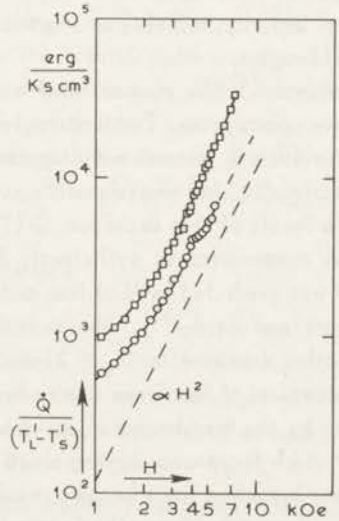

Fig. 3. $\dot{Q}/(T_L' - T_s')$ versus H on a logarithmic scale for $CuCs_2(SO_4)_2.6H_2O$. The dashed line corresponds to the results obtained for a 10 mm thick sample[14].

○ : d = 5.0 mm □ : d = 2.3 mm

results of the 10 mm thick sample have already been published[14] and are represented in fig. 3 by the dashed line which corresponds to the approached H^2 dependence. According to eq. (14) and a hot phonon lifetime of the form $t_{ph} = \eta d/2v_o$, $\dot{Q}/(T_L' - T_s')$ is expected to be inversely proportional to the crystal thickness d. At for instance H = 3000 Oe, where the H^2 dependence of $\dot{Q}/(T_L' - T_s')$ is established to a good approximation, we find the results given in table I.

Table I

	$\dot{Q}/(T_L' - T_s')$ (erg/K cm^3 s)	d(mm)
sample I	1.08×10^3	10.0
sample II	2.0×10^3	5.0
sample III	3.7×10^3	2.3

From these results we may remark that the relation $\dot{Q}/(T_L' - T_s') \propto 1/d$ is approximately fulfilled, indicating a spin-lattice energy transfer which takes place at the crystal boundaries. The small anomaly in the $\dot{Q}/(T_L' - T_s')$ versus H curve at 3.8 kOe as reported for the 10 mm thick sample[14], was found to be slightly present in the 5.0 mm thick sample and did not occur in the 2.2 mm sample. Since the three samples were grown from different aqueous solutions, the occurrence of the anomaly may be related to the presence of an impurity, which can shorten the spin-bath relaxation time in a limited magnetic field region.

As was suggested previously[14] the phonon band width, ΔH, depends on the degree of magnetization of the spin system. For a strongly magnetized system, i.e. $X_s \equiv g\beta H/kT_s \gg 1$, the line width will decrease and approach zero for a completely magnetized spin system. Specifically, our measurements suggested that for $X_s \geq 2$, ΔH decreases markedly. As a result of this decrease, $\dot{Q}/(T_L' - T_s')$ also decreases at a constant field when the temperature is sufficiently lowered, as can be seen from eq. (14). Such an effect was predicted by McMillan and Opechowski[30] and was found experimentally by Svare and Seidel[31]. The reduction of the phonon band width in the copper salt is rather drastical for $X_s \geq 2$, probably because of the fact that the spin resonance line consists of four lines due to hyperfine coupling ($I = 3/2$) which are coalesced into one by the broadening of the dipolar interactions. At low temperatures the dipolar line width decreases, having practically no influence on the overall line width until the four hyperfine lines become resolved.

From the results obtained on the 10 mm thick sample, a hot phonon lifetime t_{ph} was calculated with the aid of relation (14), in which A equals 8×10^{-12} erg/Oe^3 cm^{3}K. Taking for the phonon band width, ΔH, the value of the electron spin resonance line width of 400 Oe[30] which exists in the direction of the crystallographic K_2 axis in which direction the magnetic field was applied, we can calculate $t_{ph} = 4 \times 10^{-5}$s. This value of t_{ph} is much larger than the value found in concentrated

CMN (section 4.2) and that found by Scott and Jeffries[1] and Ruby, Benoit and Jeffries[2], from experiments on dilute rare-earth double nitrates. These latter experiments indicated a t_{ph} being approximately equal to the time needed for the phonons to traverse one half of the crystal thickness. With the relation $\eta = t_{ph}.2v_o/d$ and taking d = 10 mm, $v_o = 2.5 \times 10^5$ cm/s, we obtain for $CuCs_2(SO_4)_2.6H_2O$ a value for η of about 20. From this result it may be concluded that the phonons can only transfer their energy to the bath after being reflected ten times at the crystal boundaries. A similar result was obtained by Nash[23] on $Cu(NH_4)_2(SO_4)_2.6H_2O$, namely $t_{ph} = 2.5 \times 10^{-6}$ s for a 1 mm thick crystal, yielding a value for η of about 13.

As a final result of our experiments on copper tutton salt it was found that the $\dot{Q}/(T_L' - T_s')$ versus H relation did not show a dependence on the contact area between the sample and the metal plates, which were glued to the crystal surface. More specifically, the spin-lattice energy transfer appeared to be constant within the experimental error (≈10%) after changing the crystal to metal contact area from about 2 to 0.3 cm^2. This result is to be understood on the basis of a hot phonon lifetime which is determined by inelastic scattering at the crystal boundaries.

4.2. $Ce_2Mg_3(NO_3)_{12}.24H_2O$, results

Cerium magnesium nitrate crystallizes in the trigonal system. The crystal structure has been determined by Zalkin et al.[32]. The energy levels of the $^2F_{5/2}$ ground state is split by the crystal field into three Kramers doublets. The lowest-lying doublet is separated from the next higher-lying doublet by an amount $\Delta/k \approx 34$ K. Below 1 K merely the lowest doublet is populated so we deal with effective spin ½. The energy level splitting of the lowest doublet is described by an anisotropic splitting factor $g = (g_{//}^2 \cos^2\theta + g_\perp^2 \sin^2\theta)^{1/2}$, where $g_\perp = 1.84$ and $g_{//} = 0.024$.

4.2.1 Field dependence

In fig. 4 the quantity $\dot{Q}/(T_L' - T_s')$ per cm^3 for concentrated CMN has been plotted versus magnetic field, H, on a logarithmic scale. The spin-lattice heat contact was studied while the field made an angle with the crystallographic c axis of 90°, 20° and 10°. All data have been taken at approximately the same temperature of T = 0.25 K. As can be seen from this figure, $\dot{Q}/(T_L' - T_s')$ is proportional to H^2 for $\theta = 90°$ over the whole magnetic-field region measured, which corresponds to the presence of a phonon bottleneck. According to eq. (14) the experimental data correspond to a proportionality constant of $\dot{Q}/(T_L' - T_s')$ with H^2 of $At_{ph}^{-1}\Delta H = 3.05 \times 10^{-3}$ erg Oe^{-2} cm^{-3} $K^{-1}s^{-1}$. For the constant A one obtains for $\theta = 90°$ with $g_\perp = 1.84$ and $v_o = 2.5 \times 10^5$ cm/s a value of $A = 5.69 \times 10^{-12}$ Oe^{-3} cm^{-3} K^{-1}. If we take for ΔH in the maximum g direction a value of 118 Oe[33] which corresponds to the elec-

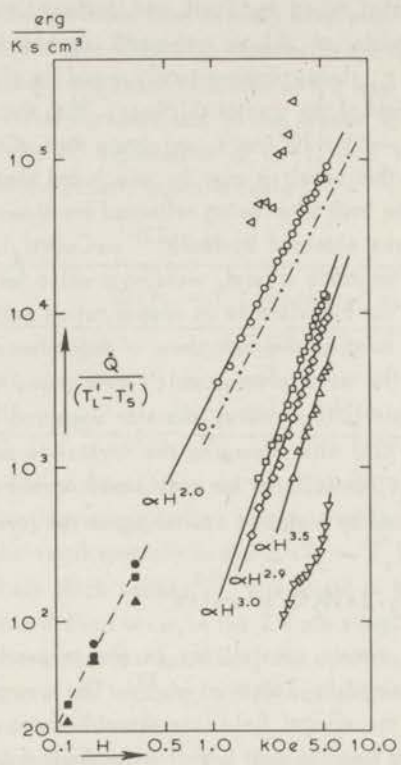

Fig. 4. $\dot{Q}/(T_L' - T_s')$ versus H on a logarithmic scale for CMN, T = 0.25 K.

○: $\theta = 90°$, 100% pure sample, d = 1.6 mm
□: $\theta = 20°$, 100% pure sample, d = 1.6 mm
△: $\theta = 10°$, 100% pure sample, d = 1.6 mm
◇: $\theta = 90°$, 10% diluted sample, d = 2.3 mm
▽: $\theta = 20°$, 10% diluted sample, d = 2.3 mm
◁: $\theta = 20°$, 100% sample + 0.1% Cu, d = 1.6 mm
dash-dotted line: Results of Ruby et al.[2)], extrapolated to a 100% sample, (see text).
dashed line: Low-temperature results (section 4.2.6), d = 1.5 mm.

tron spin resonance line width at half height, $(\Delta H)_{1/2}$, a hot phonon lifetime of $t_{ph} = 2.2 \times 10^{-7}$ s is obtained. The electron spin resonance line width of the sample used, was determined by EPR measurements[33)] at about 1.5 K. The value obtained of 118 Oe, agrees with the value reported by Hudson et al.[34)].

For $\theta = 20°$ and 10° the experimental results yield a higher field dependence of $\dot{Q}/(T_L' - T_s')$ on H, i.e. for $\theta = 20°$ proportional to $H^{3.0}$ and for $\theta = 10°$ proportional to $H^{3.5}$. Actually, the $\theta = 90°$ results presented in fig. 4 were obtained in

three different runs. Two runs were made on different days without removing the sample from between the metal plates and one run was made after the crystal had been removed and polished again without substantially affecting the crystal thickness. No systematic difference in the relaxation data was found between the three runs, the accuracy being about 10%.

4.2.2 Temperature dependence

Spin-lattice contact data have been taken for $\theta = 90°$ in constant magnetic field strengths of respectively 4.4, 3.3 and 2.2 kOe. $\dot{Q}/(T_L' - T_s')$ was determined as a function of the temperature such that $X_s \equiv g\beta H/kT_s$ varied approximately between 6 and 1. As a result of these measurements it was found that $\dot{Q}/(T_L' - T_s')$ was temperature independent in H = 4.4 kOe for $X_s \leq 2.0$. A similar result was found in 3.3 kOe for $X_s \leq 1.6$ and in 2.2 kOe for $X_s \leq 1.3$. These phenomena are similar to those found in the copper tutton salt where the low-temperature data, i.e. for $X_s \geq 2$, could also be described by assuming ΔH to be a function of H/T_s only. At relatively high temperatures $\dot{Q}/(T_L' - T_s')$ was found to be temperature independent.

4.2.3 Angular dependence

The angular dependence of $\dot{Q}/(T_L' - T_s')$ at a constant temperature of T = 0.25 K has been established in magnetic fields of 4.4, 3.3 and 2.2 kOe. The results are shown in fig. 5. From eqs. (7) and (13) one can derive that in a constant magnetic field in the presence of a phonon bottleneck, $\dot{Q}/(T_L' - T_s')$ will be proportional to g^2, if $\Delta\nu = g\beta\Delta H$ is independent of the direction of the magnetic field. It was observed[33] that the full line width at half height, $(\Delta\nu)_{1/2}$, was constant within 5% to θ values of about 20°. For smaller θ values it was found to increase rapidly. Numerical evaluation of the second moment of the resonance line[35], using the formulae of Pryce and Stevens[36], yielded a constant value down to $\theta = 15°$. As can be seen from fig. 5 the g^2 proportionality is fairly well met in a magnetic field of 4.4 kOe to a θ value of about 10°. No relaxation data could be obtained with a reasonable accuracy for $\theta < 10°$, the heat capacity of the sample becoming too small to establish a temperature difference, $(T_L - T_s)$, without warming up the sample appreciably. In a field of 2.2 kOe, $\dot{Q}/(T_L' - T_s')$ decreased faster than proportional to g^2 with decreasing θ, as is apparent from fig. 5.

4.2.4 Concentration and thickness dependence

In fig. 4 also data are presented obtained for a diluted sample of 2.3 mm thickness. The cerium ions were greatly replaced by lanthanum ions and from chemical analysis the cerium-ion concentration, c, was determined to be c = 0.10. The relaxation data were taken in the directions $\theta = 90°$ and 20°. As can be seen from fig. 4, $\dot{Q}/(T_L' - T_s')$ is lowered by approximately a factor 10 for $\theta = 90°$ at H=5000 Oe,

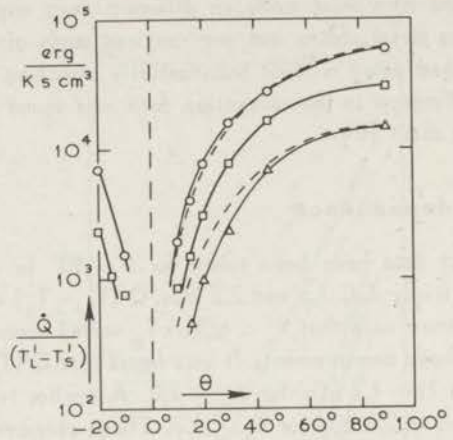

Fig. 5. Angular dependence of $\dot{Q}/(T_L' - T_s')$ for the 100% CMN sample of thickness 1.6 mm, at T = 0.25 K.

○: H = 4.4 kOe
□: H = 3.3 kOe
Δ: H = 2.2 kOe
The dashed lines are proportional to g^2.

compared to the concentrated sample. The field dependence is found to be proportional to $H^{2.9}$, i.e. somewhat more strongly dependent on magnetic field than must be expected for a bottlenecked spin-bath energy transfer. The data obtained for $\theta = 20°$ show a still steeper field dependence towards high fields and show a deviation between 3 and 4 kOe.

Several CMN samples were examined on a thickness dependence of $\dot{Q}/(T_L' - T_s')$. However, a variation in thickness from 4.0 to 1.0 mm of the same single crystal did not show a different $\dot{Q}/(T_L' - T_s')$ versus H relation within the accuracy of the experiment.

4.2.5 Effect of impurities

Most of the experiments were performed on a 1.6 mm thick sample which was grown from very pure cerium nitrate (no detectable impurity present, i.e. $< 10^{-6}$). Additional measurements were performed on a CMN sample of the same thickness, in which 0.1% copper nitrate was added to the aqueous solution. The results of these measurements are also indicated in fig. 4. No relaxation data in the direction $\theta = 90°$ could be obtained because the spin-lattice relaxation time appeared to be too fast to establish a noticeable temperature difference, $(T_L - T_s)$. At H = 1100 Oe a rough estimate can be made of $\dot{Q}/(T_L' - T_s') \approx 1.1 \times 10^6$ erg/cm^3 K s, compared to 0.37×10^4 erg/cm^3 K s for the pure, concentrated sample of 1.6 mm thickness.

Some data were also obtained for $\theta = 20°$, which, however, were too inaccurate in a small field range to establish a field dependence. The addition of 0.1% Pr to the aqueous solution yielded a spin-bath relaxation time which was about 10 times shorter at H = 4000 Oe, than the relaxation time in the concentrated, pure sample. The field dependence of $\dot{Q}/(T_L' - T_s')$, however, could not accurately be determined, but tended to a $H^{3.6}$ dependence. The measurements on a sample in which 4% Nd had been added to the aqueous solution did not give a different $\dot{Q}/(T_L' - T_s')$ versus H relation than that in the concentrated, pure sample. Similar measurements on a concentrated sample CMN containing 5% added Nd or Pr were reported by Hoffman and Sapp[37]. However, in the temperature range of 1.9 K to 3 K and in magnetic fields ranging from 30 to 2880 Oe they did not find an influence on the spin-lattice relaxation time due to the presence of these impurities.

When the experiments on the spin-lattice heat transfer in CMN were started, no special precautions were taken with regard to the presence of several impurities. The measurements on the copper tutton salt did not show a scatter in the results of different samples, and agreed fairly well with each other. The relaxation data obtained for different specimens of CMN with the same thickness, however, did not agree with each other within a factor of two. Most of these $\dot{Q}/(T_L' - T_s')$ data for $\theta = 90°$ were lying above the curve of the concentrated sample of 1.6 mm thickness, presented in fig. 4. Such a behaviour corresponds to a decreased value of the spin-bath relaxation time τ_b. Also some samples showed an anomaly in the $\dot{Q}/(T_L' - T_s')$

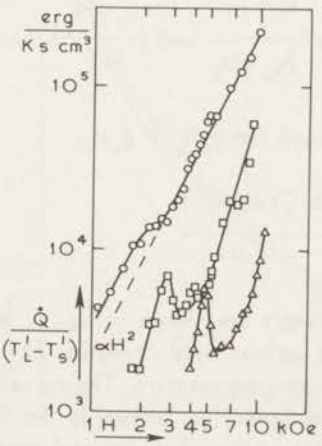

Fig. 6. $\dot{Q}/(T_L' - T_s')$ versus H on a logarithmic plot for a concentrated, impure CMN sample, thickness 4.0 mm.

○: $\theta = 90°$
□: $\theta = 20°$
△: $\theta = 10°$

versus H relation which shifted towards higher fields and became more pronounced towards smaller values of $\bar{\theta}$. An example of a specimen with such an anomaly is shown in fig. 6. No further information on the kind of impurity to which the anomaly may be attributed, was obtained.

4.2.6. Very low temperature and low field experiments *)

The effect of a phonon bottleneck can also be observed at much lower temperatures ($0.02\ K < T < 0.1\ K$) and in lower magnetic fields ($H < 1$ kOe) than was discussed in the above sections. This bottlenecked spin-bath energy transfer becomes apparent when one cools a slab of CMN in thermal contact with a brass plate of much lower temperature. A thin layer of Apiezon N grease between the CMN and the brass plate served to improve the thermal contact. The cooling rate was found to be much lower for pure CMN than for a specimen to which a small amount of Cu ions was added.

The data were obtained in the following way. The susceptibility, χ, was measured as a function of time, while the CMN cooled down to low temperatures. A magnetic field was present in a direction (x direction) perpendicular to the direction in which χ was measured (z direction, lying in the $g_\perp$ plane). From χ and $d\chi/dt$ we derived respectively the temperature, T_s, and the heat flow, $\dot{Q}$, out of the sample, using the following formulae.

$$\chi \equiv \frac{C}{T^*} = \frac{Ng_z^2\beta^2}{4kT^*} = \frac{Ng_z^2\beta^2}{2g_x\beta H_x} \tanh\left(\frac{g_x\beta H_x}{2kT}\right) . \tag{15}$$

In the above relation it is assumed that $g_x H_x \gg g_z H_z$.

$$\dot{Q} = N \frac{g_x^2\beta^2(H_x^2 + b/C)}{4k} \frac{d(1/T^*)}{dt} \tag{16}$$

The results of these measurements are shown in fig. 7, where $\dot{Q}$ per unit contact area is plotted versus $1/T_s$ for various field strengths. The temperature of the metal plate was much lower than the spin temperature. The curves for $H = 440$ Oe and 660 Oe almost coincide; for higher fields (not shown in the figure) approximately the same heat flow was found. The results of the crystal containing some copper impurities are shown in fig. 8. From spectroscopic analysis the Cu content was estimated to be $Cu : Mg = 5 \times 10^{-4}$. In the solution from which the crystal was grown, the ratio was $Cu : Mg = 10^{-2}$.

It can be noticed from figs. 7 and 8 that for fields higher than 400 Oe in the

*) These data were obtained by J. Lubbers.

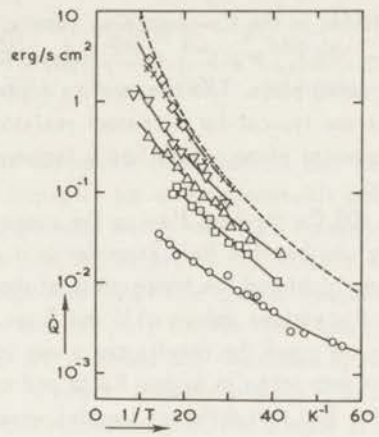

Fig. 7. Relation between the heat flow per cm^2 out of a CMN crystal and the spin temperature. The crystal of thickness of 1.5 mm was glued to a much colder brass plate. The magnetic field was applied along the $g_\perp$ direction.

○ : H = 0 Oe ▽ : H = 320 Oe
□ : H = 110 Oe × : H = 450 Oe
△ : H = 175 Oe ◇ : H = 660 Oe

The dashed line corresponds to $\dot{Q} = 10^5 T^4$ erg/s cm^2.

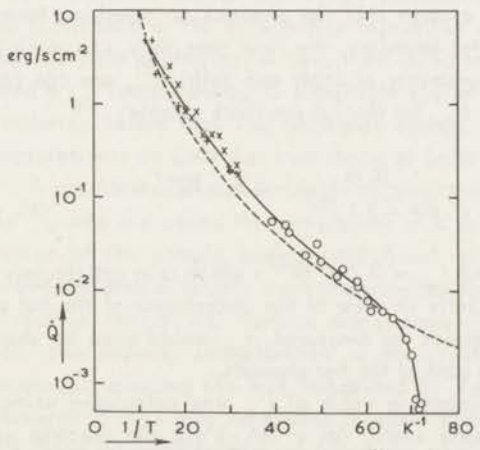

Fig. 8. Relation between the heat flow per cm^2 out of a CMN crystal, containing 0.05% Cu, and the spin temperature. The crystal, with a thickness of 3.8 mm, was glued to a much colder brass plate. The magnetic field was applied along the $g_\perp$ direction.

○ : H = 0 Oe × : H = 100 Oe △ : H = 300 Oe

The dashed line corresponds to $\dot{Q} = 10^5 T^4$ erg/s cm^2.

Cu-free sample and for all fields in the Cu-containing sample, the heat flow can be given by the relation $\dot{Q}/A = 10^5.T_L^4$ erg s^{-1} cm^{-2}, where A is the contact area between the crystal and the metal plate. The temperature dependence as well as the magnitude of the coefficient are typical for a contact resistance of a grease layer between the crystal and the metal plate, which has a temperature much lower than the temperature of the crystal.

In fields smaller than 400 Oe the heat flow in the copper-free sample is field dependent. In order to verify whether this field dependence is due to a bottlenecked spin-lattice heat transfer, we calculated the temperature of the lattice, T_L, from the relation $T_L = (\dot{Q}/10^5 A)^{1/4}$. For various values of H and T we calculated from fig. 7 values for $\dot{Q}/(T_s' - T_L')$ per cm^3, and the results are given in fig. 4 by the dashed line. The agreement with the data taken at higher fields and at a higher temperature is satisfactory considering the fact that different samples were used.

4.3. Discussion of the CMN results

Clearly the field, temperature and angular dependence of $\dot{Q}/(T_L' - T_s')$ indicate the presence of a phonon bottleneck in CMN, as has already been reported by Ruby, Benoit and Jeffries[2] for a 0.2 and 2% cerium in lanthanum magnesium nitrate crystal. Our measurements did not show a dependence of $\dot{Q}/(T_L' - T_s')$ on the smoothness of the crystal surface, nor was a thickness dependence established. For a diluted cerium sample a thickness dependence of τ_b was established by Ruby et al.[2] and Brya et al.[6]. If we assume that the phonons on speaking terms are inelastically scattered at the crystal boundary, the first time they can reach it, as may be concluded from the measurements of Scott and Jeffries[1], one can calculate for the hot phonon time constant, t_{ph}, for the 1.6 mm thick sample:

$$t_{ph} = \frac{d}{2v_o} = \frac{0.16}{2 \times 2.5 \times 10^5} = 3.2 \times 10^{-7} \text{s}.$$

Experimentally we find $t_{ph} = 2.2 \times 10^{-7}$ s which is in satisfactory agreement with the calculated t_{ph}, especially in view of the uncertainty of the hot phonon band width. For the less pure samples we measured, t_{ph} would even be shorter, corresponding to a shorter mean free path of the hot phonons.

From our experiments a value of t_{ph} was calculated using eq. (14) in which for the hot phonon band width, $\Delta H = (h\Delta\nu)/g\beta$, the electron spin resonance line width of approximately 118 Oe was taken[34]. However, in the case of a sufficiently fast direct relaxation rate the hot phonon band width may have a value which is appreciably larger than the spin resonance line width. For a Gaussian shaped spin resonance line, Giordmaine and Nash[16] derived for the hot phonon band width, $\Delta\nu$, the relation

$$\Delta\nu = \frac{g\beta\Delta H}{h(\ln 2)^{1/2}} \{\ln[\tfrac{1}{2} (\frac{\ln 2}{\pi})^{1/2} (\frac{h\nu}{kT_L})^2 \frac{hNt_{ph}}{\rho(\nu)g\beta\Delta H\tau_d}]\}^{1/2} \qquad (17)$$

where ΔH is the spin resonance line width in Oe. However, they argued that the bottlenecked energy transport for a homogeneously broadened spin resonance line does not occur by the phonons which have their frequency near the central frequency of the spin resonance line, but occurs by the phonons which have a frequency in the wings of the spin resonance line. The central-frequency phonons interact strongly with the spin system and can only deliver their energy to the bath by a diffusion process in which they are absorbed and re-emitted by the spins many times (phonon imprisonment) and so, in effect, they are trapped. For the phonons with frequencies in the wings of the spin resonance line, the sample is more or less transparent and they can have mean free paths of the order of the crystal dimensions. So, because of this being trapped of the central-frequency phonons, the effective phonon band width will decrease. No concrete conclusion can be drawn about the value of the hot phonon band width and one may only guess that it is of the order of magnitude of the electron spin resonance line width. In this connection it may be mentioned that Larson and Jeffries[4] conclude from their measurements on the angular dependence of the bottlenecked spin-bath relaxation time of dilute cerium and praseodymium in lanthanum magnesium nitrate, that the spins interact only with the phonons within the paramagnetic line width. A similar result was obtained by Brya et al.[18] who measured a phonon bottleneck in the spin-lattice relaxation of a 1% Ni doped MgO sample, using Brillouin light scattering. A result as obtained for the copper tutton salt, which indicated a t_{ph} corresponding to a multiple scattering of the hot phonons at the crystal boundaries before they can exchange energy with the bath, did not follow from our measurements on CMN nor from those of Scott et al.[2], Ruby et al.[2] and Brya et al.[17]. A possible explanation for these results on double nitrates was suggested by Mills[38], who discussed the possibility of a thin porous layer formed by partial dehydration of the sample surface and filled with helium causing the crystal surface to become almost totally non-reflecting for the hot phonons. It may also be possible that at the crystal surface many magnetic ions have different magnetic properties. Furthermore, irregularities at the crystal surface may result in a very strong magnetic coupling (as was suggested by Van Vleck[39], groups of three or more paramagnetic ions may be closer together than usual). If there is a wide distribution of these different energy splittings the crystal surface, the phonon bottleneck becomes related to the average distance to the crystal surface. Other mechanisms which could determine t_{ph}, such as phonon-phonon scattering or the presence of chemical impurities with different energy splittings, must be rejected since they will result in a t_{ph} which is either frequency (field) or temperature dependent.

As to the temperature dependence of the phonon band width in a constant field

while varying the temperature such that X_s varied between approximately 6 and 1 (section 4.2.2), the following considerations may be taken into account. If, as a result of a fast direct relaxation rate, the band width of the phonons on speaking terms is wider than the spin resonance width and the central-frequency phonons are strongly coupled to the spin system, it may occur that for increasing $g\beta H/kT_s$, the spin resonance line width decreases, but at the same time τ_d will lengthen (see eq. (10)) so that the ineffective central-frequency phonons are somewhat less coupled to the spins. The decrease in spin resonance line width and the increasing effectiveness of the central-frequency phonons in transporting energy to the bath may to some extent cancel, with the result that the apparent phonon line width is initially more or less independent of increasing X_s. When the temperature is further lowered, $\dot{Q}/(T_L' - T_s')$ will finally decrease because of decreasing spin resonance line width. In a smaller magnetic field τ_d, being approximately proportional to H^{-4}, will be longer with the result that the phonon band width is less determined by the phonons with frequencies in the wings of the resonance line and more by the central-frequency phonons. On lowering the temperature in a constant field, the effective band width will sooner decrease with increasing X_s than in a higher magnetic field. The experimental results of section 4.2.2 may be interpreted by the above-given mechanism.

The results of Ruby et al.[2] on a 0.2% and 2% cerium in lanthanum magnesium nitrate sample at temperatures below 1 K and in a field of 3.8 kOe along the $g_\perp$ direction, show a bottlenecked spin-bath relaxation time of

$$\frac{1}{\tau_b} = A \coth^2\left(\frac{g\beta H}{2kT_L}\right) \qquad (18)$$

in which A equals 2.4 for the 0.2% sample and 0.8 for the 2% sample. To compare these results with the data we obtained on the concentrated sample, we may expect that according to eq. (13) τ_b^{-1} is dependent on the cerium concentration, c, through the term $\Delta\nu/c$. From e.g. relation (20) of chapter I, which gives the mean square width of a spin resonance line determined by dipolar interactions only, we may conclude that on diluting a magnetic spin system with diamagnetic ions, $\Delta\nu$ will depend on concentration as $\Delta\nu \propto \sqrt{c}$. Consequently τ_b^{-1} is expected to be proportional to $1/\sqrt{c}$; so we may calculate for the results of Ruby et al., obtained for a 2% cerium sample of 1.0 mm thickness, extrapolated to concentration c = 1, $\tau_b^{-1} = 0.114 \coth^2 (g\beta H/2\ kT_L)$. Together with eq. (7) this result yields

$$\frac{\dot{Q}}{(T_L' - T_s')} = 2.6 \times 10^4 \left(\frac{H}{3800}\right)^2$$

This relation is indicated in fig. 4 by the dash-dotted line. As $\dot{Q}/(T_L' - T_s')$ is expected to be inversely proportional to the crystal thickness (eq. (14)), the above

relation should be divided by a factor 1.6 in order to compare the results of Ruby et al. with our measurements on a concentrated sample with a thickness d = 1.6 mm. With the aid of fig. 4 the so obtained $\dot{Q}/(T_L' - T_s')$ versus H curve lies about a factor of 2.5 below our experimental curve. However, the measured spin resonance line width of the 2% sample of Ruby et al.[1] amounted to 8 Oe, compared to the value of the measured line width of 118 Oe in the concentrated CMN sample. So we may conclude that the relation $\Delta\nu \propto \sqrt{c}$ is an underestimate of the increase of $\Delta\nu$ with increasing concentration. As a consequence the dash-dotted curve in fig. 4 will shift, after having taken into account a possible thickness dependence towards higher values and it may be noticed from fig. 4 that the extrapolated results of Ruby et al. roughly agree with our results. The concentration dependence of the spin resonance line width i.e. varying c with a factor 50 resulting in an increase of line width of a factor of about 15, is not understood.

As to our measurements on a 10% cerium sample of 2.3 mm thickness, we may expect a proportionality constant of $\dot{Q}/(T_L' - T_s')$ with H^2 which is $\sqrt{10} \times 2.3/1.6 \approx$ 4.5 times smaller compared to the results of the concentrated sample on behalf of eqs. (7) and (13). The measured[33] full half width of the resonance line of the 10% sample was determined to be approximately 47 Oe which is not in severe disagreement with the relation $\Delta H \propto \sqrt{c}$. At 5000 Oe where the experimental points of the diluted sample are most reliable, a difference of a factor of approximately 10 can be deduced. A possible explanation for this discrepancy in the calculated and experimental difference of $\dot{Q}/(T_L' - T_s')$ for the 100% and 10% cerium sample may be found in a higher dependence on cerium concentration of the hot phonon band width than proportional to $\sqrt{c}$, as is also suggested by eq. (17). Such dependence would result in a lower value of $\dot{Q}/(T_L' - T_s')$ than according to the expected factor of $\sqrt{c_1/c_2}.d_2/d_1$, where c_1, c_2 and d_1, d_2 are the concentrations and thicknesses for the two samples respectively. The occurrence of a slightly different field dependence of $\dot{Q}/(T_L' - T_s')$ viz. $\propto H^{2.9}$ as was found for the 10% sample (fig. 4) is not understood, although one may expect that upon diluting a sample, the phonon bottleneck will become less important, which may result in a higher field dependence.

The addition of 0.1% copper ions to the solution of concentrated CMN was found to cause a much shorter spin-bath relaxation time τ_b as can be observed from fig. 4. Such a shortening of τ_b after adding some copper nitrate to CMN was also reported by Lubbers (section 4.2.6) and Van Kempen[40]. They found that the time constant of a CMN susceptibility thermometer in zero magnetic field after applying a step in the temperature of the system to which the CMN is thermally connected, is shortened by about a factor of four compared to a thermometer of pure CMN, by adding some copper to CMN. When we assume the cerium spins to interact with the copper spins through spin-spin interactions, this shortening of the spin-bath relaxation time may be due to a shorter spin-lattice relaxation time of the copper ions. Furthermore it may be due to a larger Zeeman splitting of the copper ions than the cerium ions. So the copper ions can interact with a phonon band at higher frequencies, where

there are more lattice oscillators ($\propto \nu^2$). Besides, the copper ions may have a wider spin resonance line width than the cerium ions because of hyperfine interactions ($I = 3/2$). A similar shortening of the spin-bath relaxation time, although less than found for a copper impurity, was found after adding some praseodymium to the CMN solution. Addition of some Nd ions did, however, not show an effect on the $\dot{Q}/(T_L' - T_s')$ versus H relation within 10%, in spite of the wider Nd line width due to hyperfine interactions.

The results, obtained for the supposedly impure CMN samples (section 4.2.5) from which an anomaly occurred in the $\dot{Q}/(T_L' - T_s')$ versus H relation, may be explained by the presence of an impurity which has a shorter spin-bath relaxation time than Ce and with which the Ce ions can exchange energy through spin-spin interactions. The field at which the anomaly occurs may be related to a decreasing contact between Ce and impurity spins. At higher fields we may expect that the spin-bath heat transfer is not influenced by the impurities. As can be seen from fig. 6 the field at which the anomaly occurs is angular dependent and it is more pronounced towards smaller θ values.

Brya and Wagner[26] performed paramagnetic relaxation measurements on a lanthanum magnesium nitrate sample containing a few tenths of a percent cerium. From their measurements at low Zeeman frequencies they deduced an unbottlenecked spin-bath relaxation time (i.e. the direct process relaxation time), in the approximation of $g\beta H \ll kT$, of $1/\tau_d = 93\ T\ s^{-1}$ at $H = 4330$ Oe. From this value of $1/\tau_d$ we may estimate the value of the bottleneck factor, σ, at $T = 0.25$ K and in a magnetic field of 5000 Oe, parallel to the $g_\perp$ direction. Under these conditions one can derive for E_{spins}/E_{ph}, where E_{spins} equals the Zeeman energy of the spin system and E_{ph} the energy of the phonons on speaking terms, a value of 1.14×10^7. For the bottleneck factor we then find approximately $\sigma = (E_{spins}/E_{ph}).(t_{ph}/\tau_d) \approx 150$, which value should be regarded as an order of magnitude estimate only. Since σ appears to be much bigger than unity, a phonon bottleneck must be expected which is also apparently observed experimentally.

Our data for the concentrated CMN sample indicate a field dependence of $\dot{Q}/(T_L' - T_s')$ higher than proportional to H^2 for $\theta = 20°$ and $10°$. From the angular dependence of $\dot{Q}/(T_L' - T_s')$ at constant magnetic field, we observe at 2.2 kOe for decreasing θ, a proportionality of $\dot{Q}/(T_L' - T_s')$ with the splitting factor, higher than g^2, as one should expect on basis of relations (7) and (13) for a bottlenecked spin-bath relaxation. As the field and angular dependence of the bottleneck factor is given by the relation $\sigma \propto H^4 \sin^4\theta$ (eqs. (10) and (12)) in the high-temperature approximation, we expect for e.g. $\theta = 10°$ and $H = 1000$ Oe, a bottleneck factor which is about 10^5 times smaller than for $H = 5000$ Oe parallel to the $g_\perp$ direction. Such a decrease in σ would case it to be much smaller than unity, in which case we may expect the spin-bath relaxation to be determined by the direct process relaxation rate. As the direct process is expected to yield $\dot{Q}/(T_L' - T_s')$ to be proportional to $g^3 \sin^2\theta\ H^5 \tanh(g\beta H/2kT)$, (eq. (10)), the behaviour of the angular and field de-

pendence, which was found towards small values of θ, may indicate the onset of the direct process.

5. Conclusions

The field dependence of $\dot{Q}/(T_L^* - T_s^*)$ in $CuCs_2(SO_4)_2.6H_2O$ and $Ce_2Mg_3(NO_3)_{12}.24H_2O$ strongly suggest the presence of a phonon bottleneck. As a result of the $\dot{Q}/(T_L^* - T_s^*)$ versus H relation it may be concluded that in the copper salt the hot phonons can exchange their energy with their surroundings after multiple reflection at the crystal boundaries. In the cerium salt the hot phonons seem to be inelastically scattered the first time they reach the crystal boundary; some of our measurements even suggest a still shorter t_{ph}, which may be related to the presence of e.g. cracks in the sample. The absence of an experimentally observed thickness dependence of $\dot{Q}/(T_L^* - T_s^*)$ would be in accordance with a breakdown of the phonon bottleneck, not primarily determined by the crystal boundaries. Also indications are found that the hot phonon band width is more or less determined by the direct relaxation rate and may exceed the spin resonance line width. The response time of a CMN sample, used as a thermometer, is greatly improved by adding some copper as an impurity. Experimental indications for the occurrence of the direct process are found in the dependence of $\dot{Q}/(T_L^* - T_s^*)$ on magnetic field strength and on θ, at least at small values of θ.

References

1) Scott, P.L. and Jeffries, C.D., Phys.Rev. 127(1962)32.
2) Ruby, R.H., Benoit, H. and Jeffries, C.D., Phys.Rev. 127(1962)51.
3) Schulz, M.B. and Jeffries, C.D., Phys.Rev. 149(1966)270.
4) Larson, G.H. and Jeffries, C.D., Phys.Rev. 141(1966)461; 145(1966)311.
5) Van den Broek, J. and Van der Marel, L.C., Physica 29(1963)948; 30(1964) 565.
6) Brya, W.J. and Wagner, P.E., Phys.Rev. 157(1967)400.
7) Orbach, R., Proc.Roy.Soc. A264(1961)458.
8) Gill, J.C., Proc.Phys.Soc. 82(1963)1066.
9) Cooke, A.H., Finn, C.B.P., Mangum, B.W. and Orbach, R.L., J.Phys.Soc. Japan 17(1962)462.
10) Van Vleck, J.H., Phys.Rev. 59(1941)724.
11) Gorter, C.J., Van der Marel, L.C. and Bölger, B., Commun. Leiden, Suppl. No. 109c; Physica 21(1955)103.
12) Giordmaine, J.A., Alsop, L.E., Nash, F.R. and Townes, C.H., Phys.Rev. 109 (1958)302.
13) Faughnan, B.W. and Strandberg, M.W.P., Phys.Chem.Sol. 19(1961)155.
14) Miedema, A.R. and Mess, K.W., Commun. Leiden 340c; Physica 30(1964)1849.

15) Stoneham, A.M., Proc.Phys.Soc. 86(1965)1163.
16) Giordmaine, J.A. and Nash, F.R., Phys.Rev. 138(1965)1510.
17) Brya, W.J. and Wagner, P.E., Phys.Rev.Lett. 14(1965)431.
18) Brya, W.J., Geschwind, S. and Devlin, G.E., Phys.Rev.Lett. 21(1968)1800.
19) Berman, R., Proc.Roy.Soc. A208(1951)190.
20) Bömmel, H. and Dransfeld, K., Phys.Rev.Lett. 2(1959)298.
21) Jacobsen, E.H., Phys.Rev.Lett. 2(1959)249.
Jacobsen, E.H., Shiren, N.S. and Tucker, E.B., Phys.Rev.Lett. 3(1959)81.
22) Bömmel, H. and Dransfeld, K., Phys.Rev. 117(1960)1245.
23) Nash, F.R., Phys.Rev.Lett. 7(1961)593.
24) Nash, F.R., Phys.Rev. 138(1965)1500.
25) Schedewie, F.J., Phys.Stat.Sol. 30(1868)251.
26) Brya, W.J. and Wagner, P.E., Phys.Rev. 147(1966)239.
27) Bailey, C.A., Proc.Phys.Soc. 83(1964)369.
28) Hudson, R.P. and Kaeser, R.S., Physics 3(1967)95.
29) Bleaney, B., Penrose, R.P. and Plumpton, B.I., Proc.Roy.Soc. 198(1949)406.
30) McMillan, M. and Opechowski, W., Canad. J.Phys. 38(1960)1168.
31) Svare, I. and Seidel, G., Phys.Rev. 134(1964)172.
32) Zalkin, A., Forrester, J.D. and Templeton, D.H., J.Chem.Phys. 39(1963)2881.
33) Zimmerman, N.J., private communication.
34) Hudson, R.P., Kaeser, R.S. and Radford, H.E., VII Int.Conf. on Low Temp. Phys. Toronto 1969, pg. 100.
35) De Boo, N., private communication.
36) Pryce, M.H.L. and Stevens, K.W.H., Proc.Phys.Soc. 63(1950)37.
37) Hoffman, J.T. and Sapp, R.C., J.Appl.Phys. 39(1968)837.
38) Mills, D.L., Phys.Rev. 133(1964)876.
39) Van Vleck, J.H., Conf. on Quantum Electronics, Bloomfield, N.J. (1959).
40) Van Kempen, H., Thesis Leiden, 1965.

Chapter V

MAGNETIC PROPERTIES AND SPIN-LATTICE RELAXATION OF $CoCs_3Cl_5$ AND $CoCs_3Br_5$

1. Introduction

Recently the occurrence of lambda-type specific-heat anomalies in $CoCs_3Cl_5$ and $CoCs_3Br_5$ at $T_N = 0.527$ K and $T_N = 0.282$ K respectively were reported[1,2]. These two salts both constitute a relatively simple magnetic system. EPR measurements[3] show that all Co ions are magnetically equivalent. From the crystal structure determination and from the magnetic equivalence of all Co ions, it can be argued that the Co ions are arranged in a simple tetragonal Bravais lattice, the ratio of the c and a axis being approximately 1.11[5]. The EPR results show further that the fourfold degenerate ground state is split into two doublets due to a tetragonal distortion of the cubic crystalline field along the crystallographic c axis. The zero-field splitting of the two doublets amounts to $2D/k = -12.4$ K and -15.4 K for the chloride and bromide respectively, the $s_z = \pm 3/2$ doublet being lowest. At low temperatures, i.e. in the region around 1 K, only this lowest doublet is populated. Hence it may described by an effective spin ½ with a very anisotropic splitting factor, i.e. $g_{//} = 7.20$ and $g_{\perp} = o$ for the chloride and $g_{//} = 7.26$ and $g_{\perp} = o$ for the bromide. The very anisotropic g value and the occurrence of a phase transition in both salts at temperatures much below D/k, imply that the exchange interaction between the Co ions may be described by the Ising model.

On the basis of crystal structure, paramagnetic resonance and specific heat data it was found that the molecular field in $CoCs_3Cl_5$ is predominantly due to strongly anisotropic nearest neighbour exchange. From the heat-capacity data it was possible to derive an average value for the exchange constants, which were found to agree with the results[3] of electron paramagnetic resonance measurements on exchange coupled pairs of Co ions substituted in $ZnCs_3Cl_5$. From these results it followed that the Co ion is coupled to its six nearest neighbours with approximately equal strength, which mainly originates from exchange and further also from dipolar interaction, and that further neighbours can be neglected to a good approximation. For many purposes the chloride can be considered therefore, to be a three-dimensional, almost simple cubic, Ising system.

The results of the heat-capacity measurements on $CoCs_3Br_5$ differ appreciably from those on the chloride, since entropy and energy involved in short-range ordering are much larger than in the chloride and indicate a predominantly two-dimensional character of spin ordering.

The experimental heat-capacity versus temperature curve shows similarity to the theoretical curve, based on exact calculations of Onsager on the two-dimensional simple square lattice of Ising spins.

It will be seen in this chapter that antiferromagnetic interactions predominate in these salts and that the chloride and bromide show interesting features when compared to theoretical calculations on the Ising model, applied to antiferromagnetic ordering in two and three-dimensional spin systems.

2. Experimental method

The inner apparatus used, was the same as that shown schematically in fig. 1 of chapter IV. In all measurements described in this chapter a lead heat switch was used. The following experiments were performed on both cobalt salts.

2.1. Susceptibility measurements

Since both $CoCs_3Cl_5$ and $CoCs_3Br_5$ single crystals have a $g_\perp$ value zero at low temperature, the crystals were mounted horizontally in the measuring coils. Rectangular flat single crystals were mounted between two brass plates with Apiezon N grease. One of the plates was connected to the carbon resistor, the other one to the heater and to the heat switch. In most of the susceptibility measurements the switch was kept in the normal state, while the desired temperature could easily be obtained by heating the sample with the heater. Measurements were taken only when a stationary temperature was obtained.

2.2. Specific-heat measurements

The specific-heat measurements on single crystals in a magnetic field were carried out with the same apparatus. However, the crystal had to be mounted vertically, because the magnetic field which had to be directed along the $g_{//}$ direction, was horizontal. The heater and the thermometer were connected to the same brass plate. In this apparatus we were able to study the specific heat anomaly as a function of magnetic field strength. Accurate specific heat data could be obtained by heating temperature differences between the before period and after period of about 1.5 millidegrees.

2.3. Magnetic field versus temperature diagram

Magnetic field vs temperature diagrams for $CoCs_3Cl_5$ and $CoCs_3Br_5$ single crystals were derived by observing the temperature variation as the magnetic field, which was directed along the c axis, was slowly varied. The isentropes for the chloride, shown in fig. 8, were determined by following the temperature while the magnetic field was varied from 0 to about 2500 oersteds in 150 seconds. At temperatures above 0.3 K the variation of temperature, the field being changed up- or downwards, was reversible. Below this temperature an irreversible temperature rise in

low fields, when going to higher fields, was observed. This is probably caused by Joule heating in the brass plates of the sample, the specific heat being very small in this temperature region. At the lowest temperatures the temperature minima were determined by cooling the sample in a magnetic field of 2500 oersteds to the desired temperature and lowering the field while the temperature change was observed. Precise measurements were made by following the temperature and field variation on a recorder in the immediate vicinity of the line connecting the temperature minima in the H vs T diagram. In the bromide crystals a similar procedure was followed. In order to obtain reasonable temperature variations the field had to be changed at a rate three times slower than in the case of the chloride,

2.4. Relaxation measurements

Some relaxation data below 1 K were obtained for both salts. The mounting was the same as for the susceptibility measurements. The experimental procedure was identical to the one described extensively in chapter III, section 2. A typical example of an experimental point obtained for $CoCs_3Cl_5$ is shown in fig. 1. From the known heat flow between the lattice and the spin system and the recorded temperature change at t_2, spin-lattice relaxation data can be obtained. In the temperature range shown in fig. 1, the whole procedure lasted for about 120 seconds. At 0.2 K this time increased to 600 seconds.

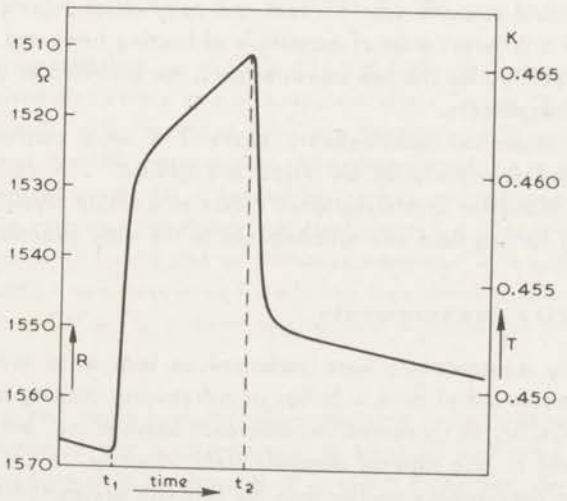

Fig. 1. Temperature and resistance of the carbon resistor as a function of time. At t_1 the sample heating is started, at t_2 heating is stopped.

As a definition of relaxation time, τ, we take [4]

$$\frac{dT_s}{dt} = -\frac{T_s - T_L}{\tau} . \tag{2.1}$$

in which T_L and T_s equal the lattice and spin temperature respectively. This definition is a high-temperature approximation to the definition of spin-lattice relaxation time (chapter IV, eq. (3)) and holds if the temperature difference $(T_L - T_s) \ll T_L$. In the case shown in fig. 1, we obtain $T_s - T_L = 0.010\ K \ll T_L = 0.46\ K$. One can also write for the heat flow to the spin system

$$\dot{Q} = c\frac{dT_s}{dt} \tag{2.2}$$

in which c is the specific heat of the spin system. Equations (2.1) and (2.2) yield

$$\frac{1}{\tau} = \frac{dT_s/dt}{(T_L - T_s)} = \frac{\dot{Q}}{c(T_L - T_s)} . \tag{2.3}$$

By measuring the spin temperature T_s, and the lattice temperature T_L, at a given heat flow $\dot{Q}$, and if one knows the specific heat of the sample, one can determine τ. In principle one could measure specific heat and spin-lattice relaxation simultaneously. Because of a different order of magnitude of heating times and a slight modification in the apparatus for the two measurements, we preferred to obtain the data in two different arrangements.

Spin-lattice relaxation measurements above 1 K were carried out with an apparatus described previously by De Vries and Livius[28]. A constant magnetic field was applied along the crystallographic c axis of a single crystal of $CoCs_3Cl_5$ and a sinusoidally varying field was superimposed in the same direction.

3. Susceptibility measurements

Susceptibility measurements were performed on both salts with the aid of a ballistic galvanometer and of an a.c. bridge at a frequency ranging from 20-260 Hz. As far as the $CoCs_3Br_5$ is concerned, no difference between a.c. and d.c. measurements was observed in zero external magnetic field. However, in $CoCs_3Cl_5$ the a.c. susceptibility was considerably smaller than the ballistic susceptibility at $T < 0.9$ K. The different behaviour of the two salts may be related to the difference in spin-lattice relaxation times (cf. section 5). The results of the susceptibility measurements along the c axis of single crystals are shown in fig. 2A and 2B for $CoCs_3Cl_5$ and in fig. 2C–2D for $CoCs_3Br_5$. No appreciable susceptibility in directions perpen-

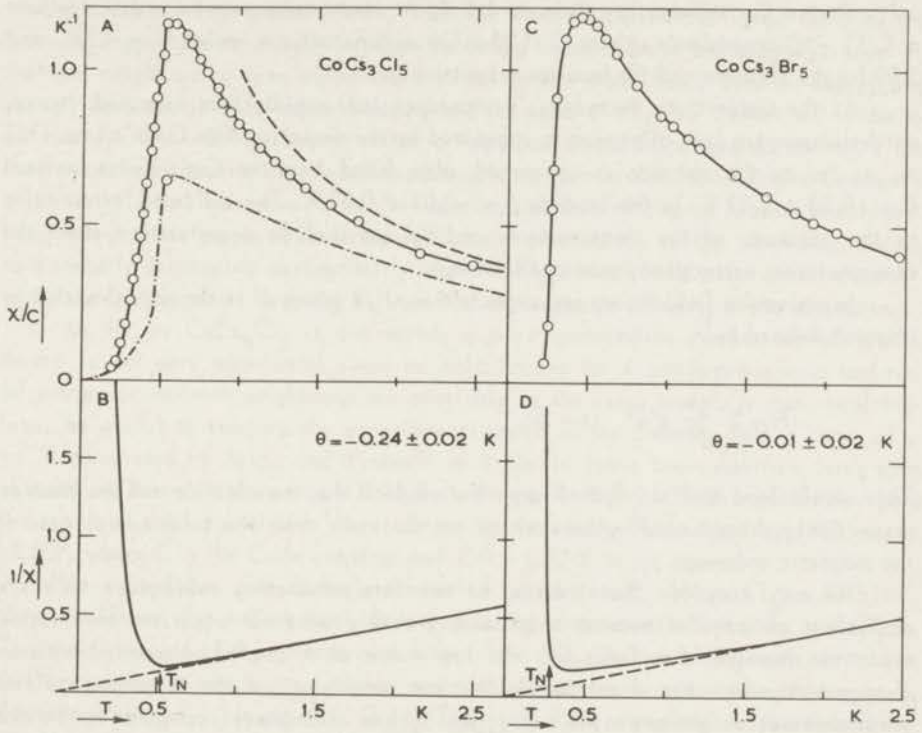

Fig. 2. Molar susceptibility, χ, of $CoCs_3Cl_5$ and $CoCs_3Br_5$ versus temperature T. χ has been measured along the c axis of a single crystal. Curves 2B and 2D are derived from fig. 2A and 2C with the aid of the Curie constants, 4.99 and 5.09 per mole for the chloride and bromide respectively. The dash-dotted curve in 2A is Sykes' and Fisher's theoretical result for a two-sublattice s.c. antiferromagnet (6 antiparallel n.n.); the circle indicates the theoretical Néel point T_N. The scale factors for this curve are based on C = 4.99 and an exchange parameter $J'/k = 0.12$ K, taken from ref. 1. The dashed curve represents Curie's law from which it is seen that the Curie-Weiss constant of $CoCs_3Cl_5$ is much smaller than according to Sykes e.a. for 6 antiparallel n.n.

dicular to the c axis could be found. Demagnetizing corrections were not applied to the data; we estimate that a correction of at most 5% has to be applied to χ, the correction being largest in the bromide at $T \approx 0.5$ K; further, the Curie-Weiss constant may require an upward correction of at most 0.04 K. Small corrections to the data between 2 K and 4 K (not shown on the graph, but significant for determining the Curie-Weiss constant) were applied for the population density of the higher doublet at $2D/k = 12.4$ K and $2D/k = 15.4$ K in the chloride and bromide respectively. After subtraction of the higher doublet contribution it is found (cf. fig. 2) that both

salts obey a Curie-Weiss law down to 1.5 K. At lower temperatures χ deviates from a $C/(T-\theta)$ dependence, where C is the Curie constant per mole, C = 4.99 and 5.09 for the chloride and the bromide respectively.

As the temperature decreases, χ increases less rapidly than expected. Hence, antiferromagnetic spin alignment is suggested by the deviation from Curie's law. This is, as far as the chloride is concerned, also found from the Curie-Weiss constant $\theta = -0.24 \pm 0.02$ K. In the bromide $\theta = -0.01 \pm 0.02$ K. The indicated errors refer to the accuracy of the measurements and do not include uncertainties about the demagnetizing corrections, mentioned above.

In molecular-field theory one expects $\theta = zJ'/k$ where J' is the (Ising)-exchange integral defined by[1)]

$$H = \sum_{i,j} \frac{J'}{s^2} s_i^z s_j^z \quad (s = \tfrac{1}{2}).$$

This would lead to $\theta = -0.66$ K and $\theta = -0.44$ K for the chloride and the bromide respectively, based on J' values which are derived[1)] from the total energy gain of the magnetic ordering.

We may conclude that ordering in two interpenetrating sublattices with six equivalent antiparallel nearest neighbours probably does not occur in the chloride or in the bromide. For $CoCs_3Cl_5$ the low value of θ can be reconciled with an arrangement which has 4 antiparallel nearest neighbours in the ab plane and two parallel nearest neighbours in the c direction. Such an arrangement, compared to the two interpenetrating sublattices, is the next most simple one in accordance with the crystal symmetry and does give a much lower θ. Then on the basis of molecular field theory θ would be 1/3 of that for six antiparallel neighbours, i.e. $\theta = -0.22$ K., to be compared to the experimental value -0.24 ± 0.02 K.

However, very recently Hamman[5)] performed neutron diffraction experiments on $CoCs_3Cl_5$ at a temperature of 0.31 K. As a result of these experiments a magnetic structure was proposed in which each Co ion is surrounded by four antiparallel nearest neighbours in the ab plane and by two next-nearest neighbours along the c axis which are also antiparallel to the central Co ion. This arrangement along the c axis is opposite to that which was assumed above, on basis of the observed Curie-Weiss constant. To explain the stability of the newly proposed magnetic structure, which is not the simplest one in view of the relatively large ferromagnetic exchange interaction along the c axis[3)], third- and fourth-neighbour interactions have to be assumed. However, a consistent analysis, involving two extra exchange constants can not be made in view of the total ordering energy gain and the Curie-Weiss θ, so it may be concluded that the magnetic structure of $CoCs_3Cl_5$ has not been established without ambiguity and additional experimental results are required.

If one supposes strong resemblance between the chloride and the bromide with respect to the kind of magnetic ordering, as we assumed for the chloride on basis

of the susceptibility measurements, then the small experimental value for θ in the bromide suggests a relatively stronger exchange interaction of ferromagnetic sign of the two neighbouring ions along the c axis. On the other hand, data on energy and entropy involved in short-range ordering and the ratio of kT_N/zJ' (where zJ' is derived from $\frac{1}{2}zJ'/k = E/R$) suggest rather a two-dimensional Ising system; in ref. 1 the theoretical heat capacity of a two-dimensional Ising spin system (according to Onsager's exact calculation) was seen to fit the experimental data of c quite reasonably. Therefore, we suppose magnetic ordering to occur predominantly in the ab plane, leading to a steadily decreasing susceptibility when $T \to T_N$, which is to some extent cancelled by the ferromagnetic coupling between the net magnetic moments of the ab planes.

As far as $CoCs_3Cl_5$ is concerned, a more quantitative comparison of χ with theory is not very meaningful since no calculations for 4 antiferromagnetic and two ferromagnetic nearest neighbours are available in the Ising model. It may, nevertheless, be useful to compare the experimental result of the chloride with a curve of χ vs T calculated by Sykes and Fisher[6] in a simple cubic two-sublattice Ising spin system; the latter is shown as a dash-dotted curve in fig. 2A. Sykes and Fisher give the result of their calculation as a relation between $zJ'\chi/Nm^2 = (zJ'/k)(\chi/C)$ versus kT/zJ', where C is the Curie constant and $J'/k = 0.12$ K in our case.

Since in Sykes and Fisher's theoretical estimates T_N obeys $kT_N = 0.751zJ'$, they would find $T_N = 0.54$ K as compared to the experimental value $T_N = 0.527$ K. The main interest of this comparison arises from the position of T_N with respect to the temperature at which χ_{max} occurs and with respect to the steep ascent of χ vs T. Experimentally it is found that $(T_{max}/T_N)_{exp} = 1.06$, compared to the theoretical result of $(T_{max}/T_N)_{theor} = 1.10$ for a simple cubic lattice; the ratio of $\chi(T_N)$ and χ_{max} equals 0.98, whereas Sykes and Fisher predict $\chi(T_N)/\chi_{max} = 0.97$[5]. This is to be contrasted with the situation in the bromide. Taking Sykes and Fisher's calculations of χ for a two-dimensional simple square Ising spin system, we arrive at: $(T_{max}/T_N)_{theor} = 1.537$ to be compared to the experimental result $(T_{max}/T_N)_{exp} = 1.60$; similarly[5] $(\chi(T_N)/\chi_{max})_{theor} = 0.64$, while $(\chi(T_N)/\chi_{max})_{exp} = 0.53$. We may conclude from these comparisons that the magnetic susceptibility of the bromide has features more or less in common with the two-dimensional Ising antiferromagnet.

It is interesting to compare the behaviour of χ for $CoCs_3Br_5$ at the critical point with Sykes and Fisher's calculated asymptotic formula:

$$\chi T/C \sim B_{\pm} \left|1 - \frac{T_N}{T}\right|^{\ln \left|1 - \frac{T_N}{T}\right|} + \xi_c \qquad (3.1)$$

where

$$B_+ = 0.317 \quad (T > T_N)$$
$$B_- \leq 0.317 \quad (T < T_N)$$
$$\xi_c = 0.157$$

for a simple square two-sublattice antiferromagnet.

The experimental result is shown in fig. 3; although the functional behaviour of χ vs T agrees with eq. (3.1), the parameters $(B_+)_{exp} = 0.43$, $(B_-)_{exp} > 0.5$ and $(\xi_c)_{exp} = 0.205$ are much larger than Sykes and Fisher's theoretical values mentioned above.

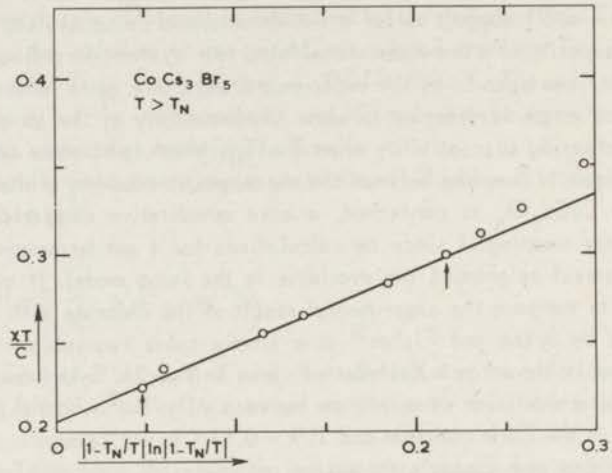

Fig. 3. Susceptibility of $CoCs_3Br_5$ at temperatures slightly above the Néel point, plotted versus

$$\left|1 - \frac{T_N}{T}\right| \ln \left|1 - \frac{T_N}{T}\right|.$$

The two points indicated by arrows refer to $T/T_N = 1.01$ and $T/T_N = 1.10$.

We do not claim sufficient accuracy of the χ measurements at the critical point for an experimental proof of the validity of eq. (3.1), but the above comparison serves to illustrate the steep ascent of χ vs T at the critical point, the latter being defined by the peak in the heat capacity. This steepness does not seem to be characteristic for the three-dimensional Ising system, since theoretically the $B_\pm$ values for three-dimensional antiferromagnets are not larger than $B_\pm$ values for two-dimensional antiferromagnets. We ascribe the steep rise at T_N to the influence of ferromagnetic couplings (partly of dipolar origin) between nearest neighbours along the c axis.

D.c. susceptibility measurements were also carried out in magnetic fields of moderate strength both on $CoCs_3Cl_5$ and $CoCs_3Br_5$. In $CoCs_3Cl_5$, a small magnetic field is already sufficient to let the temperature, at which χ_{max} occurs, coincide with $T_N(H)$, as can be concluded from table I.

In fig. 4 the d.c. susceptibility of $CoCs_3Cl_5$, divided by the Curie constant is shown for several longitudinal magnetic fields.

In $CoCs_3Br_5$ the results show distinctly that the position of the maximum susceptibility, χ_{max}, shifts towards $T_N(H)$, in other words the temperature at which

Table I

H(Oe)	$T_N(H)$ (K)	T_{max} (K)	$T_N(H)/T_{max}$
0	0.527	0.56	0.94
510	0.508	0.52	0.98
1020	0.463	0.46	1.0

Comparison of the Néel point in a magnetic field, $T_N(H)$, and the temperature at which the susceptibility has a maximum, T_{max}, for $CoCs_3Cl_5$.

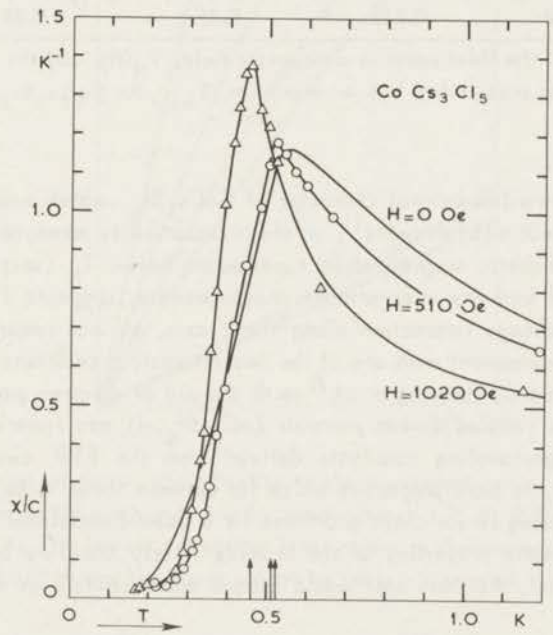

Fig. 4. Parallel d.c. susceptibility of $CoCs_3Cl_5$ in a magnetic field H, applied along the crystalline c axis. The position of the specific heat singularity, $T_N(H)$, is indicated by the three vertical arrows at $T_N(0) = 0.523$, $T_N(510) = 0.508$ and $T_N(1020) = 0.460$ K.

O : 510 Oe, Δ : 1020 Oe.

χ_{max} occurs is decreased more strongly than T_N when applying a magnetic field along the crystalline c axis, as can be seen from table II. Further, the maximum in the susceptibility curve becomes higher and sharper.

In this connection it may be noted that an increase in χ at temperatures below T_N and also the occurrence of a singularity of χ in the presence of a magnetic field is predicted on the basis of exact calculations by Fisher[7] on his

super exchange two-dimensional Ising antiferromagnet. Although we find in $CoCs_3Br_5$ results of χ measurements in the presence of a magnetic field, which are similar to those in $CoCs_3Cl_5$, we note that the sharp maximum in χ is more clearly observed in the three-dimensional $CoCs_3Cl_5$ than in the predominantly two-dimensional $CoCs_3Br_5$.

Table II

H(Oe)	$T_N(H)$ (K)	T_{max} (K)	$T_N(H)/T_{max}$
0	0.282	0.45	0.63
1020	0.212	0.25	0.85

Comparison of the Néel point in a magnetic field, $T_N(H)$, and the temperature at which the susceptibility has a maximum, T_{max}, for $CoCs_3Br_5$.

In spite of the two-dimensional character of $CoCs_3Br_5$, which conclusion is based on the specific-heat measurements[1], on the susceptibility measurements and on the results of the adiabatic magnetization experiments below T_N (section 4.2), the low θ value, as found from the susceptibility measurements, suggests a relatively strong ferromagnetic exchange interaction along the c axis, as was remarked before. This suggestion is in agreement with one of the two alternative solutions for the exchange constants measured by Henning et al.[3] with the aid of electron paramagnetic resonance of exchange coupled Co-ion pairs in $ZnCs_3Br_5$. It was remarked by Wielinga[2] that the exchange-coupling constants derived from the EPR measurements would suggest $CoCs_3Br_5$ to have properties which lie between those to be expected for the one-dimensional Ising linear chain and those for a three-dimensional Ising system. As to the thermodynamic properties of the bromide it may therefore be quite possible, although accidental, that this salt would behave approximately as a two-dimensional Ising system.

The magnetization of $CoCs_3Cl_5$ as a function of the magnetic field was measured*) by a Faraday balance method and is shown in fig. 5.

From the saturation value of σ at large H and T = 1.35 K we deduce that there is agreement to within the measuring accuracy (< 1%) with the results of the g-value measurements mentioned in refs. 1 and 3.

The Brillouin curves on basis of those g values have not been drawn in fig. 5, but they deviate only slightly from the measured points, the difference being smaller than a few hundred oersteds on the horizontal scale and this might be due to demagnetizing effects. The straight lines referring to the $g_\perp$ direction are due to admixture of the excited states into the ground state by the magnetic field which is related to the (in first order) temperature independent Van Vleck paramagnetism.

*) These measurements were performed by J.J. Giesen.

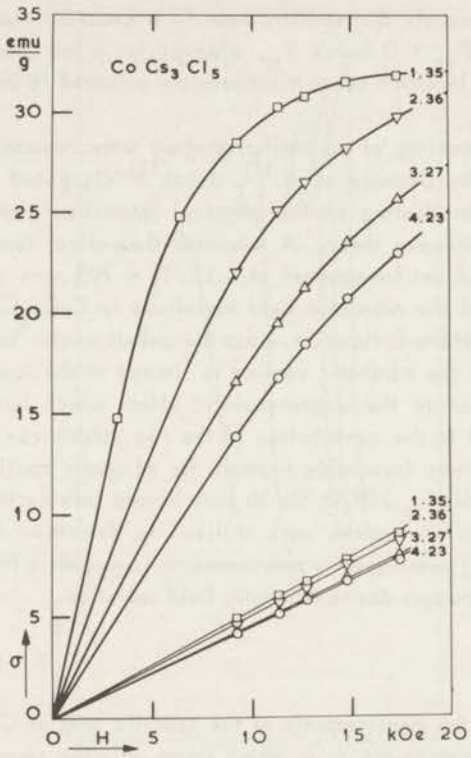

Fig. 5. Magnetization, σ, of $CoCs_3Cl_5$ in electromagnetic units as a function of magnetic field strength and for temperatures 1.35 K, 2.36 K, 3.27 K and 4.23 K. The lowest set of four lines refers to the magnetic moment in the $g_\perp$ direction and the upper curves to the $g_{//}$ direction.

4. Phase boundary

In order to obtain supporting evidence that $CoCs_3Cl_5$ and $CoCs_3Br_5$ are antiferromagnetic below the transition point, we tried to demonstrate the existence of a phase boundary between the paramagnetic and antiferromagnetic region. As is well known, an antiferromagnet displays a critical-field curve in the H – T plane[8,9,27]. When a magnetic field is applied adiabatically along the preferred axis of magnetization and at a temperature below the critical point in zero field, $T_N(0)$, a cooling of the sample is observed on account of the thermodynamic relation for the magnetocaloric effect

$$\left(\frac{dT}{dH}\right)_S = -\frac{T}{c_H}\left(\frac{\partial M}{\partial T}\right)_H ,$$

in which relation c_H equals the specific heat in a constant magnetic field. For an antiferromagnet $(\partial M/\partial T)_H > 0$ below T_N, whereas for a ferromagnet or paramagnet usually $(\partial M/\partial T)_H < 0$, in which cases a temperature increase is observed on applying a field adiabatically.

Experiments on cooling of an antiferromagnet were reported a.o. by Schelleng and Friedberg[10] and by Giauque et al.[11]. Joenk[12] discussed the dependence of adiabatic magnetization cooling on the physical quantities characterizing an antiferromagnet, using spin-wave theory. A maximum theoretical temperature change for a hypothetical uniaxial antiferromagnet of $-\Delta T/T_i = 70\%$ was derived. As a result of the measurements of the adiabatic field variations in $CoCs_3Cl_5$ a maximum value of $-\Delta T/T_i = 40\%$ was obtained. However, since the cobalt nuclei have a non-zero magnetic moment ($I = 7/2$) the adiabatic cooling is limited at the lowest temperatures by the nuclear contribution to the magnetocaloric effect which has the opposite sign ($\partial M/\partial T > 0$) compared to the contribution of the two sublattices. As will be shown in chapter VI a much more favourable example for adiabatic cooling is found in antiferromagnetic $Ni_3La_2(NO_3)_{12}.24H_2O$, the Ni ions having zero nuclear spin.

Two experimental procedures were utilized to determine the phase boundary for both cobalt salts; 1) heat-capacity measurements in magnetic fields and 2) measurements of temperature changes due to adiabatic field variation.

4.1. $CoCs_3Cl_5$

Some results on the measurements of the specific heat of $CoCs_3Cl_5$ in external magnetic fields are shown in fig. 6, in which figure only the smoothed curves through the experimental points are shown. The position of the specific-heat maximum shifts to lower temperatures with increasing H. It is found that it broadens when H increases and this ultimately restricts the accuracy of the determination of the position $T_N(H)$, of the anomaly in c_H. No attention was paid to changes in the form of the curve, but, for instance the steep slope at the high-temperature side of T_N remains practically unaltered and provides additional means for determining the shift of the singularity. $T_N(H)$ is plotted versus H^2 in fig. 7, from which it is seen that the experimental points can be fitted by a linear relation between T_N and H^2, namely

$$T_N(H)/T_N(0) = 1 - AH^2 = 1 - 1.10 \times 10^{-7}H^2 \quad (H \text{ in Oe}). \tag{4.1}$$

From the thermodynamic relation between magnetization M, entropy S, temperature T and magnetic field H:

$$\left(\frac{\partial T}{\partial H}\right)_S = -\left(\frac{\partial M}{\partial S}\right)_H \tag{4.2}$$

one derives, by differentiating with respect to H and keeping S fixed

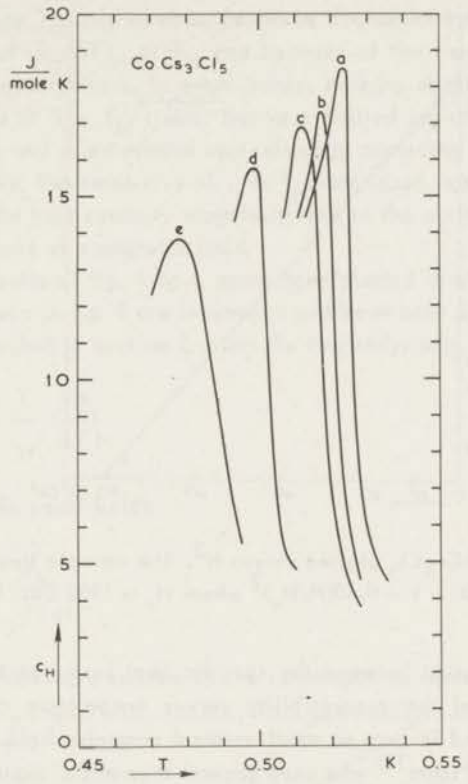

Fig. 6. Heat-capacity curves of $CoCs_3Cl_5$ in various externally applied magnetic fields:

a: 0 Oe
b: 220 Oe
c: 440 Oe
d: 660 Oe
e: 880 Oe

$$\left(\frac{\partial^2 T}{\partial H^2}\right)_S = -\left\{\frac{\partial}{\partial H}\left(\frac{\partial M}{\partial S}\right)_H\right\}_S = -\left(\frac{\partial \chi}{\partial S}\right)_H = -\frac{T}{c_H}\left(\frac{\partial \chi}{\partial T}\right)_H . \qquad (4.3)$$

For small χ, compared to $\partial\chi/\partial T$, we may write:

$$c_H = -\frac{1}{\left(\frac{\partial^2 T}{\partial H^2}\right)_S} T\left(\frac{\partial \chi}{\partial T}\right)_H = -\frac{1}{\left(\frac{\partial^2 T}{\partial H^2}\right)_S}\frac{\partial(\chi T)}{\partial T} . \qquad (4.4)$$

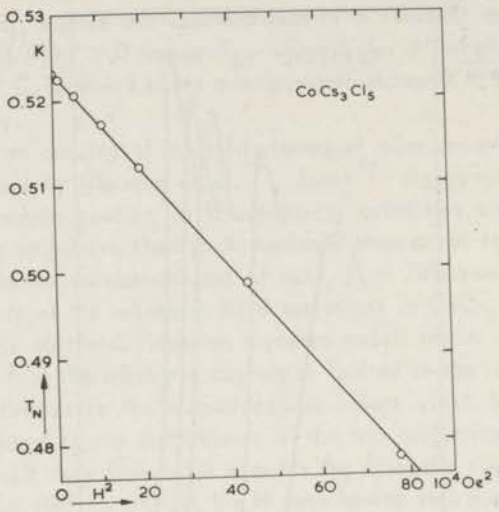

Fig. 7. $T_N(H)$ of $CoCs_3Cl_5$ plotted versus H^2. The straight line corresponds to $T_N(H)/T_N(0) = 1 - 0.40(H/H_c)^2$ where $H_c = 1900$ Oe.

Eq. (4.4) gives a relation between the specific heat in a constant small magnetic field and the slope of the susceptibility versus temperature curve, taken at the critical temperature and in zero or small external magnetic field. Relation (4.4) was originally derived by Fisher[13] who used general theoretical arguments and compared it with experimental results of MnO and MnF_2. Skalyo et al.[14] gave some additional discussion to eq. (4.4) and compared it with experimental results on $CoCl_2 6H_2O$.

If it is found that in a (H,T) diagram the isentrope, which starts at $T = T_N$ and $H = 0$, follows the boundary between paramagnetic and antiferromagnetic phases, then we see that $(\partial^2 T/\partial H^2)_S$ may be equated to $2AT_N(0)$ where A is the constant in eq. (4.1). Theoretically[13], at $T = T_N$ both $c_H(H = 0) = c$ and $(\partial\chi/\partial T)_H$ may become infinite, but the relation holds also for a finite interval about T_N. Taking the interval between $0.97T_N$ and T_N we find

$$\left[\int_{0.97T_N}^{T_N} c\,dT\right] / \left[\chi T\right]_{0.97T_N}^{T_N} = 1/(1.23 \times 10^{-7}). \qquad (4.5)$$

This is to be compared with $2AT_N(0) = 1.15 \times 10^{-7}$. For a similar comparison above T_N we did not have a sufficient number of points in the small temperature region between T_N and the temperature at which the maximum in χ occurs. Extending the interval limits to $0.95T_N$ and T_N, we get for the ratio in eq. (4.5) a slightly lower value. The moderate agreement between relations (4.1) and (4.4) we find in a small

temperature region near T_N may to some extent be accidental because of the strong changes in both c and $(\partial\chi/\partial T)_H$ at T_N and because of the limited accuracy of the d.c. susceptibility measurements. In other words, nothing about the validity of eq. (4.4) has been proved at $T = T_N$ itself. But in a limited region around T_N we find that the heat capacity and χ are related approximately according to eq. (4.4).

Stated differently, the steep rise of χ at T_N mentioned in section 3, is related to the sharpness of the heat capacity singularity and to the shift of the Néel temperature under the influence of a magnetic field.

In fig. 8 the results of fig. 7 have again been plotted in a phase-boundary diagram. The drawn curves in fig. 8 are isentropes and have been determined according to the procedure described in section 2. From the thermodynamic relation

$$\left(\frac{\partial T}{\partial H}\right)_S = -\frac{T}{c_H}\left(\frac{\partial M}{\partial T}\right)_H \tag{4.6}$$

one sees that, since in small fields

$$\left(\frac{\partial M}{\partial T}\right)_H = H\left(\frac{\partial \chi}{\partial T}\right)_H \tag{4.7}$$

the occurrence of temperature minima in the isentropes is related to maxima in the

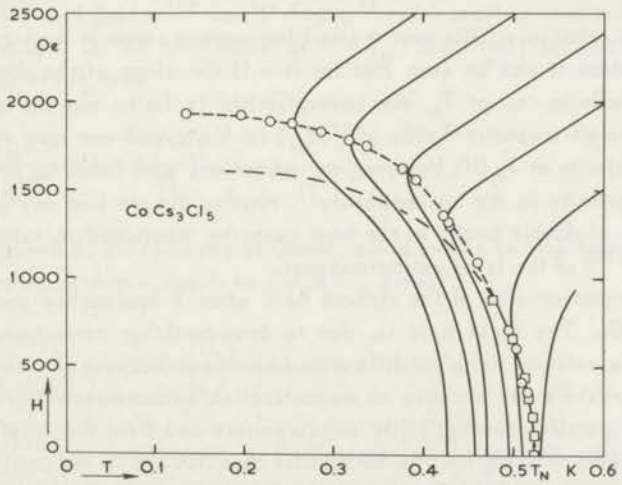

Fig. 8. Phase diagram of $CoCs_3Cl_5$. The drawn line are isentropes, the circles indicate the temperature minima in these isentropes; the locus of these minima is indicated by the upper dashed line (phase boundary); the lower dashed line indicates the locus of inflection points of the isentropes. The square points are obtained from fig. 6.

susceptibility versus temperature curves. We are, however, not primarily interested in the susceptibility maxima, but in the phase transition, which is associated with singularities in $(\partial M/\partial T)_H$, $(\partial \chi/\partial T)_H$ and c_H. From the result of fig. 4 it was found that in a magnetic field of a few hundred oersted the singularity in c_H occurs at the same temperature as the maximum in the susceptibility (see tabel I). Leaving aside the singular behaviour of c_H and χ at $T_N(H)$, there is clearly a change of sign of $(\partial \chi/\partial T)_H$. Hence (eq. (4.6)) the temperature minimum in the isentropes is associated with the phase transition and the locus of minima in fig. 8 denotes the phase boundary. It may be mentioned that sometimes[15] inflection points in the isentropes are associated with the phase boundary. In fig. 8 the locus of the inflection points of the isentropes is indicated by the lower dashed line. As can be seen from this figure the temperature at which $(\partial T/\partial H)_S = 0$ is much lower than the temperature at which $(\partial^2 T/\partial H^2)_S = 0$. As we found that in a relatively weak magnetic field $T_N(H)/T_{max}$ approximates unity (table I) the locus of the inflection points does not yield a phase boundary in our case, except possibly at low field strengths. It may be noted that this phase boundary (critical field versus temperature) fits smoothly to the T_N vs H data obtained in specific heat measurements up to a field of 880 Oe.

Sawatzky and Bloom[15] derived the relation

$$\frac{c_H}{T} = \left(\frac{dH}{dT_N}\right)^2 \chi_T + A$$

where A varies relatively little over a small temperature range in the vicinity of T_N. From this relation it can be seen that for $H = 0$ the slope of the phase boundary, (dH/dT_N) is infinite, as at T_N the susceptibility is finite and the specific heat infinite. For small magnetic fields (dH/dT_N) is finite and one may expect χ_T to display a singularity at $T_N(H)$. However, no indications were found for the occurrence of such a singularity in the susceptibility[7]. Neither did we find any indication for the occurrence of double peaks in the heat capacity, mentioned in some theoretical treatments[8,17,18] of the Ising antiferromagnet.

The asymptotic value of the critical field when T approaches zero is approximately 1900 Oe. The local field is, due to demagnetizing corrections, somewhat smaller than the external field; the difference is unknown because of a non-ellipsoidal shape of our crystals and because no magnetization measurements were performed. However, from parallel susceptibility measurements and from the crystal shape we estimate the demagnetizing field to be smaller than 100 Oe in the antiferromagnetic phase. The value H_c = 1900 Oe is considerably lower than the molecular field at T = 0 K, deduced from the energy yield of the ordering process[1]. This discrepancy may be qualitatively explained on the basis of the kind of ordering discussed in section 3, in which it was suggested that each Co ion has four antiparallel neighbouring spins in the ab plane and two parallel neighbouring spins along the c axis. Hence, if one assumes ferromagnetic linear chains along the c axis, the molecular

field on such a chain is the exchange field of four neighbour chains of antiparallel spins and a certain part of the total dipolar field. The field which is required to reverse a chain as a whole in the field of its neighbours may be smaller than the above-mentioned molecular field. It may also be mentioned that the critical field, as was obtained from neutron diffraction measurements[5], amounts to approximately 2000 Oe which agrees reasonably with our results in spite of the proposed different magnetic structure.

The existence and form of a transition curve between antiferromagnetic and paramagnetic regions was discussed by Garret[8], Ziman[17], Burley[18], Fisher[7] and recently by Bienenstock[19]. Garret[8] finds a boundary between paramagnetic and antiferromagnetic solutions of the free energy in non-zero magnetic field, using molecular-field theory. Ziman's[17] method and result is similar to that of Garret, except that the BPW method is applied. Numerical solutions for the transition point, $T_N(H)$, in the presence of a magnetic field, H, are customarily plotted as $T_N(H)/T_N(0)$ versus H/H_c, where H_c is the critical field at $T = 0$, above which no antiferromagnetic solution is stable. The molecular-field model seems to be more reliable for $T \approx T_N$ and small H than for $H \approx H_c$ and $T \approx 0$. This is rather obvious from the way in which the model is applied and from the "bulging" transition curve at small T leading to transition fields, which are even larger than H_c for $T \approx 0$, and also to the prediction of two specific-heat singularities. Such predictions are not borne out by experimental results and also conflict with theoretical calculations e.g. of Kasteleijn[20], of Burley[18] and of Fisher[7], who applied combinatorial methods to the Ising model. On the other hand, at $T \approx T_N$, practically all models give a quadratic relation of the form

$$\frac{T_N(H)}{T_N(0)} = 1 - a\left(\frac{H}{H_c}\right)^2 . \qquad (4.8)$$

In the molecular-field calculations of Garret, $a = \frac{1}{4}$ (which is also found by Nagamiya et al.[21]). The experimental result on $CoCs_3Cl_5$ gives

$$\frac{T_N(H)}{T_N(0)} = 1 - 0.40\left(\frac{H}{H_c}\right)^2 \quad \text{where } H_c = 1900 \text{ Oe.} \qquad (4.9)$$

Bienenstock[19] has carried out a Padé-approximant machine calculation of the Helmholtz free energy in an Ising spin system. His calculations apply to spin ½ and nearest neighbour interaction only and to simple square, simple cubic and b.c.c. lattices. Within the spread of the computer results there is no difference between s.c. and b.c.c. lattices and his curve has been plotted as a dash-dot line in fig. 9. In comparison with the drawn experimental curve taken from fig. 8 there is a discrepancy, taking into account that both H_c and T_N are fitted parameters. The discre-

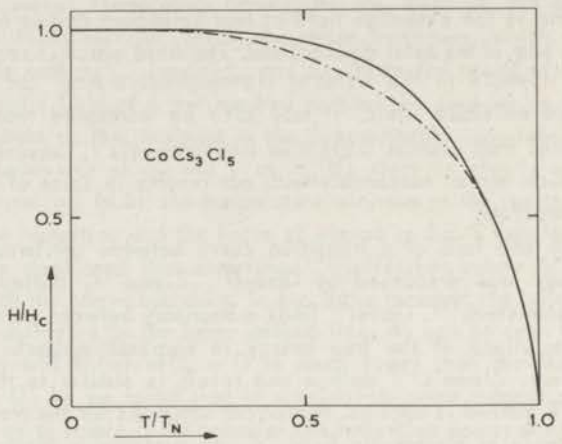

Fig. 9. Experimental phase boundary of $CoCs_3Cl_5$ (drawn line) in comparison with Bienenstock's calculation on a simple cubic antiferromagnet (6 antiparallel n.n.) indicated by a dash-dot line and fitted to the experiment at $T = 0$, $H = H_c$ and $T = T_N$, $H = 0$.

pancy cannot simply be ascribed to an apparent higher coordination number in this salt, which was suggested by the comparison of thermodynamic quantities in ref. 1. Since the theoretical curves of Bienenstock coincide for s.c. and b.c.c. lattices, such an explanation may be ruled out. We feel that the occurrence of ferromagnetic coupling along the c axis is predominantly responsible for the deviation, since (in the Ising model) magnetic properties are not symmetric with respect to reversal of the sign of the exchange interaction. For the s.c. lattice Bienenstock finds that the expression

$$\frac{T_N(H)}{T_N(0)} = \left[1 - \left(\frac{H}{H_c}\right)^2\right]^b \quad \text{with } b = 0.35 \tag{4.10}$$

fits his computational results at $T \approx T_N$. Eq. (4.10) is, for small H, equivalent to eq. (4.8) if $a = b = 0.35$; for $H/H_c \approx 0.4$, however, one finds that eq. (4.9) and (4.10) give equal $T_N(H)/T_N(0)$ ratio's if $a = 0.39$ (and $b = 0.35$). In other words, considerably more accurate data are required in order to distinguish between the occurrence of a factor a and an exponent b in eq. (4.8) and eq. (4.10).

4.2. $CoCs_3Br_5$

The experimental results on the phase boundary in $CoCs_3Br_5$ show features, which differ appreciably from those of $CoCs_3Cl_5$. Before discussing these differences, it may first be pointed out, however, that $CoCs_3Br_5$ shows an antiferromag-

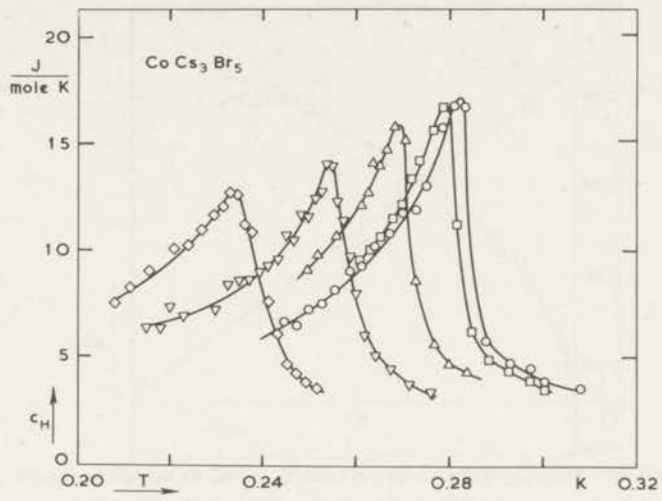

Fig. 10. Heat-capacity curves of $CoCs_3Br_5$ in various external magnetic fields:

○: 0 Oe ▽: 660 Oe
□: 220 Oe ◇: 880 Oe
△: 440 Oe

netic phase transition and a phase boundary.

In fig. 10 one finds the heat capacity of the bromide when a magnetic field is applied along the crystalline c axis. In fig. 11 the position of $T_N(H)$ is again plotted versus H^2; it is seen that the data agree only approximately with eq. (4.1), in this case $T_N(H)/T_N(0) = 1 - 2.50 \times 10^{-7}H^2$. From the experimental data on energy gain of the magnetic ordering[1] it is estimated that the molecular field at T = 0 is approximately 1800 Oe. If we equate this value to the critical field, H_c, which determines the phase boundary between paramagnetic and antiferromagnetic regions at T = 0, we get

$$T_N(H)/T_N(0) = 1 - 0.81(H/H_c)^2. \qquad (4.11)$$

This gives a much larger value, a = 0.81 (eq. (4.8)), than was found for the chloride, and it has probably to be increased still further as will be seen shortly. Such a large a value is precisely what is to be expected for a two-dimensional Ising antiferromagnet, according to Fisher[7], to Burley[18] or to Bienenstock[19]. Fisher[7] gives a = 0.69; Bienenstock[19] presents his results in the form of eq. (4.10), in which b = 0.87, but this is for small H equivalent to b = a = 0.87. For larger fields ($H/H_c \approx$ 0.5) and taking b = a, eq. (4.10) predicts a stronger shift ΔT_N than eq. (4.8).

Further information is obtained from the study of the isentropes in the H vs T diagram. Again, as in the chloride, it was found that the maximum in the susceptibil-

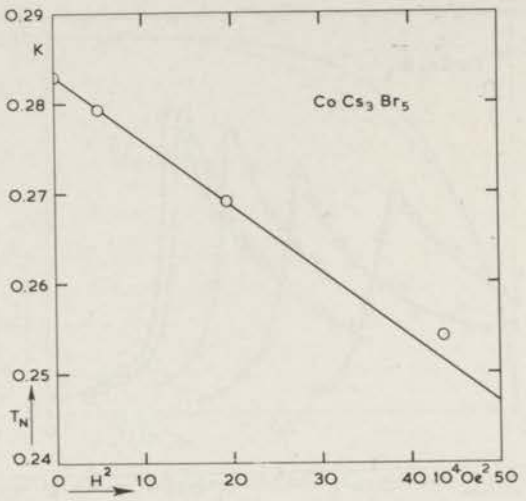

Fig. 11. $T_N(H)$ of $CoCs_3Br_5$ plotted versus H^2. The straight line corresponds to $T_N(H)/T_N(0) = 1 - 2.50 \times 10^{-7}H^2$ (H in Oe).

ity versus temperature curve measured in the presence of a magnetic field of e.g. 1 kOe falls much closer to the maximum (at $T_N(H)$) in the heat capacity than for H = 0 (see table II). In small fields, however, $T_N(H)$, may not coincide with the susceptibility maximum and in fact temperature minima in the isentropes were indeed observed also for $T > T_N$. Clearly then, the procedure of establishing minima in the isentropes does not give information about the phase boundary in small magnetic fields ($H < 1000$ Oe). However, this part of the phase boundary (up to 1 kOe), could be readily found from measurements of the position of the heat-capacity maximum, $T_N(H)$. These results, in conjunction with the determination of temperature minima in the isentropes are seen in fig. 12. The values of the critical field have to be reduced by the unknown demagnetizing field and also the temperature difference between the susceptibility maximum and the critical point have to be taken into account. We estimate that these corrections do not exceed 200 Oe and have not much effect on the most remarkable feature of the results, namely that the phase boundary does not level off towards low T, in contrast to what was found in the chloride. Bienenstock's[19] and Fisher's calculations on two-dimensional Ising systems also show this linear variation of H vs T near T = 0 K. At the absolute zero equation (4.10) predicts the phase boundary to reach the H/H_c axis horizontally, unless b = 1. Bienenstock's computational data, however, are too scarce to establish a definite behaviour at T = 0 K. Fisher[7] predicts a non-zero slope at zero temperature. Since Bienenstock's simple square lattice model may correspond most closely to the situation in the bromide, we present his H vs T phase diagram in fig. 12 as a fully drawn curve on a reduced temperature scale and based on a choice of $H_c = 2100$ Oe.

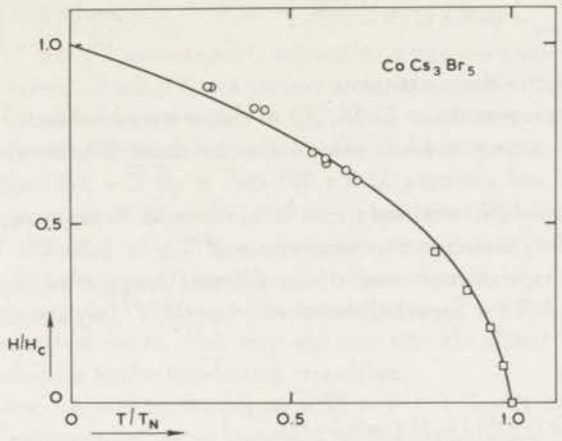

Fig. 12. Phase diagram of $CoCs_3Br_5$ on a reduced temperature and field scale, taking $H_c = 2100$ Oe at $T = 0$ K. The circles are the experimental points, uncorrected for demagnetizing field and the drawn line is Bienenstock's computed curve for a planar square Ising antiferromagnet.

One finds good agreement between theoretical curve and the experimental data available. The choice of 2100 Oe for getting an optimal fit leads to a revised value of the parameter a in eq. (4.8), namely $a = 1.10$. The above mentioned corrections affect H_c (at $T \approx 0$ K), and the parameter a, which follows from the region $T \approx T_N$. Probably the true value of H_c is below 2000 Oe and then $a < 1.00$; in any case the a value agrees better with Bienenstock's result than with the superexchange antiferromagnet in two dimensions, considered by Fisher[7].

The results on the phase-boundary measurements in $CoCs_3Br_5$ confirm strongly the two-dimensional character of the spin ordering suggested before on basis of other experimental evidence.

5. Spin-lattice relaxation

5.1. Internal field

Spin-lattice relaxation measurements above 1 K*) and at relatively high frequency (240 kHz) give the adiabatic susceptibility χ' in parallel magnetic fields up to a few kOe. From χ'/χ_0, where χ_0 is the d.c. susceptibility, one finds b by means of $\chi'/\chi_0 = b/(b + CH^2) = c/c_H$ where $c = b/T^2$ and c_H is the specific heat at constant magnetic field. Further, in the above relation the validity of Curie's law is assumed, C being the Curie constant. At low temperatures a correction has to be applied for deviations from Curie's law according to[22]

*) These measurements were performed by D. A. Curtis and A.J. van Duyneveldt.

$$(b/C)_{corr} = (b/C)\{T/(T-\theta)\}^3 \qquad (5.1)$$

in which θ is the Curie-Weiss constant.

From the measurements on $CoCs_3Cl_5$ at temperatures between 1.2 K and 4.2 K it follows that the uncorrected b/C value varies by about 50%, but $(b/C)_{corr}$ is constant to within 3% and averages 32.8×10^4 Oe^2 or $\sqrt{b/C} = 573 \pm 10$ Oe. Since the Curie constant C = 4.99, one finds $c = 0.16/T^2$ joule K per mole, in reasonable agreement with the heat-capacity measurements[1], $c = 0.20/T^2$. The difference between the two experimental results from different temperature regions could be explained on basis of the expected deviation from a $1/T^2$ dependence, e.g. according to Baker[23]

$$c/R = 3\,(\frac{J'}{kT})^2[1 + 11\,(\tanh\frac{J'}{kT})^2 + \ldots] \qquad (5.2)$$

and taking[1] $J'/k = 0.12$ K, this gives a substantial correction ($\approx$ 15%) to the $1/T^2$-dependence of c. However, the heat-capacity measurement at 1 K is not sufficiently accurate to justify a comparison in further detail. Taking the more accurate χ' measurements for the determination of b, one finds a discrepancy between the experimental result b = 0.16 J K/mole and the prediction of eq. (5.2) based on J'/k = 0.12 K, giving b $\approx$ 0.35 J K/mole. It should be mentioned that J'/k includes the dipolar coupling of nearest neighbours[1], but further dipolar interactions are neglected since they are estimated to contribute only about 2% to the b value. On the other hand, between 1 and 4 K one should not neglect the occupation of the higher doublet, at $2D/k$ = 12.4 K in the chloride. Apparently this doublet does not contribute to the heat capacity, as determined from χ' at ν = 240 kHz since e.g. at 1.27 K $b/C = 32.4 \times 10^{-4}$ and at 4.2 K we find $b/C = 32.0 \times 10^{-4}$. We conclude that further experiments above 1 K are required in order to explain the observed b value. The discrepancy becomes even more apparent in $CoCs_3Br_5$, where $\sqrt{b/C}$ = 1255 Oe was found, leading to b = 0.8 J K/mole, as compared to the result of heat-capacity measurements[1], which gave b = 0.33 J K/mole and to a value b $\approx$ 0.25 J K/mole from Onsager's calculated heat capacity vs T curve[24], some uncertainty in the latter value being caused by lack of a precise J'/k value. Unlike the situation in the chloride, here one might ascribe the difference between heat-capacity data (high b) and theory (low b) to next-nearest neighbour interactions. Further, the experimentally found parameter b as deduced from fig. 3 in ref. 1 may not correctly represent the $1/T^2$ behaviour, even at a relatively high temperature T $\approx$ 1 K. Again, however, there is a discrepancy with the adiabatic-susceptibility measurements, for which we are unable to offer any explanation.

5.2. Relaxation time

From the χ' and χ'' measurements relaxation times were determined at various temperatures between 1.2 and 4 K and various external magnetic fields (up to 4 kOe). The results on the chloride are shown in fig. 13, in combination with the relaxation times measured at temperatures below 1 K, mentioned in section 2. Four features are to be mentioned:

1. There is no pronounced dependence of the relaxation time on the external magnetic field. For instance, at 4.2 K, τ changes by a factor 2.5 when increasing H from 0 to 4 kOe and the τ vs H dependence is approximately accounted for by the Brons-Van Vleck formula[25]. Also at low temperatures, $T \approx 0.7$ K, we find τ to be only slightly dependent on H. This may indicate that the direct process does not significantly contribute to the spin-lattice relaxation.

2. The data above 1 K and in the region $0.7K < T < 1$ K may be reasonably well fitted by a T^{-7} dependence, as is indicated by the drawn curve in fig. 13. Taking only the data above 1 K, a T^{-6} dependence would fit the data better. When plotting τ vs T on a semilogarithmic scale, it is difficult to fit an exponential curve to the

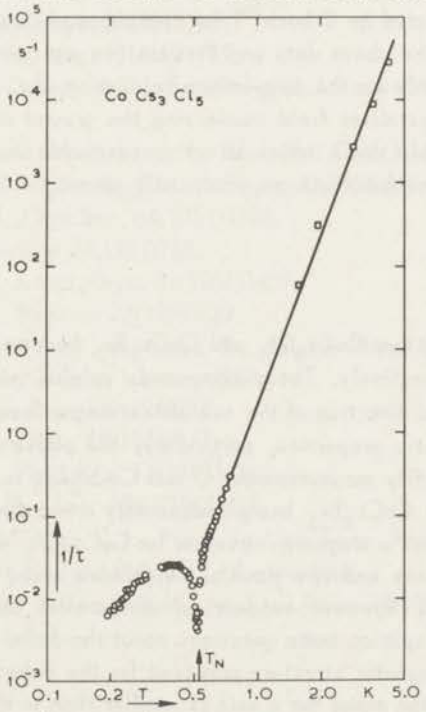

Fig. 13. Inverse of spin-lattice relaxation time, τ, versus temperature in $CoCs_3Cl_5$. The square points are obtained from χ' measurements, the circles originate from the response time to an applied heat "pulse". The straight line connecting the experimental points represents $\tau = 0.83T^{-7}$.

experimental result. Consequently, Orbach processes[26] seem to be inoperative and Raman processes are apparently mainly responsible for the spin-lattice relaxation.

3. Even at low temperatures ($0.7K < T < 1$ K) τ vs T does not correspond to a direct process ($\tau \propto T^{-1}$). In this temperature region short-range ordering in the $CoCs_3Cl_5$ is still negligible[1], i.e. the crystal would be predominantly paramagnetic and the approach to T_N is probably not yet anticipated.

4. A small decrease in a $\dot{Q}/\Delta T$ vs T plot was found in a temperature region around T_N. This result indicates that the heat transfer coefficient $\alpha = \dot{Q}/\Delta T = c_H/\tau$, is a smoothly varying function even in the temperature region where the specific heat is anomalous. The marked dip in the $1/\tau$ vs T curve at $T = T_N$ is therefore partly a consequence of the anomalous specific heat.

Quite similar results were obtained in the bromide, where the relaxation times are found to obey $\tau = 0.11T^{-7.0}$s in the temperature region of liquid He and, when extrapolated to lower temperatures, fit reasonably to the results of carbon resistance thermometry methods. Again, the magnetic field dependence is roughly accounted for by the Brons-Van Vleck relation and therefore is small compared to, for instance, a H^{-2} dependence predicted by Orbach[26] for two-phonon relaxation processes in a Kramers doublet. From the above data and discussions we conclude that the higher doublet has little influence on the spin-lattice relaxation, i.e. matrix elements of the normal modes of the crystalline field connecting the ground doublet with the next higher doublet are probably small, which is not unreasonable in view of the observation that the doublet wave functions are practically pure $s_z = \pm\frac{1}{2}$, $s_z = \pm 3/2$ states respectively.

6. Conclusion

It has been shown that $CoCs_3Cl_5$ and $CoCs_3Br_5$ become antiferromagnetic at 0.527 and 0.282 K respectively. These compounds exhibit many properties of the Ising model, the preferred direction of the sublattice magnetization being the crystalline c axis. The magnetic properties, particularly the phase diagram, support the evidence from heat-capacity measurements[1], that $CoCs_3Cl_5$ is a three-dimensional antiferromagnet and that $CoCs_3Br_5$ has predominantly a two-dimensional character. Our measurements suggest a magnetic structure for $CoCs_3Cl_5$ with four antiparallel neighbours in the ab plane and two parallel neighbours along the c axis. Neutron diffraction measurements however suggest an antiparallel spin arrangement also along the c axis. In our opinion some questions about the definite magnetic structure remain unsolved. Our magnetic structure proposed for the chloride may also exist in $CoCs_3Br_5$, but the coupling along the c axis is smaller than in the chloride.

The spin-lattice relaxation does not show the influence of Orbach processes or of the direct process, but is characterized mainly by (field independent) Raman processes.

References

1) Wielinga, R.F., Blöte, H.J.W., Roest, J.A. and Huiskamp, W.J., Commun. Leiden No. 354c; Physica 34(1967)223.
2) Wielinga, R.F., Thesis, Leiden, 1968.
3) Van Stapele, R.P., Henning, J.C.M., Hardeman, C.E.G. and Bongers, P.F., Phys. Rev. 150(1966)310; Proc. of the XIVth Colloque Ampère, Ljubljana (1966)1204.
4) Stoneham, A.M., Proc.Phys.Soc. 86(1965)1163.
5) Hammann, J., Physica 43(1969)277.
6) Sykes, M.F. and Fisher, M.E., Physica 28(1962)919,939.
7) Fischer, M.E., Proc.Roy.Soc. A254(1960)66.
8) Garret, C.G.B., J.chem.Phys. 19(1951)1154.
9) Joenk, R.J., Phys.Rev. 128(1962)1634.
10) Schelleng, J.H. and Friedberg, S.A., J.appl.Phys. 34(1963)1087.
11) Giauque, W.F., Hornung, E.W., Brodale, G.E. and Fisher, R.H., J.chem.Phys. 46(1967)1804.
12) Joenk, R.J., J.appl.Phys. 34(1963)1097 .
13) Fischer, M.E., Phil. Mag. 7(1962)1731.
14) Skalyo Jr., J., Cohen, A.F., Friedberg, S.A. and Griffiths, R.B. Phys.Rev. 164(1967)705.
15) Friedberg, S.A. and Schelleng, J.H., Proc. int. Conf. Magn. Nottingham (1964)90.
16) Sawatzky, E. and Bloom, M., Can. J. Phys. 42(1964)657.
17) Ziman, J.M., Proc.Phys.Soc. 64(1951)1108.
18) Burley, D.M., Physica 27(1961)768.
19) Bienenstock, A., J.appl.Phys. 37(1966)1459.
20) Kasteleijn, P.W., Physica 22(1956)387.
21) Nagamiya, T., Yosida, K. and Kubo, R., Adv. in Phys. 4(1955)1.
22) Van den Broek, J., Thesis, Leiden, 1960.
23) Baker, G.A., Phys.Rev. 129(1963)99.
24) Onsager, L., Phys.Rev. 65(1944)117.
25) Van Vleck, J.H., Phys.Rev. 57(1940)426.
26) Orbach, R., Proc.Roy.Soc. A264(1961)458.
27) Poulis, N.J. and Gorter, C.J., Progr. in Low Temp. Phys. I, Ch. XIII (1955), ed. C.J. Gorter (North Holland Publ. Cy., Amsterdam).
28) De Vries, A.J. and Livius, J.W.M., Appl.sci.Res., 17(1967)31.

Chapter VI

MAGNETIC AND CALORIC STUDY OF THE PHASE TRANSITIONS OF COPPER, NICKEL, MANGANESE AND COBALT LANTHANUM DOUBLE NITRATE

1. Introduction

Thermal and magnetic properties of rare-earth double nitrates, $M_3R_2(NO_3)_{12}\cdot 24H_2O$ have been fairly extensively investigated by various methods[1,2] and for various rare-earth ions, notably for Ce^{3+}[3,4], in $Ce_2Mg_3(NO_3)_{12}\cdot 24H_2O$ (see chapter III). Very little attention has so far been paid to the magnetic properties of the double nitrates in which M is an ion of the iron group and R is the diamagnetic lanthanum ion. Unlike the rare-earth ions, which do not show any significant exchange interaction since they are relatively far apart in the lattice, the divalent ions are located at appreciably smaller distances. They are all surrounded by octahedra of water molecules and it may be interesting to investigate the superexchange interaction between iron group ions in this compound for which crystal structure and single ion properties are well defined by X-ray and NMR measurements and by EPR measurements respectively.

From EPR data, summarized in table I, we note that there are two kinds of divalent ions, two thirds of the ions being at crystallographic X sites and the remaining one third are at Y sites. The divalent ions at X sites are located at small mutual distances and have very nearly octahedral crystalline fields. The latter may be inferred, for instance, from the practically isotropic g value of the Co ion at X sites, the average g value being 4.32 compared to 13/3 to be expected for perfect octahedral symmetry. Since the proton positions in La-Mg-nitrate are determined by NMR, by double resonance techniques[32] and by neutron diffraction, one may be able to evaluate theoretically the superexchange interaction strength. Some experimental results regarding the exchange interactions between iron group ions at X sites will be presented in this chapter. However, we shall be mainly concerned in our experimental study with the caloric and magnetic properties connected with the magnetic phase transitions in these compounds. The single-ion properties are expressed by a spin Hamiltonian

$$H = g_{//}\beta H_z s_z + g_{\perp}\beta(H_x s_x + H_y s_y) + D\left\{s_z^2 - \frac{s(s+1)}{3}\right\} +$$

$$+ A s_z I_z + B(s_x I_x + s_y I_y).$$

The constants for Cu^{2+}, Ni^{2+}, Mn^{2+} and Co^{2+} are given in table I.

Table I

Ion	$Mn^{5)}$		$Co^{6,7)}$		$Ni^{8,19)}$		$Cu^{9,10)}$	
	X	Y	X	Y	X	Y	X	Y
$g_{//}$	2.00	2.00	4.37	7.36	2.23	2.23	2.41	2.41
$g_{\perp}$	2.00	2.00	4.31	2.34	2.23	2.23	2.10	2.10
D/k	−0.0070	−0.0310	–	–	+0.288	−3.24?	–	–
A/k	−0.0129	−0.0129	+0.0142	+0.042	–	–	−0.016	−0.016
B/k	−0.0129	−0.0129	+0.0136	≈0	–	–	+0.002	+0.002

Parameters of the spin Hamiltonian for Mn, Co, Ni and Cu ions in lanthanum double nitrate as measured in EPR experiments. D, A and B are expressed in units kT.

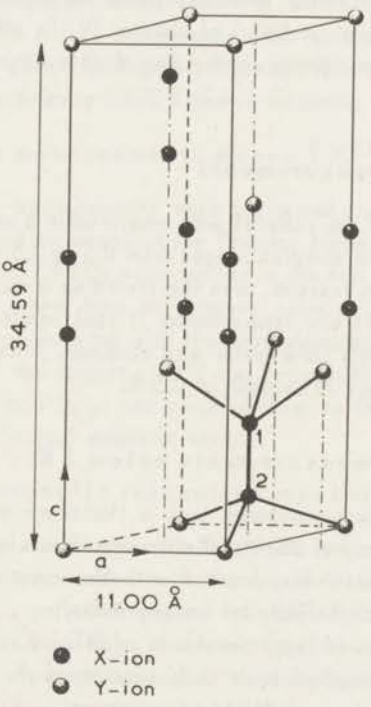

Fig. 1. Hexagonal unit cell of lanthanum magnesium nitrate containing 3 molecules. Only the divalent ions are indicated in the figure and these are all surrounded by slightly distorted octahedrons of water molecules. Two thirds of the ions are at crystallographic X sites and one third at Y sites. The lanthanum site is at $\pm(0,0,\frac{1}{4})$ + $(0,0,0; \frac{1}{3},\frac{2}{3}, \frac{2}{3},\frac{2}{3}, \frac{1}{3},\frac{1}{3})$. Each of the vertical lines represents an axis of trigonal symmetry. Two Y sites outside the unit cell are drawn in order to indicate the n.n. neighbours of X ions number 1 and number 2, which are nearest neighbours of each other at 5.0 Å. Nearest neighbours of Y ions are mutually shielded by large $La(NO_3)_6$ complexes.

It may be remarked that both for Cu^{2+} and for Mn^{2+} ions the X sites and Y sites are practically identical as far as single-ion properties are concerned.

The crystal structure for the double nitrates has been determined by Zalkin, Forrester and Templeton[11]. The hexagonal unit cell is drawn in fig. 1, in which only the magnetic divalent ions are indicated. The interionic distance of nearest neighbours at X sites is 5.0 Å, while all other distances between magnetic ions exceed 7.14 Å. The c axis coincides with the $g_{//}$ direction for the forementioned divalent ions at X sites as well as at Y sites.

2. Experimental method

The apparatus has already been described extensively in chapter II. Schematically the setup is shown in fig. 1 of chapter IV. In all the experiments a lead switch was used. The experiments on the four double nitrates can be divided into the following sections.

2.1. Specific-heat measurements

The specific heat of the samples was measured in a temperature range of 0.06 to 0.8 K. The weight of the samples ranged from 0.5 to 1.5 g. The temperature drift, as measured by the carbon resistor, was registered on a recorder; heating times of 20 seconds were used. At low temperatures it took about 1000 seconds before a stationary temperature in the calorimeter was obtained. This time decreased towards higher temperatures to about 30 seconds at 0.5 K.

2.2. Susceptibility measurements below 1 K

The susceptibility was measured with a Hartshorn mutual inductance bridge, which operated at a frequency of 260 Hz; d.c. measurements were done with a ballistic galvanometer. The samples were mounted with the crystallographic c axis either vertical or horizontal and the parallel susceptibility, $\chi_{//}$, and perpendicular susceptibility, $\chi_{\perp}$, was measured respectively. In addition d.c. external magnetic fields up to 1500 Oe could be applied by a coil, outside of the cryostat, in a direction parallel to that of the a.c. susceptibility measurement.

2.3. Adiabatic field variations

Measurements were performed in which the magnetic field was varied adiabatically and the temperature change of the sample was observed by the carbon resistor. From such observations, isentropes in the H–T phase diagram could be obtained. In the case of Ni-La nitrate in which the lowest temperatures in a field were obtained, the magnetic field was varied in steps of about 150 Oe. About 200

seconds were needed to obtain thermal equilibrium below 0.05 K, which time rapidly decreased towards higher temperatures.

2.4. Nuclear orientation

Measurements were carried out on the anisotropy of the gamma-ray intensity, emitted from radioactive ^{54}Mn, grown as an impurity in a Mn-La nitrate single crystal. A sample of Mn–La nitrate of a few tenths of a gram could not be cooled down to a low enough temperature, because of its rising hyperfine specific heat and decreasing thermal contact with the cooling salt. Therefore, a sample was used, which consisted of a diamagnetic single crystal of Mg–La nitrate, on which a 0.5 mm thick layer of Mn–La nitrate was grown. The gamma-ray intensity was detected by means of four NaJ scintillation counters, which were located in directions along the crystallographic c axis and perpendicular to that axis. The pulses of the counters were analyzed on a 256 channel analyzer. The gamma-ray anisotropy was measured at temperatures down to 0.028 K and in magnetic fields up to 5.5 kOe.

2.5. Susceptibility measurements above 1 K*)

The susceptibility measurements were performed in the temperature range of liquid helium and hydrogen by means of the Faraday balance method. Inhomogeneous magnetic fields from 3.3 tot17.6 kOe were applied in the horizontal plane. The samples were cut from crystals, grown from an aqueous solution and were about 20 mg in weight. The crystals, were mounted with the crystallographic c axis in a horizontal direction; by rotation of the magnetic field the susceptibility could be measured in a direction along the c axis ($\chi_{//}$) and perpendicular to that axis ($\chi_{\perp}$). The c axis was found to be also a principal magnetic axis.

2.6. EPR and paramagnetic relaxation measurements**)

Ni–La nitrate samples, diluted with Mg nitrate were investigated by EPR and paramagnetic relaxation measurements in the liquid-helium temperature region. In the EPR measurements a reflection-type 3 cm ESR spectrometer with a VA203B (6975) klystron locked on the TE_{102} mode rectangular cavity with a 10 kHz automatic frequency control system was used. Measurements could be taken in any crystal direction by turning either the crystal or the magnet. Paramagnetic relaxation phenomena have been measured using a bridge with a frequency range of 200 Hz to 1 MHz. The equipment has been described in detail by De Vries[12]. The samples are placed in an external magnetic field H_c on which an oscillating field of amplitude h is applied. The output signal of the bridge gives information about the real and imaginary parts of the susceptibility.

*) These measurements were performed by J.J. Giesen.

**) The EPR data were obtained by N.J. Zimmerman and the relaxation results were obtained by A.J. van Duyneveldt.

3. Cu-La nitrate

3.1. Heat capacity

The heat capacity of $Cu_3La_2(NO_3)_{12}.24H_2O$ was measured between 0.05 K and 0.5 K by the method described in section 2. The result is shown in fig. 2 on a logarithmic scale. In addition to the rather sharp singularity at 0.089 K it is seen that a broad anomaly is present at appreciably higher temperatures. The total entropy change can be fairly precisely determined from the heat-capacity curve since only minor extrapolations are required. The entropy yield between 0.05 and 0.5 K is 0.638 R per gramion Cu. When extrapolating the high-temperature data according to $cT^2/R = 0.018K^2$ and the low-temperature data by fitting a straight line on the logarithmic graph of c versus T, we find for the total entropy involved in magnetic ordering, $S/R = 0.691$ which is very close to the expected value $\ln(2s + 1) = \ln 2$. The values of c and S per gramion Cu which are given in table II represent smoothed

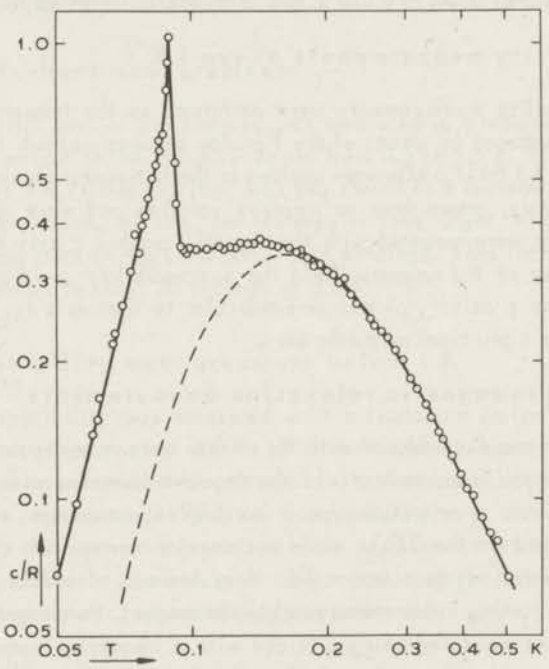

Fig. 2. Heat capacity of Cu–La nitrate per gramion Cu versus temperature on a logarithmic scale. The maximum corresponds to $T_N = 0.089$ K. The dashed line represents the theoretically calculated heat capacity for antiferromagnetically coupled ion pairs at X sites. The corresponding singlet-triplet splitting was taken to be $-2J/k = 0.46$ K, in order to fit the position of the theoretical curve on the temperature scale to the experimental points.

Table II

$Cu_3La_2(NO_3)_{12}\cdot 24H_2O$			
T	c/R	S/R	−E/R
∞	0	0.693	0
0.50	0.07	0.66	0.036
0.46	0.08^5	0.65	0.039
0.42	0.10	0.64	0.043
0.38	0.12^5	0.63	0.047
0.34	0.15^5	0.61^5	0.053
0.30	0.19	0.60	0.060
0.26	0.23^5	0.56	0.068
0.22	0.29	0.51^5	0.079
0.18	0.34^5	0.45	0.091
0.16	0.36	0.41	0.098
0.14	0.36^5	0.36	0.106
0.12	0.35^5	0.31	0.113
0.11	0.35	0.27^5	0.116
0.10	0.35	0.24	0.120
0.09^5	0.35^5	0.22	0.122
0.09	0.75	0.19^5	0.124
0.089	1.04^5	0.18	0.125
0.08^5	0.58	0.13^5	0.129
0.08	0.45^5	0.11	0.131
0.07	0.26^5	0.06	0.135
0.06	0.14	0.03	0.137
0.05	0.07	0.01^5	0.138
$T_N = 0.089$ K		$\Delta E/R = 0.139$ K	
$cT^2/R = 0.018$ K^2		$\Delta S/R = 0.691$	

data taken from the drawn curve in fig. 2. Also the energy yield, obtained by integrating c with respect to T, has been tabulated.

From these results it is clear that all Cu ions participate in the magnetic phase transition, but the magnetic ordering apparently occurs in two steps since above the critical temperature the entropy yield involved in short-range ordering is 0.511 R, i.e. more than 2/3 of the total entropy. This leads to the suggestion that the ions at crystallographic X sites have an appreciably stronger interaction than the ions at Y sites. We anticipate approximately isotropic exchange interaction between nearest neighbour ions at X sites (X ions). This is motivated by experimental evidence on other ionic Cu compounds involving octahedral $Cu(OH_2)_6$ complexes, which do not exhibit directed valence bonding causing anisotropic super-

exchange. Therefore, according to the Heisenberg model the interaction between two X ions may be expressed as:

$$H = -2J\ \vec{s}_1 . \vec{s}_2 \tag{3.1}$$

which leads to a singlet-triplet splitting of 2J, the singlet having an energy $+3J/2$ and the triplet having an energy $-J/2$. In fig. 2 the calculated heat capacity associated with a singlet antiferromagnetic ground state and a triplet at $-2J/k = 0.46$ K is plotted as a dashed line and approximately accounts for the anomaly above the critical point. It should be emphasized that, while the horizontal scale for the calculated Schottky type anomaly can be adjusted by choosing J/k, the vertical scale is fixed and it is therefore significant that the height of the maximum of the experimental curve agrees with that of the Schottky anomaly.

Further justification for this model of pair-exchange coupling is provided by the following considerations:

1. The distance between two X ions is 5.0 Å, while the distance between X ions and Y ions is at least 7.14 Å, that between various Y ions at least 11.0 Å and that between X ions belonging to different pairs is at least 7.31 Å. Hence it is not surprising that X ion pairs have the strongest exchange coupling.
2. The dipolar interactions at high temperatures in this crystal can be calculated according to the formula of Daniels[13], (eq. (19), chapter I). We carried out this summation for the La-double-nitrate lattice for the X- and Y-ion sites separately, and the averaged result for Cu–La nitrate is given by $c_{dip} T^2/R = 1.78 \times 10^{-4}$ K^2, which value is negligible compared to the experimental result of 180×10^{-4} K^2.

The dipolar coupling of a pair may be seen as a pseudo-exchange coupling, expressed by

$$H_{dip} = \frac{g^2\beta^2}{r^3}(\vec{s}_1 . \vec{s}_2 - 3s_{1z}s_{2z}), \tag{3.2}$$

if one takes the z axis along the line connecting the two ions, which is for the X-ion pairs in keeping with our notation throughout this chapter. Since H_{dip} provides some anisotropy in the total pair coupling, our singlet-triplet level scheme will be modified into levels at

$$\tfrac{3}{2}J,\ -\tfrac{1}{2}J - \frac{D}{2},\ -\tfrac{1}{2}J - \frac{D}{2},\ -\tfrac{1}{2}J + D, \text{ where } D \equiv \frac{g^2\beta^2}{r^3} = 0.03\ k.$$

However, although the heat capacity for this level scheme is slightly different from that used in fig. 2, it does not affect our conclusion, namely that at relatively high temperature the specific heat is predominantly determined by pair coupling. Apart from a minor correction due to dipolar coupling of ions outside of pairs no interactions other than superexchange interactions are expected to contribute significant-

ly to the heat capacity. Specifically, crystalline field splittings are much too large and hyperfine interactions much too small. For the h.f.s. contribution one derives for $T > T_N$,

$$c_{h.f.s.}/R = \tfrac{1}{9}\, s(s+1)\, I(I+1)\, \frac{A^2+B_x^2+B_y^2}{k^2T^2} = \frac{0.86 \times 10^{-4}}{T^2} \qquad (3.3)$$

where A, B_x and B_y are the h.f.s. constants taken from EPR data.

3.2. Susceptibility

Measurements of the isothermal susceptibility have been carried out both by a.c. bridge and d.c. galvanometer methods. The single crystal was mounted with its c axis either parallel to the axis of the measuring coils or perpendicular to that axis and the corresponding susceptibilities, $\chi_{//}$ and $\chi_{\perp}$ respectively, were first measured in the temperature range of liquid helium and thereafter at lower temperatures by intermediary of the cooling salt. The quantity $T^* = C/\chi$, where C is the Curie constant, was found to be a linear function of T in the liquid-helium temperature range, intersecting the temperature scale at practically zero temperature. Hence we conclude that $T = T^*$ down to at least T = 1 K. The results at lower temperatures have been plotted in fig. 3 and they show that Cu–La nitrate behaves as an antiferro-

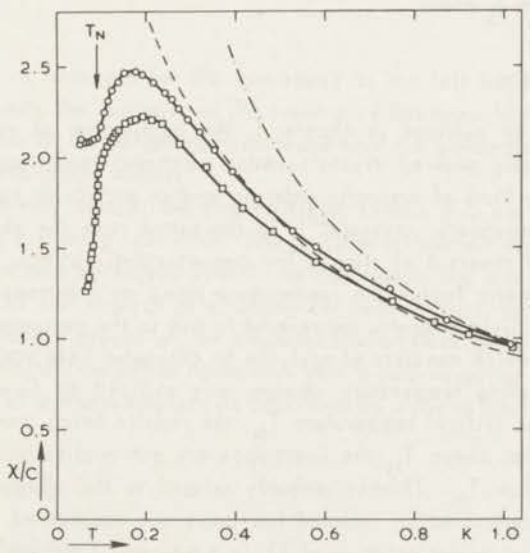

Fig. 3. Magnetic susceptibility of Cu–La nitrate, divided by the Curie constant. The dashed curve is a theoretical curve based on the assumption that two thirds of the ions are exchange coupled pairwise (eq. (3.4)). The dash-dotted curve represents Curie's law. The experimental points refer to measurements along the c axis and perpendicular to the c axis. ○: $\chi_{//}$, □: $\chi_{\perp}$.

magnet. However, the maxima in $\chi_{//}$ and $\chi_{\perp}$ lie at temperatures appreciably above that of the heat-capacity singularity ($T_N = 0.089$ K). Referring to the model introduced in section 3.1, namely predominance of pair coupling of 2/3 of the ions (X ions) and 1/3 of the ions (Y ions) remaining paramagnetic down to T_N, we may compare the susceptibility data with a calculation based on relative populations of singlet and triplet. This gives

$$\chi_{//} = \frac{2}{3} \frac{g_{//}^2 \beta^2}{kT} \frac{e^{-2J/kT}}{1 + 3e^{-2J/kT}} + \frac{1}{12} \frac{g_{//}^2 \beta^2}{kT} \qquad (3.4)$$

and similarly for $\chi_{\perp}$.

The resulting χ/C, based on a singlet-triplet splitting of $-2J/k = 0.46$ K, has been plotted as a dashed line in fig. 3 and accounts approximately for the deviation of the experimental data from Curie's law (dash-dotted line). When expanding the exponential functions in eq. (3.4) one easily derives that the Curie-Weiss constant $\theta = J/3k$ or $\theta \approx -0.075$ K. The experimental data above 1 K indicate that θ is practically zero, hence it is suggested that the Y ions have exchange coupling of positive sign, presumably with their nearest neighbours, i.e. X ions.

Below T_N one finds $\chi_{//}/C_{//} > \chi_{\perp}/C_{\perp}$ which may suggest a preference for spin alignment in the $g_{\perp}$ plane.

3.3. H–T diagram

As was already outlined in chapter I, the application of external magnetic fields to magnetically ordered crystals under adiabatic conditions may yield information about the kind of magnetic ordering and in particular may give a phase diagram in antiferromagnetic crystals[14]. In the latter case the phase boundary is associated with the reversal of sign of the magnetocaloric effect. Whereas usually in the antiferromagnetic region the temperature along an isentrope decreases with increasing magnetic field strength, the reverse is true in the paramagnetic region.

This method, which consists of applying an adiabatic field variation and measuring the corresponding temperature change, was utilized on Cu–La nitrate both above and below the critical temperature T_N, the results being presented in fig. 4. We notice firstly that above T_N the isentropes are not qualitatively different from those measured below T_N. This is probably related to the aforementioned model, in which in first approximation isolated ion pairs are considered, which are characterized by a singlet-triplet splitting of 2J. In a magnetic field one of the magnetic substates of the triplet may cross the singlet ground state and this will in principle, like for instance in Ni salts,[15,16] lead to a temperature decrease. For a splitting of $2J/k = -0.46$ K one expects level crossing at $g_{//}\beta H = 2J$, that is at $H \approx 3$ kOe. This rather close to the magnetic field strength of 3.7 kOe at which a minimum in

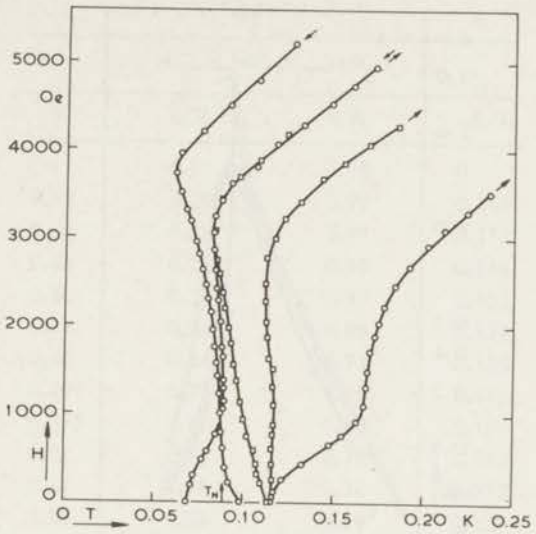

Fig. 4. Isentropes in the H–T diagram for Cu–La nitrate.

○ : H // c axis, □ : H ⊥ c axis.

The arrows at the end of the isentropes indicate whether the field was varied up or downwards.

the temperature is observed for the isentropes at the left hand side in fig. 4. For higher temperatures the minimum in the isentropes becomes less pronounced, which is presumably due to the temperature increase from the paramagnetic Y ions, having a positive magnetocaloric effect.

Or alternatively stated: the singlet-triplet system may not be able to cool the Y ions effectively when $g_{//}\beta H \approx kT$. The problem of determining the temperature as a function of H could be solved exactly for our model, but this does not seem warranted in view of the neglect of coupling between X ions and Y ions and of the somewhat qualitative aspect of the magnetocaloric-effect measurements. However, the data are definitely in better agreement with a pair-coupling model than with the usual behaviour of antiferromagnets as described by a phase boundary below T_N.

4. Ni–La nitrate

4.1. Heat capacity

The heat capacity of $Ni_3La_2(NO_3)_{12}.24H_2O$ is shown in fig. 5; at $T_c = 0.393$ K a sharp singularity is found. The total entropy change associated with the heat-capacity anomaly is $\Delta S = 1.07$ R which is close to R ln 3 = 1.10 R per Ni ion. Hence neither the X ions nor the Y ions have crystalline-field splittings of the order

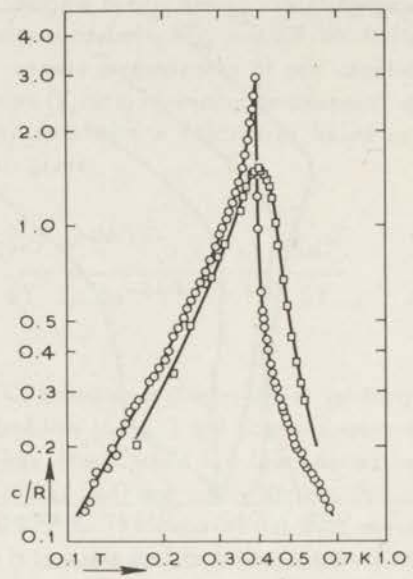

Fig. 5. Heat capacity (O) of Ni–La nitrate per gramion Ni versus temperature on a logarithmic scale. The maximum defines $T_c = 0.393$ K. The heat capacity was also measured in the presence of a magnetic field of 880 Oe along the c axis (□).

of magnitude of 1 cm^{-1} or larger, as has been suggested by EPR measurements[8]. If for one third of the ions, i.e. the Y ions, $D/k = -3.24$ K, then one would expect that the average entropy yield below 0.6 K would amount to 0.88 R ln 3 per gramion Ni. Other possibilities like $D > 0$ at the Y site or large D values for X ions would correspond to still smaller values of the entropy yield. In view of the smallness of the uncertainty in the experimental result all these possibilities may be dismissed. It should also be mentioned that the EPR measurements[8] refer to a crystal containing 1% Ni merely. In table III smoothed data are summarized for c/R, S/R and E/R.

The crystalline field splitting for the X ions ($D/k = 0.29$ K) as reported by Hoskins et al.[17] for a diluted salt contribute to the heat capacity at relatively high T according to $cT^2/R = \frac{2}{9}(D/k)^2$, which yields $cT^2/R = 0.0187\ K^2$ for one gramion Ni. We calculate for the dipolar contribution to the specific heat a value of $c_{dip}T^2/R = 1.15 \times 10^{-3}\ K^2$. The experimental value of cT^2/R cannot be accurately determined because the specific heat was measured to temperatures merely up to 1.7 T_N. The asymptotic value can be estimated as $cT^2/R \approx 0.055\ K^2$; this value corresponds to $b/C = 3.7 \times 10^6\ Oe^2$, where C is the Curie constant. It is seen that the sum of the contributions to cT^2/R from crystalline field interactions and dipolar coupling is much smaller than the experimental value. Since there is practically no h.f.s. inter-

Table III

$Ni_3La_2(NO_3)_{12}\cdot 24H_2O$			
T	c/R	S/R	−E/R
∞	0	1.10	0
0.52	0.20[5]	0.99[5]	0.106
0.50	0.22[5]	0.99	0.111
0.48	0.25[5]	0.98	0.116
0.46	0.29	0.97	0.121
0.44	0.34[5]	0.95	0.127
0.42	0.44	0.93	0.135
0.40	0.71	0.91	0.146
0.393	2.97	0.87[5]	0.159
0.38	2.13	0.79	0.192
0.37	1.78	0.74	0.212
0.36	1.58	0.69[5]	0.229
0.34	1.26	0.61	0.257
0.32	1.06	0.54	0.281
0.30	0.91	0.48	0.300
0.28	0.78	0.42	0.317
0.24	0.56	0.32	0.344
0.20	0.38[5]	0.23	0.363
0.16	0.25[5]	0.16	0.375
0.12	0.15	0.10[5]	0.383
T_N = 0.393 K		$\Delta E/R$ = 0.390 K	
cT^2/R = 0.055 K^2		$\Delta S/R$ = 1.07	

action, we may sately ascribe the difference to exchange interactions. This is also suggested by the sharp descent of the heat capacity above T_c, which is in marked contrast to the behaviour of magnetic compounds exhibiting predominantly dipolar and crystalline field interactions, e.g. Gd salts[18] Cr alums[19].

Since there is only one rather sharp singularity, the heat-capacity data suggest that the X ions and the Y ions are not behaving as separate systems, but must be rather tightly coupled by exchange interaction.

The heat capacity has also been measured in the presence of an external magnetic field H, applied in the $g_{//}$ direction (fig. 5). The magnitude of the field was chosen at 880 Oe, being large enough as to make $g_{//}\beta H$ comparable to kT_c and on the other hand small enough as not to change the shape of the c versus T curve significantly. It was found that the heat capacity curve is shifted to slightly higher T, which indicates that the crystal behaves ferromagnetically in low fields. The shift in T_c is 4 ± 1% and the change in the shape of the curve is hardly noticeable

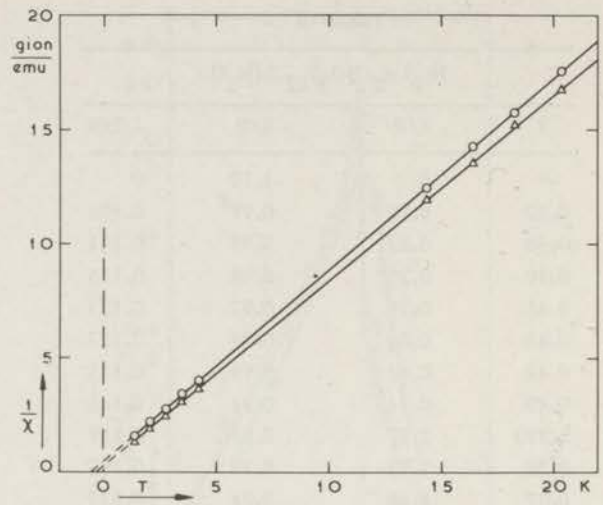

Fig. 6. The reciprocal susceptibility, $1/\chi$, in gramion/emu., of Ni–La nitrate versus temperature.

O: parallel c axis □: perpendicular c axis.

except that there is an excess heat capacity at $T > 0.5$ K. The excess at $T = 0.6$ K amounts to 25%, which is quite reasonable in view of $b/C = 3.7 \times 10^6$ Oe^2 and H^2 being 0.77×10^6 Oe^2, the relative increase being expected to be CH^2/b.

4.2. Susceptibility above 1 K

Fig. 6 shows the dependence of $1/\chi$ on T. At temperatures of liquid helium paramagnetic saturation was observed. The graphs can be described with the Curie-Weiss law: $\chi = C/(T - \theta)$. For the direction parallel the c axis we found:

$$\theta_{//} = -0.31 \text{ K}; \; C_{//} = 1.232 \text{ emu.K/gion and } g_{//} = 2.23$$

and for the direction perpendicular to the c axis:

$$\theta_{\perp} = -0.53 \text{ K}; \; C_{\perp} = 1.189 \text{ emu.K/gion and } g_{\perp} = 2.18.$$

Borrowing from the results of section 4.6 we take $J_{XX}/k = -0.36$ K. Antiferromagnetic coupling, $-2J_{XX}\vec{s}_1.\vec{s}_2$, for pairs of ions at X sites would give a Curie-Weiss constant of $\theta_{ex} = \frac{4}{3} J_{XX}/k$ for two thirds of the ions. These ions have, in addition, a crystalline field splitting parameter $D/k = +0.29$ K and this will give $\theta^{//}_{cr} = -\frac{1}{15}(D/k)(2s - 1)(2s + 3) = -0.10$ K and $\theta^{\perp}_{cr} = -\frac{1}{2}\theta^{//}_{cr} = +0.05$ K. Therefore, we get

$$\theta^{//}_{2/3} = \theta^{//}_{ex} + \theta^{//}_{cr} = -0.48 - 0.10 = -0.58 \text{ K},$$

$$\theta^{\perp}_{2/3} = \theta^{\perp}_{ex} + \theta^{\perp}_{cr} = -0.48 + 0.05 = -0.43 \text{ K}.$$

For the crystal as a whole we shall then predict θ values which are 2/3 times the above numbers, or $\theta^{//} = -0.39$ K, and $\theta^{\perp} = -0.29$ K. The above consideration should be extended to include the interactions of Y ions. Since, according to section 4.1 the crystalline field interaction of the Y ions is small, we conclude that exchange interactions of the Y ions contribute significantly to the Curie-Weiss constant.

4.3. Susceptibility below 1 K

The results of the susceptibility measurements below 1 K are given in fig. 7. When measuring in the $g_{//}$ direction it is seen that χ versus T rises rapidly with decreasing temperature and reaches a maximum value at T_c. There is a sharp peak in χ' when utilizing the a.c. bridge (ν = 260 Hz), corresponding to increased a.c. losses (χ'') at T_c, whereas the d.c. susceptibility (χ_o) remains practically constant below T_c. The maximum value of χ_o agrees approximately with the estimated reci-

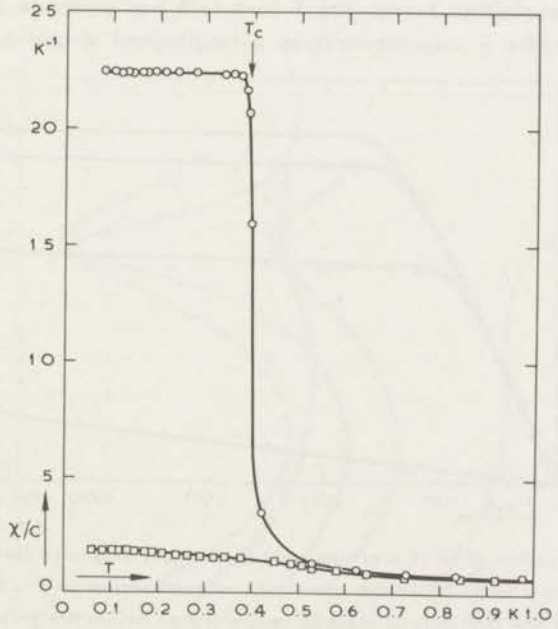

Fig. 7. Susceptibility of Ni–La nitrate, divided by the Curie constant, below 1 K.
○: d.c. susceptibility parallel to c axis.
□: d.c. susceptibility perpendicular to c axis.

procal value of the demagnetizing factor N, i.e. $\chi_o^{max} \approx 1/N$. These results show, therefore, that Ni–La nitrate becomes ferromagnetic at $T_c = 0.393$ K. Measurements of χ_o in rather small external longitudinal magnetic fields (H = 40 Oe or H = 100 Oe) show very different results. This indicates that the anisotropy energy has a minimum in the $g_{//}$ direction.

The susceptibility in the $g_\perp$ direction does not reach such high values at T_c (fig. 7). There is no difference between the results of a.c. and d.c. susceptibility measurements in the $g_\perp$ direction. Since furthermore χ is practically constant as a function of temperature, we conclude that ferromagnetic alignment of the Ni ions occurs along the $g_{//}$ direction. The occurrence of spontaneous magnetization along the trigonal crystal axis is in keeping with magnetic group theory.

4.4. Magnetization below T_c

Measurements of the isothermal susceptibility χ_o in the presence of longitudinal fields, applied in the $g_{//}$ direction, may be used to obtain the value of the saturation magnetization. For sufficiently small fields, however, it may be expected that only the domain magnetization is rotated, or, in our case, more probably reversed. One then measures essentially the spontaneous magnetization and it was our intention to ascertain whether X ions and Y ions both participate in the ferromagnetic alignment. From the χ measurements in a longitudinal magnetic field we obtain

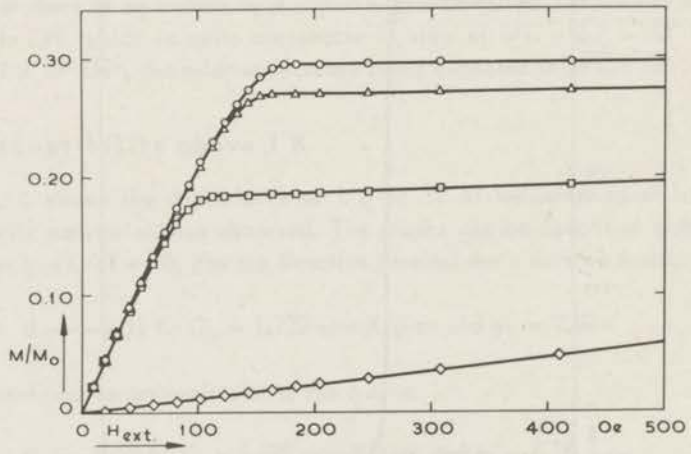

Fig. 8. Magnetization of Ni–La nitrate versus external magnetic field, H_{ext}, applied along the c axis. M_o is the saturation magnetization at T = 0 K.
Three of the four curves refer to temperatures below the critical temperature ($T_c = 0.393$ K) and the lowest curve refers to a temperature above T_c.

○: T = 0.097 K. □: T = 0.306 K.
△: T = 0.200 K. ◇: T = 0.550 K.

(by integrating with respect to the variable H) M versus H and the result is shown in fig. 8. The M versus H curve at the lowest temperature (T = 0.097 K) clearly shows that a) saturation is obtained at comparatively low values of H, b) the magnitude of the saturation magnetization pertains to one third of the Ni ions, hence very probably to the Y ions.

4.5. H–T diagram

We have utilized the method of measuring isentropes in the H–T diagram, described in section 2, particularly on Ni–La nitrate. This crystal shows ferromagnetic behaviour according to measurements of χ below T_c, but it has a Curie-Weiss constant of antiferromagnetic sign according to χ measurements in the temperature range far above T_c.

Our measurements were carried out in magnetic fields along the $g_{//}$ direction and also along the $g_{\perp}$ direction and the results are given in fig. 9.

It may be seen that in relatively small fields there is a positive magnetocaloric effect, which agrees with ferromagnetism. When further increasing the magnetic field strength, however, there is a very strong decrease of temperature if the field is in the $g_{//}$ direction and also a slight decrease if the field is in the $g_{\perp}$ direction. We may explain these results qualitatively by assuming an antiferromagnetic exchange coupling between the X ions, which is roughly isotropic. Furthermore, the initial

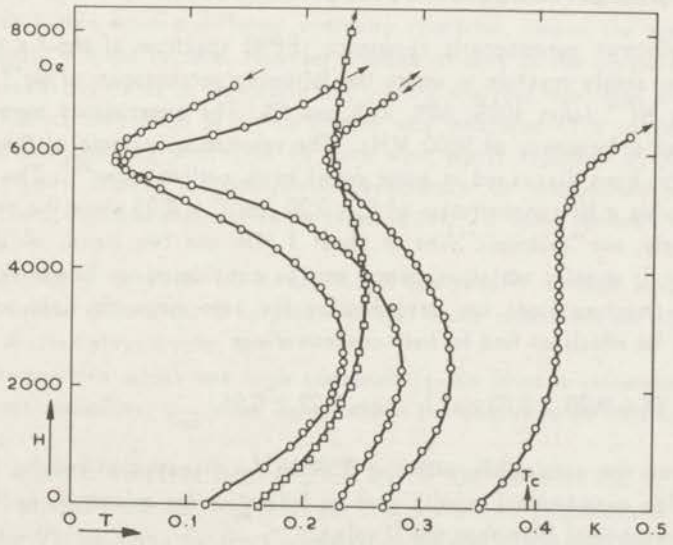

Fig. 9. Isentropes in the H–T diagram for Ni–La nitrate.
○: H // c axis, □: H ⊥ c axis.
The arrows indicate whether the magnetic field was varied up or downwards.

temperature rise may be due to ferromagnetic alignment of the Y ions. According to the susceptibility measurements in the $g_\perp$ direction it is not surprising that the magnetocaloric effect in that direction is smaller than in the $g_{//}$ direction. The positive magnetocaloric effect in the $g_\perp$ direction extends to higher magnetic fields and presumably cancels to some extent the negative magnetocaloric effect at high fields (> 2kOe), the latter due to the X ions.

The assertion that the antiferromagnetic coupling between X ions is roughly isotropic is based on the observation that the sign reversal of the magnetocaloric effect occurs at magnetic field strengths, which are approximately equal for H // c axis and H $\perp$ c axis.

Finally it may be remarked that the cooling obtained when applying an external magnetic field adiabatically is particularly strong in this crystal when compared to other compounds having antiferromagnetic ordering, such as for instance $CoCs_3Cl_5$ (chapter V) and $NiSiF_6.6H_2O$[15]. We ascribe this phenomenon to the circumstance that the X-ion pairs are decoupled in rather high magnetic fields both from each other and from Y ions such that one deals effectively with a paramagnetic system. In that case entropy exchange among different spin systems may be negligible and this may present a more favourable situation for cooling than, for instance, in the case of two antiferromagnetically coupled sublattices considered in a molecular field approach of this cooling effect[14].

4.6. EPR and paramagnetic relaxation results

The electron paramagnetic resonance (EPR) spectrum of Mg–La nitrate was measured for single crystals in which the following percentages of Mg^{++} ions were replaced by Ni^{++} ions: 100%, 60%, 20%, and 5%. The experiments were performed at 4.0 K and a frequency of 9600 MHz. The resonance patterns of these various samples have been discussed in some detail in an earlier paper[20]. The spectra of crystals having a Ni concentration of C = 0.20 and C = 0.05 show the same constituents, namely, one "isotropic" line at about 1 kOe and two lines, which follow a $(3\cos^2\phi - 1)$ angular variation, hence may be considered as fine-structure lines. These fine-structure lines are described by the zero magnetic field energy level splitting D, for which we find for both concentrations

$$|D| = 0.20 \pm 0.03\ \text{cm}^{-1}; \quad g = 2.29 \pm 0.05.$$

These values are compatible with the 0.5% Ni^{++}-concentration results of Hoskins et al.[17]. The experimental results gave no indication for anisotropy in the g value or for the presence of more than one D value.

To understand the occurrence of the "isotropic" line for which the resonance fields are

$C = 0.20\ Ni^{++}$ crystal: $H_o = 980$ Oe,

$C = 0.05\ Ni^{++}$ crystal: $H_o = 1100$ Oe,

we propose a spin Hamiltonian, H, including an isotropic exchange interaction J between X ions 1 and 2, belonging to one pair:

$$H = g_1\beta\,\vec{H}.\vec{s}_1 + g_2\beta\,\vec{H}.\vec{s}_2 - 2J\vec{s}_1.\vec{s}_2 + D_1\{s_{1z}^2 - \tfrac{1}{3}s(s+1)\} + \\ + D_2\{s_{2z}^2 - \tfrac{1}{3}s(s+1)\} \qquad (4.1)$$

where $s = s_1 = s_2$. Taking $g_1 = g_2 = g$ and $D_1 = D_2 = D > 0$, an energy level scheme results for the external field parallel to the c axis, as has been given in fig. 10. It is suggested that the "isotropic" line may be identified as the transition between the two lowest levels. From the energy difference of these levels we obtain

$C = 0.20\ Ni^{++}$ crystal: $J = 0.23\ cm^{-1}$;

$C = 0.05\ Ni^{++}$ crystal: $J = 0.24\ cm^{-1}$.

We did not find any indication of an absorption line corresponding to a high D value, due to the Y ions. This line, of which the intensity should increase greatly with increasing ϕ, has been reported by Culvahouse[8] for a C = 0.01 crystal.

Strictly speaking, no transitions between s = 0 and s = 1 states are expected, since these states have a different symmetry character. Hence the matrix element for a magnetic rf field is zero. However, random strains in the crystals or the presence of electric rf fields in the cavity may yield a non-zero transition probability[31].

Spin-lattice relaxation of Ni–La nitrate was measured in a concentrated salt and in various samples where the Ni ions were partly replaced by Mg ions. The relaxation times showed a complicated dependence on temperature and external magnetic field. Detailed information is given in ref. 21. Some features will be mentioned here.

1. At temperatures between 1.2 K and 4.2 K the results at high magnetic fields showed a double relaxation. It is plausible that cross relaxation between pairs of Ni ions at X sites plays a role.

At frequencies which are high compared to the inverse relaxation time, the adiabatic susceptibility, χ_{ad}, was measured. In the concentrated salt we found two b/C values:

a. At low magnetic fields we found $b/C = 2.5 \times 10^6\ Oe^2$ at T = 1.2 K, a result obtained by correcting the measurements for the deviations of the Curie law[22] (eq. (5.1) chapter V), by using for the Curie-Weiss constant $\theta_{//} = -0.31$ K (see section 4.2). The corrected b/C values slightly varied as a function of temperature (20% decreasing from 1 K to 4.2 K), and also differ from $b/C = 3.7 \times 10^6\ Oe^2$ as obtained from the specific-heat measurements. The so obtained b/C value is presumably

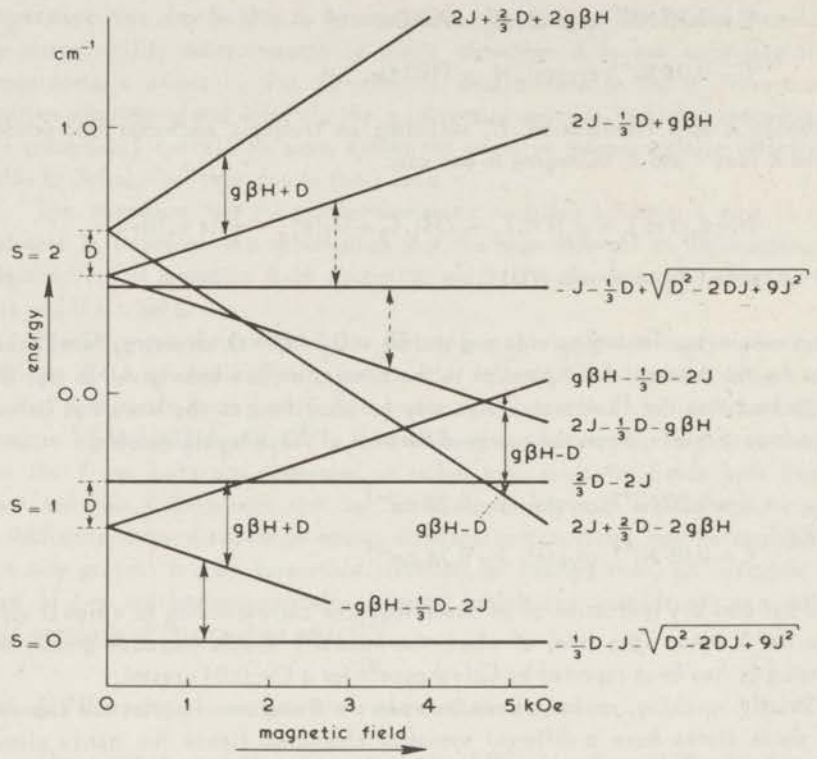

Fig. 10. Energy level scheme of exchange coupled pairs (eq. (4.1)) in which the absolute value of J has been used, versus magnetic field parallel to the c axis in Ni–La nitrate. Observed resonances are indicated by vertical arrows.

correlated with a situation of the system of Ni-ion pairs being "partially" in equilibrium. If one assumes the energy level diagram of the Ni ions to be roughly the same as in the case of the 5% salt (fig. 10), it is doubtful whether all Ni pairs are in equilibrium.

b. At high magnetic fields b/C is varying from 50 x 10^6 Oe^2 at T = 4.2 K to 17 x 10^6 Oe^2 at T = 1.2 K. When we calculate b/C from the spin-energy levels (fig. 10) we find b/C = 22 x 10^6 Oe^2 at temperatures high compared to the level splittings. This value would decrease when the temperature is lowered, while on the other hand deviations from the Curie law would increase b/C. Further experiments are required to explain the observed b/C values.

2. The measurements on the second relaxation mechanism in the concentrated salt indicates that cross-relaxation processes between neighbouring Ni ion pairs occur. In order to verify this, a crystal grown from a solution containing 5% Ni was examined. Various maxima in the χ'' versus H_c curve were found, which correspond ob-

viously to fast relaxation processes. From these curves we found a series of external magnetic field strengths for which cross-relaxation processes are possible. From the energy level scheme of the Ni pairs, calculated on basis of the measured D and J values obtained from EPR measurements, one obtains the field strengths at which cross relaxations may be expected. The agreement is found to be quite satisfactory, which strongly supports the idea of X-site Ni ions occurring as exchange-coupled pairs, as proposed in eq. (4.1).

4.7. Heat capacity of magnetically diluted Ni–La nitrate

For magnetically diluted Ni–La nitrate the heat capacity was measured as a function of temperature, according to the methods of section 2.1.

The concentrations of Ni used were, as determined by chemical analysis 83.9%, 72.6%, 68.2% and 57%, and the specific heat exhibited a maximum at T = 0.297, 0.236, 0.204 and 0.133 K, respectively. The results are shown in fig. 11. In all cases the heat-capacity anomaly remains observable in the temperature range accessible to our experimental technique, but it is seen that the singularity is

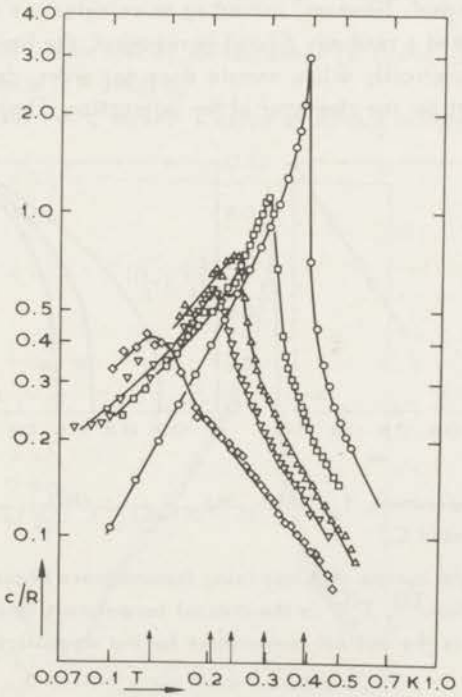

Fig. 11. Heat capacity per mole of magnetically diluted $Ni_{3C}Mg_{3(1-C)}La_2(NO_3)_{12}\cdot 24H_2O$ on a logarithmic scale.
O: C = 1, □: C = 0.84, Δ: C = 0.73, ∇: C = 0.68, ◇: C = 0.57.

strongly broadened. Particularly for the crystal containing 57% Ni it becomes difficult to determine the position of the maximum heat capacity on the temperature scale. Plotting the temperature of the maximum in the heat capacity versus concentration, we obtain fig. 12a. The latter figure suggests that the critical temperature goes to zero when the concentration decreases to 45 ± 10%. This is still a relatively high concentration. We may e.g. compare this result with one of the few calculations made for diluted ferromagnets, namely with those of Essam and Garelick[23] on Ising systems and applying the technique of Syozi[24]. Their results for a plane square lattice give a critical concentration $p_c = 0.5$ and their relation of $T_c^{(C)}/T_c^{(1)}$ versus C, where C is the concentration, is given in fig. 12b. For other lattices the shape of the curve is practically the same, but p_c is considerably lower for cubic lattices and even for the diamond lattice amounts to only 0.375. We may conclude that the coordination number in Ni–La nitrate is low, as might have been anticipated from the crystal structure if only the ion pairs at X sites are considered. On the other hand, the X-site pair is surrounded by two triangles of ions at Y sites; for comparison we may mention that p_c for a honeycomb lattice amounts to 0.648.

Of course the Ising model may not be appropriate and moreover Ni–La nitrate is not a simple ferromagnet. However, according to calculations of Rushbrooke and Morgan[25], who considered a randomly diluted ferromagnet, the limiting concentration, p_c, below which a magnetically dilute sample does not order, depends only on the lattice structure and not on the character of the interaction. They further predict an

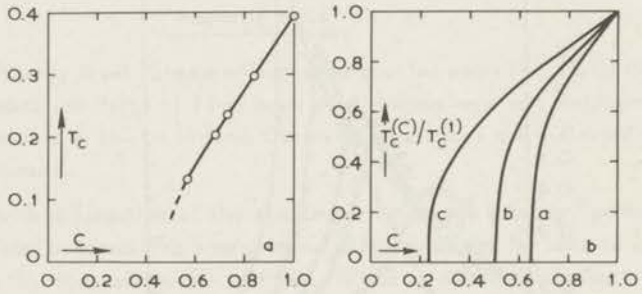

Fig. 12 a) Curie temperature, T_c, of $Ni_{3C}Mg_{3(1-C)}La_2(NO_3)_{12}{\cdot}24H_2O$ versus Ni concentration C.

b) Theoretical curves of dilute Ising ferromagnets according to Essam and Garelick[23], $T_c^{(C)}$ is the critical temperature at concentration C and $T_c^{(1)}$ is the critical temperature for the magnetically undiluted crystal.

curve a: honeycomb lattice,
curve b: plane square lattice,
curve c: simple cubic lattice.

initial decrease of $T_c^{(C)} = CT_c^{(1)}$ for the Ising model and $T_c^{(C)} < CT_c^{(1)}$ for the Heisenberg model near $C = 1$. Experimentally a slope in fig. 12a near $C = 1$ is observed which is in agreement with predictions for the Heisenberg model. A further, rather important conclusion which may be drawn from the heat-capacity results at low concentrations is that e.g. the heat capacity at 0.5 K decreases by a factor 2.1 when the concentration is decreased from 100 to 72.6%. This cannot be reconciled with a significant contribution from crystalline field splittings to the heat capacity and neither with the possibility of a large D value ($D/k \approx 3K$) for part of the Ni ions. On the other hand, the number of exchange coupled pairs going approximately as C^2 for $C \approx 1$, satisfactorily accounts for the factor 2.1 just mentioned.

4.8. Heat capacity of Ni–Nd nitrate

In order to further investigate the magnetic ordering of Ni–La nitrate an auxiliary heat-capacity measurement on Ni–Nd nitrate was carried out. This was motivated by the consideration that the Nd ion, presumably not participating in exchange interactions, may serve as a probe for estimating the effective local magnetic field in the ordered state.

The result of the heat-capacity measurement is shown in fig. 13, the curve shows a sharp maximum at $T = 0.420$ K.

A comparison with the c versus T curve of Ni–La nitrate (fig. 5) shows that

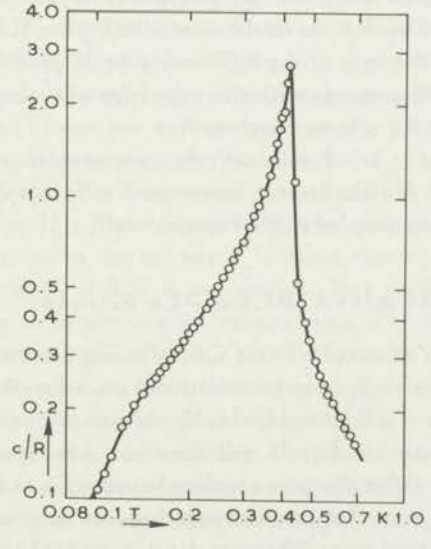

Fig. 13. Heat capacity per mole of $Ni_3Nd_2(NO_3)_{12}\cdot 24H_2O$ versus temperature on a logarithmic scale. The curve exhibits a maximum at $T = 0.420$ K.

a. T_c is shifted upwards by about 8%.
b. the shape of the curve is practically unaffected except for T up to about 0.15 K. For instance, at T = 0.125 K Ni–Nd nitrate has 30% larger heat capacity than Ni–La nitrate. One may roughly estimate the "excess" heat capacity to be represented by $c_{excess} T^2/R \approx 0.002\ K^2$/mole.
c. the entropy content of the heat-capacity curve above 0.04 K gives almost precisely k ln 3/Ni ion, hence no entropy change due to Nd ions is noticeable above that temperature.

We conclude that the Nd spin system remains in the paramagnetic state down to 0.04 K. We note that the heat capacity of Nd–Mg nitrate can be estimated to be $cT^2/R = 1.6 \times 10^{-4} K^2$/mole from dipolar interactions according to Daniels'[13] formula. However, an effective field at low T along the trigonal axis of 680 Oe would give a Zeeman splitting and a Schottky type anomaly in the heat capacity, which in the region of 0.1 K may be approximated by $cT^2/R = 0.002\ K^2$/mole. Similarly an effective field of 115 Oe in the $g_\perp$ direction would give the same "high"-temperature contribution to the heat capacity.

We also conclude that in the ordered state of the Ni system the effective (molecular) field does not exceed about ½ kOe, which is certainly very much smaller than, for instance, the magnetic field required for bringing Ni–La nitrate into a paramagnetic state (H > 6 kOe), at small T.

Furthermore, it may be mentioned that considering the nearest neighbours of a Nd ion, there is one close-lying Ni ion at an X site at 6.17 Å. When the spin of the X ions would be aligned along the $g_{//}$ axis of the crystal at low temperatures, the dipolar energy, E_d, of the Nd ion would amount to $E_d/k = 0.10$ K. (A much larger coupling would result if the spin of the Ni^{++} would be aligned in the $g_\perp$ direction). From the comparison of this energy with the experimentally observed upper limit in the effective fields at the Nd site we conclude that
a. molecular field concept is at variance with the experimental results.
b. the Ni-ion pairs at the X sites are not ferromagnetically coupled, but may be in a state of total spin 0, hence coupled antiferromagnetically.

4.9. Heat capacity of mixed (Ni,Co)–La nitrate

The heat capacities of mixed Ni- and Co-lanthanum nitrate show singularities, from which the critical point T_c may be determined as a function of concentration. For nickel concentrations C = 0.83 and C = 0.42, we found T_c = 0.360 K and 0.264 K, respectively. This is shown in fig. 14 and does not give a surprising behaviour. The result suggests that either the pair coupling between Co and Ni is intermediate between Ni–Ni and Co–Co or that the exchange between ions at X sites and those at Y sites plays an essential role. Otherwise for a system of isolated pairs and for a crystal containing 50% Ni–50% Co one would expect only roughly 25% Ni–Ni pairs and 25% Co–Co pairs and hence a noticeable depression of the critical temperature

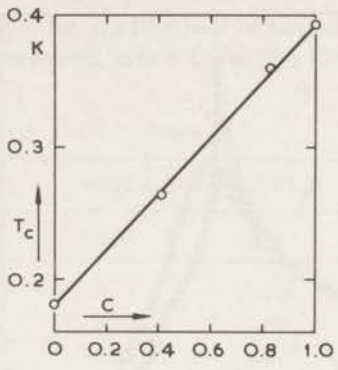

Fig. 14. Critical temperature of mixed cobalt-nickel lanthanum nitrate, $Co_{3(1-C)}Ni_{3C}La_2(NO_3)_{12}\cdot 24H_2O$ versus nickel concentration, C.

for such concentrations. The latter suggestion contradicts the experimental results, hence presumably the total X–Y coupling is comparable to the X–X coupling taking into account that an X ion has only one X neighbour but has three Y neighbours.

5. Mn–La nitrate

5.1. Heat capacity

The heat capacity of $Mn_3La_2(NO_3)_{12}\cdot 24H_2O$ has been measured between 0.08 and 0.7 K (fig. 15). A singularity was observed at 0.230 K. At about 0.1 K the c versus T curve is not so sharply decreasing with diminishing temperature as found in the Cu and Ni compounds below the critical temperature. This is a familiar aspect of Mn compounds and is due the nuclear spin specific heat. On basis of the known hyperfine structure constants one calculates for $T < T_N$, $c_{hfs}T^2/R = 0.003\ K^2$ and this was subtracted from the data in order to obtain the electronic heat capacity (dashed curve in fig. 15). When extrapolating the corrected heat capacity to zero temperature and calculating the entropy it is found that at 0.08 K the electron spin system retains an entropy of 0.27 R per gramion. This number may be in error by as much as 25%, due to uncertainty in the extrapolation. The data at high temperatures were extrapolated according to $cT^2/R = 0.060\ K^2$, which fits the data reasonably well above 0.35 K. As a result, the total entropy change is found to be $\Delta S = 1.76$ R, which is to be compared to the theoretical value R ln $(2s + 1)$ = R ln 6 = 1.79 R. Although for this compound a considerable fraction of the entropy is found in the extrapolated region towards low temperatures, experience on many other magnetic compounds has shown that extrapolation according to straight lines on a logarithmic plot of c versus T usually leads to rather precise entropy evaluations. Therefore, it may be safely concluded that all electron spins participate in the phase transition at $T_N = 0.230$ K.

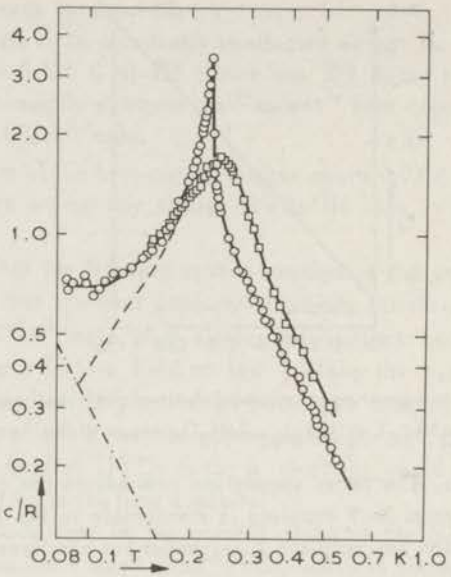

Fig. 15. Heat capacity of Mn–La nitrate per gramion Mn versus temperature (○). The dash-dotted line represents the nuclear specific heat; the dashed line is obtained by subtracting the nuclear specific heat from the experimental data. The maximum yields $T_N = 0.230$ K. The heat capacity was also measured in a magnetic field of 660 Oe, directed along the c axis (□).

The smoothed data for c/R per gramion Mn, corrected for the nuclear specific heat, and S/R are presented in table IV, in which also the energy has been tabulated.

The value of $cT^2/R = 0.060K^2$ may be compared with the value preliminarily reported by Sapp et al.[26], namely $0.070 \pm 0.002\ K^2$.

Crystalline field interactions and hyperfine interactions, calculated from EPR data, give contributions at $T > T_N$, of

$$c_{cr}T^2/R = \frac{1}{45}\, s(s+1)(2s-1)(2s+3)\, D^2/k^2 = 0.0022\ K^2,$$

$$c_{hfs}T^2/R = \frac{1}{9}\, s(s+1)\, I(I+1)(A^2+2B^2)/k^2 = 0.0041\ K^2.$$

Hence, after subtraction we find $cT^2/R = 0.054\ K^2$ for dipolar and exchange contributions to the magnetic heat capacity of the electron spins in the high-temperature approximation. We calculated the dipolar contribution to be $c_{dip}T^2/R = 0.013\ K^2$, leaving $cT^2/R = 0.041\ K^2$ for exchange interactions.

The heat capacity has also been measured in the presence of an external magnetic field of 660 Oe, applied along the $g_{//}$ direction. As can be seen from fig. 15, the sharp peak for H = 0 is rounded off and the curve is shifted towards higher

temperatures. At T = 0.5 K the specific heat in magnetic field is increased by about 35%, which is in good agreement with a factor $(b + CH^2)/b$, where $b/C = 1.14 \times 10^6$ Oe^2.

Table IV

$Mn_3La_2(NO_3)_{12}\cdot 24H_2O$			
T	c/R	S/R	−E/R
∞	0	1.79	0
0.40	0.38	1.60	0.152
0.38	0.42	1.57[5]	0.160
0.36	0.47	1.55	0.169
0.34	0.52[5]	1.52	0.179
0.32	0.59	1.49	0.190
0.30	0.66[5]	1.45	0.202
0.29	0.71	1.42[5]	0.209
0.28	0.76[5]	1.40	0.217
0.27	0.83	1.37	0.225
0.26	0.91	1.34	0.233
0.25	1.04	1.30	0.243
0.24	1.25	1.25[5]	0.254
0.23[5]	1.48	1.23	0.261
0.230	3.43	1.17	0.273
0.22	2.14	1.05	0.301
0.21	1.73	0.96	0.320
0.20	1.46	0.88	0.336
0.18	1.09[5]	0.75	0.362
0.16	0.83	0.63[5]	0.381
0.14	0.68	0.53	0.397
0.12	0.54[5]	0.43[5]	0.409
0.10	0.37[5]	0.35	0.418
0.08	0.29	0.27	0.425
T_N = 0.230 K		$\Delta E/R$ = 0.437 K	
cT^2/R = 0.060 K^2		$\Delta S/R$ = 1.76	

5.2. Susceptibility above 1 K

Fig. 16 shows the dependence of $1/\chi$ versus T in the temperature range of liquid hydrogen and liquid helium. At the lowest temperatures paramagnetic saturation was observed. No temperature-independent paramagnetic part of the susceptibility was found. We obtained for the direction parallel to the c axis a Curie-Weiss

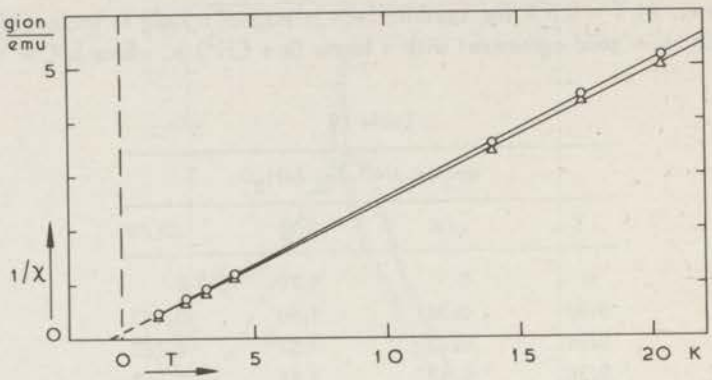

Fig. 16. Reciprocal susceptibility, $1/\chi$, of Mn–La nitrate versus temperature.
Δ : parallel c axis, O : perpendicular c axis.

constant $\theta_{//} = -0.47$ K. For a direction perpendicular to the c axis, $\theta_{\perp} = -0.42$ K. This result is to be compared with measurements of Sapp et al.[26], who reported $\theta_{//} = -0.31$ K and $\theta_{\perp} = -0.49$ K.

5.3. Susceptibility below 1 K

The isothermal susceptibility was measured by means of the a.c. bridge and also by using the d.c. galvanometer method; the two methods did not give noticeably different results down to 0.1 K. The measurements were performed with the crystal c axis mounted parallel to the axis of the measuring coils ($\chi_{//}$), and also with the c axis perpendicular to the coil axis ($\chi_{\perp}$). Furthermore, the $\chi_{//}$ measurements were carried out in the presence of longitudinal external fields of 500 Oe and 1500 Oe. The results are summarized in fig. 17.

Below 2 K a curvature in the $1/\chi$ versus T plot is observed, which is practically absent between 4 and 2 K. The deviation from the Curie-Weiss relation below these temperatures has the antiferromagnetic sign. The susceptibility in the region of the critical temperature indicates that both ferromagnetic and antiferromagnetic interactions are operative. The increase of $\chi_{//}$ by a factor two when decreasing T from 0.3 to 0.230 K cannot be easily accounted for by pure antiferromagnetism.

In view of the results on the other isomorphous compounds it may be suggested that 1/3 of the Mn ions at Y sites have a tendency to ferromagnetic alignment along the $g_{//}$ direction. That the $g_{//}$ direction is favoured by the Y ions may be due at least partly to the value of the crystalline field splitting parameter D(D/k = –0.031 K) being negative and larger than that of the X ions. Crystalline field effects alone would cause a decrease of $\chi_{\perp}$ with decreasing temperature for the X ions. However, $\chi_{\perp}$ is practically constant below T_N and therefore our results suggest that both X

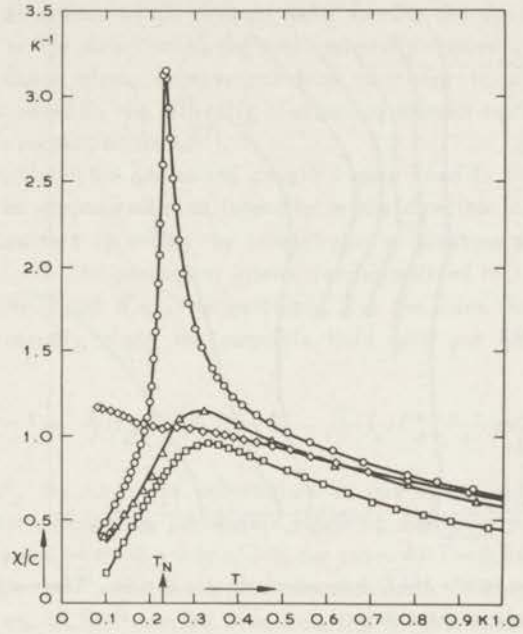

Fig. 17. Susceptibility divided by the Curie constant, χ/C, of Mn–La nitrate below 1 K. There was no difference between a.c. and d.c. measurements.

○: // c axis, H = 0 Oe
△: // c axis, H = 500 Oe.
□: // c axis, H = 1500 Oe.
◇: ⊥ c axis, H = 0 Oe.

and Y ions are aligned preferentially along the c axis and furthermore that the Y ions do not remain in a paramagnetic state but participate in the magnetic ordering.

The results of the measurements of $\chi_{//}$ in longitudinal fields show that for modest values of H the peak in $\chi_{//}$ vanishes. This result is comparable to those in the Ni compound and is likewise probably due to the rather weak spontaneous ferromagnetic moment of the crystal below T_N, being due to only 1/3 of the Mn ions.

5.4. H–T diagram

The measurements of the temperature as a function of an adiabatically applied magnetic field result in isentropes in the H–T diagram, shown in fig. 18. It is seen that a fairly complicated behaviour is found below T_N.

Like in the Ni compound temperature increases are observed in medium field strengths (up to 1.5 kOe) followed by decreases in fairly high fields (above 2 kOe). These results can only to some extent be interpreted by using the susceptibility

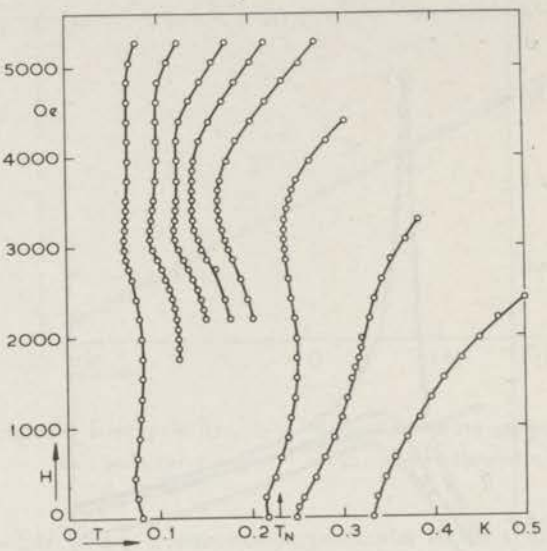

Fig. 18. Isentropes in the H–T diagram of Mn–La nitrate. The magnetic field was directed along the c axis.

data. As can be seen from this figure, the isentropes exhibit above 2 kOe two pronounced curvatures at the lowest temperatures. The region between the two curvatures, in which the temperature stays rather constant as a function of increasing magnetic field, decreases with increasing initial temperature, T_i, and the isentropes above about $T_i = 0.16$ K show only one temperature minimum as the field increases. Gamma-ray anisotropy measurements (see section 5.5) show a diminished nuclear alignment in the region between the two curvatures in the isentropes (between 3 and 5 kOe at ≈ 0.05 K). This region may therefore be characterized by a spin-flopping phenomenon in which the magnetic moments turn away from the crystallographic c axis, which is favoured as the direction in which the antiferromagnetic ordering occurs, as can be concluded from our susceptibility data.

5.5. Nuclear orientation experiments

The anisotropy in the intensity distribution of gamma radiation emitted from oriented radioactive nuclei may yield information about the internal fields at the site of the nuclei if both the nuclear decay characteristics and the temperature are known. The first requirement is met in the case of ^{54}Mn and the second can be fulfilled by the use of a calibrated carbon thermometer, as discussed in section 2. Since further for ionic Mn compounds also the magnitude of the internal field or, equivalently, of the hyperfine-structure coupling constant is known with sufficient accuracy, the method of gamma-ray anisotropy measurements can be utilized for

determining the directions of the internal field. In turn, the direction of the internal field is related to the direction of the ionic magnetic moments in the magnetically ordered state. Quite often, however, nuclear alignment in magnetically ordered ionic crystals is beset by the difficulty of attaining thermal equilibrium, due to very long nuclear spin relaxation times[27].

In our experiment the gamma-ray counters were fixed to the magnet, two counters recording the gamma-radiation intensity in the direction of the magnetic field and two other counters recording the intensity in a direction perpendicular to that of the magnetic field. The gamma-ray intensities, normalized to 1 at high temperatures, are denoted by $W(0)$ and $W(\pi/2)$ respectively. For the case that all Mn nuclei are polarized preferentially along the magnetic field axis one may use the following formula:

$$W(\theta) = 1 - \tfrac{5}{7}(f_2/f_2^m)P_2(\cos\theta) - \tfrac{2}{7}(f_4/f_4^m)P_4(\cos\theta) \qquad (5.1)$$

where P_2 and P_4 are Legendre polynomials in $\cos\theta$, f_2 and f_4 are temperature dependent nuclear orientation parameters reaching maximum values f_2^m and f_4^m at zero temperature and where $\theta = 0$ or $\pi/2$ in our case. At $T = 0.048$ K one finds $W(0) = 0.85$ and $W(\pi/2) = 1.07$[3], the deviations from the value 1 being largely due to the second term in eq. (5.1). It can be seen from fig. 19 that these values are reached when small magnetic fields are applied in the $g_{//}$ direction and this is a familiar result for paramagnetic Mn crystals. A few hundred oersteds is usually sufficient to overcome crystalline field effects and to decouple electron and nuclear spins, i.e. for the transition from the Zeeman effect region to the nuclear Paschen-Back effect region.

For a better understanding of the experimental results, it should be noted that the gamma-ray anisotropy does not depend on whether part of the nuclei are aligned in a direction antiparallel to that of the magnetic field, or in other words, f_2 and f_4 are invariant with respect to rotation of part of the nuclear spins over 180°. So, for instance, ion pairs at X sites may be aligned antiferromagnetically along the magnetic field axis without affecting the gamma-ray intensity.

From the experimental data it is seen that quite different results are obtained when H is applied in the $g_\perp$ direction. Clearly the nuclear spins, preferentially aligned along the $g_{//}$ direction in zero field, are gradually (as a function of field strength) rotated towards the magnetic field direction. However, large fields are required to polarize the nuclear spins in the magnetic field direction to a degree, allowed by the temperature $T \approx 0.05$ K. At a field of about 3.5 kOe the anisotropy practically vanishes which has to be related to vanishing of $f_2P_2(\cos\theta)$ in eq. (5.1).

This phenomenon can be discussed in two alternative ways, either by saying that $f_2 \approx 0$, or more easily by the statement that the spins are on the average aligned along a direction subtending an angle of about 54° with the magnetic field direction, which makes $P_2(\cos\theta) = 0$. At approximately the same value of H also the results for H parallel to the $g_{//}$ direction show remarkable behaviour. We suggest that at

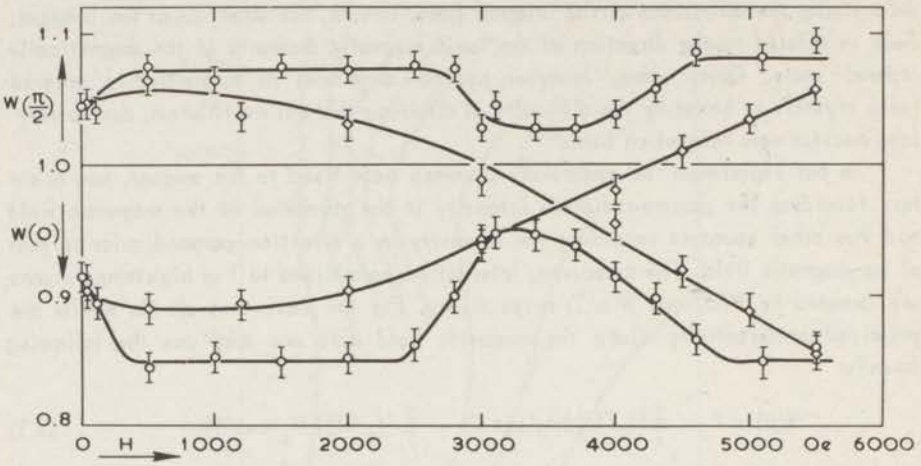

Fig. 19. Anisotropy of gamma radiation from ^{54}Mn nuclei in magnetically ordered Mn–La nitrate as a function of an externally applied magnetic field, H and at constant temperature T = 0.048 ± 0.002 K. The gamma-ray intensity, normalized to 1 at infinite temperature, was measured in a direction // c axis, W(0), and ⊥ c axis, W(π/2). The circles refer to measurements with the field // c axis, the squares to measurements with the field ⊥ c axis. The statistical error in the measuring points is indicated by vertical bars. The minimum value of W(0) and the maximum value of W(π/2) agree approximately with the theoretically expected values at T = 0.048 K for the case that the Mn nuclei at X and Y sites are all preferentially polarized in the direction of the magnetic field.

this field strength the Mn spins at X sites are flopping from antiferromagnetic alignment along the c axis to positions intermediate between the $g_{//}$ and $g_{\perp}$ direction, while at higher fields all spins are polarized with respect to the magnetic field direction. The magnitude of this field approximately agrees with the field values corresponding to the transition from antiferromagnetism to paramagnetism as obtained from the isentropes in the H–T diagram (fig. 18).

It should be remarked that the mentioned anisotropy effects of the electron spin alignment in the ordered state are not due to crystalline field splittings, which are easily suppressed by fields of a few hundred oersteds. The preferential alignment of the electron spins along the $g_{//}$ direction has therefore to be ascribed to some anisotropy in the exchange coupling.

The data of fig. 19 have been taken from measurements of the gamma-ray counting rate versus time until the fixed reference temperature T = 0.048 K was reached. Additional results were obtained by rapid variation of the crystal temperature by supplying heat to the sample from the heater. It was found that above 0.08 K the change in counting rate occurred within the time required for counting the gamma

rays, while at the lowest temperature the response time of the gamma-ray intensity was about 200 seconds. This is in remarkable contrast to nuclear spin relaxation times of many hours in some other Mn compounds[27], both in magnetically ordered crystals like $MnCl_2.4H_2O$ and in magnetically diluted crystals like Mg–La nitrate containing small amounts of Mn impurities[28]. We ascribe this phenomenon to the circumstance that Mn–La nitrate is far from complete magnetic order at $T \simeq 0.05$ K in view of the relatively low transition point, which results in relatively short electronic spin-lattice relaxation times and hence also in short nuclear spin-lattice relaxation times.

6. Co–La nitrate

6.1. Heat capacity

The heat capacity of $Co_3La_2(NO_3)_{12}.24H_2O$ has been measured as a function of temperature between 0.1 K and 0.5 K and the results are plotted in fig. 20, from which it is seen that a sharp singularity is found at $T_N = 0.181$ K. A comparatively small contribution may be expected to arise from hyperfine-structure interaction and

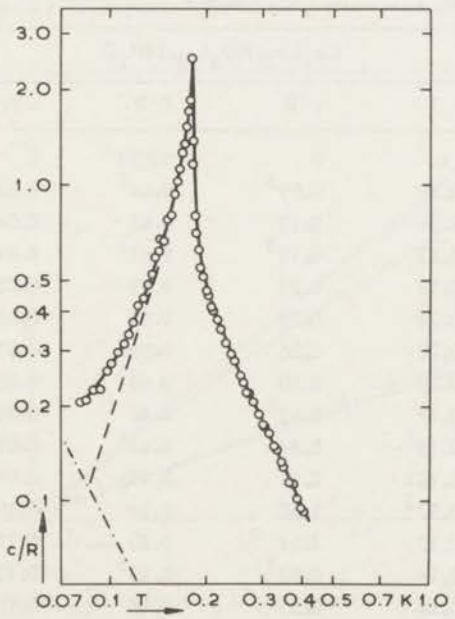

Fig. 20. Heat capacity of Co–La nitrate per gramion Co versus temperature on a logarithmic scale. The maximum corresponds to $T_N = 0.181$ K. The dash-dotted line represents the hyperfine specific heat, c_{hfs}; the dashed line is obtained by subtracting c_{hfs} from the experimental results.

was subtracted (dashed line) from the experimental data. This contribution was estimated from the h.f.s. constants as measured by EPR on paramagnetic Co ions in La–Mg nitrate and using below T_N the formula

$$c_{hfs} T^2/R = \frac{1}{3} \left(\frac{A}{2k}\right)^2 I(I+1).$$

This gives ($A^X/k = 0.014$, $A^Y/k = 0.042$, $I = 7/2$) $c_{hfs} T^2/R = 9.5 \times 10^{-4}$ K^2, which amounts to more than 50% of the measured heat capacity at T = 0.08 K, but is relatively unimportant above T = 0.15 K. The precise magnitude of the hyperfine coupling contribution to the heat capacity below T_N is uncertain due to lack of knowledge of the magnetic structure. However, the main contribution to c_{hfs} arises from 1/3 of the ions at Y sites, which have a strong preference for alignment along the z direction ($g_{//} > g_{\perp}$), hence taking only A into account is probably a good approximation in our case. The slope of the c versus T curve at the high-temperature side of T_N corresponds nearly to $c \propto T^{-2}$. When extrapolating the curve at the high-temperature side according to $cT^2/R = 0.0152$ K^2, one may calculate the entropy yield above T = 0.1K and this amounts to 0.693 R. Adding the estimated entropy yield below 0.1 K (ex-

Table V

$Co_3La_2(NO_3)_{12}\cdot 24H_2O$			
T	c/R	S/R	−E/R
∞	0	0.693	0
0.40	0.09^5	0.64^5	0.037
0.36	0.12	0.63	0.043
0.32	0.15^5	0.61^5	0.049
0.28	0.21	0.59	0.055
0.24	0.29	0.55	0.065
0.22	0.36	0.52^5	0.072
0.20	0.50	0.48^5	0.080
0.19	0.62^5	0.46	0.086
0.18^5	0.84	0.44	0.089
0.181	2.59	0.40	0.096
0.17^5	1.50	0.34	0.108
0.17	1.24	0.30	0.114
0.16	0.92^5	0.23^5	0.125
0.14	0.53	0.14	0.139
0.12	0.32	0.08	0.148
0.10	0.18	0.03	0.153
$T_N = 0.181$ K		$\Delta E/R = 0.157$ K	
$cT^2/R = 0.0152$ K^2		$\Delta S/R = 0.696$	

clusive h.f.s. coupling contributions), we find a total entropy 0.696 R, which equals R ln2 within the experimental accuracy. The entropy yield above the critical point is 0.293 R or 42% of the total value, which is an indication of a comparatively strong short-range ordering, or of a comparatively low transition point.

In table V, smoothed data are given for c/R (corrected for the hyperfine coupling contribution), S/R and E/R. The asymptotic value of $cT^2/R = 0.0152\ K^2$ for the behaviour of c at high T requires correction for the dipolar contribution, which was calculated to be $c_{dip} T^2/R = 2.20 \times 10^{-3} K^2$ on basis of the g values of table I. After subtracting the dipolar heat capacity, the value $cT^2/R = 0.0130\ K^2$ has to be interpreted on basis of exchange interactions among the Co ions.

We remark that the entropy above the transition point is larger even than of the Heisenberg model e.g. for simple cubic compounds (coordination number 6). Since short range ordering is favoured by small coordination numbers, we may suggest that in Co–La nitrate we encounter a small coordination number for magnetic interactions.

6.2. Susceptibility above 1 K

The results of the magnetization measurements are shown in figs. 21 and 22. At temperatures of liquid helium paramagnetic saturation was observed.

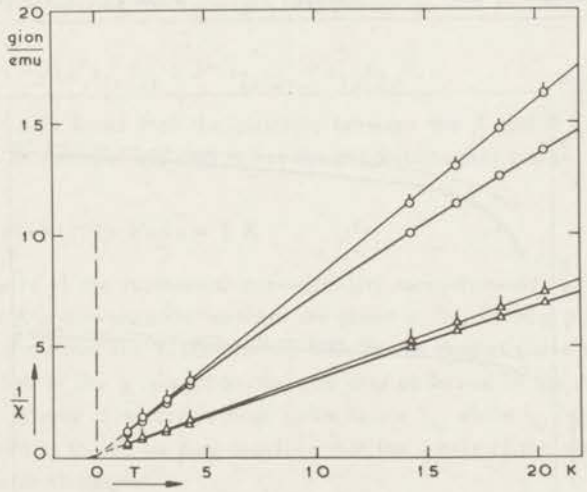

Fig. 21. The reciprocal susceptibility, $1/\chi$ in gramion/emu. of Co–La nitrate versus temperature.

Δ: // c axis
○: ⊥ c axis } experimental points

Δ: // c axis
○: ⊥ c axis } points corrected for the temperature-independent part of χ

The curves of fig. 21 had to be corrected for the temperature-independent paramagnetic susceptibility and can be described according to Van Vleck with:

$$\chi = \frac{C}{T - \theta} + \gamma$$

in which C is the Curie constant and γ is the temperature independent part of the susceptibility.

The results for γ, θ and C were derived by an iterative procedure and are given in table VI, in which also the values obtained by Leask and Wolf[29] are mentioned. Also in fig. 22 our experimental results are compared with the results of Leask and Wolf[29].

Table VI

		γ (emu / g ion)	θ(K)	C (emu K / g ion)	g
// c axis	this experiment	0.0098	−0.44	2.800	2.44
	Leask and Wolf[29]	0.00855	−0.355	2.893	
⊥ c axis	this experiment	0.0114	−0.14	1.260	1.64
	Leask and Wolf	0.0118	−0.0723	1.317	

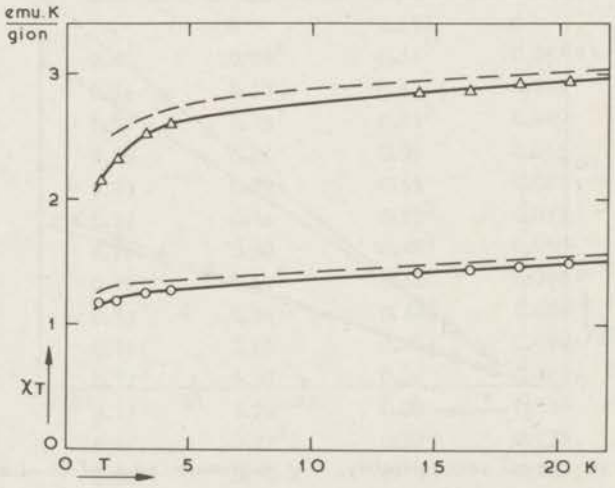

Fig. 22. χT versus T for Co–La nitrate.

Δ : // c axis, O : ⊥ c axis.

The dashed curves refer to the results of Leask and Wolf[29].

Since it is found that $|\theta_{//}| \gg |\theta_{\perp}|$, let us hypothetically propose anisotropic pair coupling of Co ions at X sites only, i.e. $H = -2J^z_{XX} s_{1z} s_{2z}$. This gives two doublets at energies $-J/2$ and $+J/2$ respectively, and one calculates for this situation $\theta_{//} = J^z_{XX}/2k$, $\theta_{\perp} = 0$. Taking the experimental value $\theta = -0.4$ K, which is an average over X and Y ions and intermediate between our value and that of Leask and Wolf, then one predicts $J^z/k = -1.2$ K and $E/R = -J^z/2k = -0.6$ K per mole. Experimentally a smaller value, viz. $E/R = -0.48$ K per mole is observed and hence the experimental θ value is relatively large. The discrepancy would increase by a factor 3 for isotropic pair-exchange interaction. From the relatively large value of θ we conclude that appreciable antiferromagnetic interaction also between X and Y ions is present, which probably is also considerably anisotropic. In this connection it may be mentioned that Culvahouse et al.[30] recently measured the hyperfine spectra of the X–X Co–ion pairs in lanthanum magnesium nitrate. The spin-spin interaction could be described by the effective hamiltonian

$$H = K_0 \vec{s}_1 . \vec{s}_2 + K_z s_{1z} s_{2z}$$

For the constants K_0 and K_z values of $+0.105$ cm^{-1} and -0.170 cm^{-1} were found respectively. After subtraction of the dipolar part in the X–X interaction one obtains $K_0 = +0.040$ cm^{-1} and $K_z = +0.024$ cm^{-1}, which values yield $J^z_{XX}/k = -0.46$ K and $J^{\perp}_{XX}/k = -0.29$ K, writing the spin-spin hamiltonian as

$$H = -2\{J^z s_{1z} s_{2z} + J^{\perp}(s_{1x} s_{2x} + s_{1y} s_{2y})\}.$$

Furthermore it was found that the coupling between the X and Y ions is relatively strong, highly anisotropic and that it has the antiferromagnetic sign.

6.3. Susceptibility below 1 K

The results of the isothermal susceptibility measurements, using both the a.c. bridge and the d.c. galvanometer method, are given in fig. 23 as a plot of χ/C versus T. One may notice that the susceptibility falls below that of Curie's law both in the $g_{//}$ direction and in the $g_{\perp}$ direction, as was also observed in the results of section 6.2. Since $\chi_{\perp}$ retains a relatively high value below T_N while $\chi_{//}$ decreases rapidly from 0.2 K down to 0.1 K, we may conclude that the c axis is the preferred axis of antiferromagnetic alignment.

Although Co–La nitrate is clearly antiferromagnetic, we may mention that a small peak in the d.c. susceptibility occurs at T_N, which for instance could be associated with ferromagnetic behaviour of the ions at Y sites. The latter suggestion is to some extent supported by the occurrence of relaxation phenomena at $T_N (\chi' < \chi_0)$.

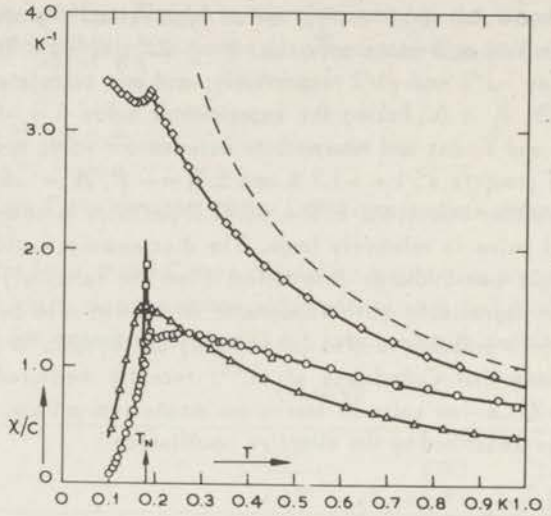

Fig. 23. Susceptibility of Co–La nitrate divided by the Curie constant below 1 K.
○: // c axis, a.c. susceptibility (260 Hz), H = 0 Oe.
□: // c axis, d.c. susceptibility, H = 0 Oe.
△: // c axis, d.c. susceptibility, H = 1000 Oe.
◇: ⊥ c axis, d.c. = a.c. susceptibility, H = 0 Oe.
The dashed line represents Curie's law.

6.4. H–T diagram

Measurements on isentropes in the H–T diagram have been carried out below T_N and also above T_N and both for H in the $g_{//}$ direction and in the $g_\perp$ direction (fig. 24). The results above T_N suggest paramagnetic behaviour and need no further discussion. Below T_N there is, like in the other three compounds, a marked minimum in T when H // c axis. The data also indicate the presence of a small positive magnetocaloric effect at relatively small values of H, which presumably originates mainly from the Y ions.

The most remarkable point is that in the $g_\perp$ direction the reversal of sign of the magnetocaloric effect (i.e. the minimum in T) occurs at much higher field strengths than for H // c axis. Similarly we see the maximum in T at small field strengths to occur at higher values of H for H ⊥ c axis than for the case H // c axis. It may be suggested that the relatively high value of $\chi_\perp$ may persist in the presence of magnetic fields and account for a stronger positive magnetocaloric effect, i.e. extending to higher fields than for H // c axis (hence only partly due to $g_\perp < g_{//}$ for the Y ions) and canceling the negative magnetocaloric effect associated with the ion pairs at X sites. More data, particularly on the heat-capacity curve in the presence of mag-

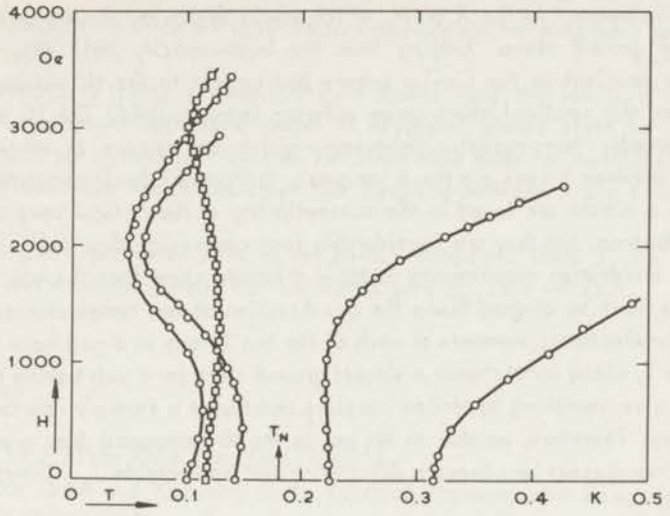

Fig. 24. Isentropes in the H–T diagram of Co–La nitrate.
O : H // c axis, □ : H ⊥ c axis.

netic fields and isothermal susceptibility measurements in longitudinal fields, are required to check this interpretation.

However, like in the other three compounds, the magnetic field strengths required for reaching a positive magnetocaloric effect and the paramagnetic state, are surprisingly large when comparing $g_{//}\beta H$ or $g_{\perp}\beta H$ to kT_N. This supports our suggestion of a predominance of pair coupling also in this compound.

7. Discussion

The main point emerging from a review of the various properties of the four iron group lanthanum double nitrates is that we encounter loosely coordinated magnetic spin systems in which pairwise exchange coupling predominates but which nevertheless show sharp phase transitions.

Further, the coupling $H = -2J_{XX}\vec{s}_1.\vec{s}_2$ between X ions is antiferromagnetic ($J_{XX} < 0$) and this would give a singlet ground state, hence vanishing magnetic moments and temperature-independent susceptibility at low temperatures. Clearly the exchange interaction, $-2J_{XY}\vec{s}_1.\vec{s}_2$, between X ions and Y ions is also important even although J_{XY} may be smaller than J_{XX}. Possibly the relative importance of J_{XY} is related to the circumstance that one X ion has three Y ions as next nearest neighbours and only one X ion as nearest neighbours, while conversely each of the Y ions has six X ions as nearest neighbours. Therefore long-range order has to be established by the Y ions linking the X pairs. In addition the Y ions may restore

some magnetic moment to the X pairs, which would otherwise remain in a non-magnetic singlet ground state. Judging from the heat-capacity data only, the ratio J_{XY}/J_{XX} is smallest in the Cu–La nitrate and largest in the Ni compound, since the latter has the smallest short-range ordering entropy yield. The Ni salt shows most pronouncedly ferromagnetic behaviour, which we assume to originate from interactions between Y ions via the X ion pairs. Indications for ferromagnetic behaviour in Mn–La nitrate are found in the susceptibility at the critical temperature and in the H–T diagram, but they are considerably less convincing than in Ni–La nitrate. The nuclear orientation experiments in Mn–La nitrate show that the electron spins of the X ions must be aligned along the $g_{//}$ direction at low temperatures; the magnitudes of the electronic moments of each of the two X ions in a pair have to be practically $s = 5/2$, since for instance a singlet ground state for a pair having total spin $s = 0$ would give vanishing hyperfine coupling and hence a strongly reduced gamma-ray anisotropy. Therefore, neither in Mn nor in the Ni compound does predominance of pair coupling present an adequate description and appreciable J_{XY} interaction has to be present.

On the other hand Cu–La nitrate shows strong deviations from the usual antiferromagnetic phase transitions in other Cu compounds and the thermal and magnetic properties definitely disagree with for instance a molecular-field treatment. This may be illustrated by estimating the molecular field from the critical temperature according to

$$H_{mol} = \frac{3kT_N}{g\beta(s+1)} = \frac{2T_N}{g(\beta/k)} \approx 1.1 \text{ kOe.}$$

The magnetic field required to bring Cu–La nitrate in the paramagnetic phase is, however, roughly 3.7 kOe. Similar discrepancies (of a factor two or three) exist for the other three salts.

In this connection it may be mentioned that Culvahouse[31] has proposed a magnetic system in which the X–Y interaction is relatively strong compared to the X–X interaction, leading to e.g. in Cu–La nitrate to a linear-chain model, having essentially the same properties as our pair model, presented in section 3.

Space does not permit to discuss the various properties of the four salts in great detail while additional experiments are required to clarify e.g. the magnetic structures below the critical temperature and to determine the magnitude of J_{XX} and J_{XY} in all of the four compounds. Summarizing we therefore limit ourselves to the following conclusions:

1. Phase transitions are observed in iron group lanthanum double nitrates indicating the establishment of long-range magnetic order due to relatively weak superexchange interactions.
2. Below the critical temperature magnetic fields of only a few hundred oersteds are required in order to bring the Y ions in the paramagnetic phase, whereas very

much larger fields (> 3 KOe) are required to overcome antiferromagnetic pair coupling of X ions.

3. While attempts to apply a molecular-field model have not led to a satisfactory description, a quantum-mechanical model of a singlet ground state for X-ion pairs and independent paramagnetic Y ions on the other hand does not adequately describe the magnetic behaviour which indicates that coupling between X and Y ions is also important.

4. EPR and cross-relaxation data in the Ni–La compound show $J_{XX}/k = -0.35$ K and thermal and magnetic data in Cu–La nitrate give $J_{XX}/k = -0.23$ K.

References

1) Trenam, R.S., Proc.Phys.Soc. A66(1953)118.
2) Al'tshuler, S.A. and Kozyrev, B.M., Electron Paramagnetic Resonance, (Academic Press Inc., 1964).
3) Hudson, R.P. and Kaeser, R.S., Physics (N.Y.) 3(1967)95.
4) Mess, K.W., Lubbers, J., Niesen, L. and Huiskamp, W.J., Commun. Kamerlingh Onnes Lab., Leiden No. 369c; Physica 41(1969)260.
5) Lubbers, J. and Huiskamp, W.J., Commun. Leiden No. 353a; Physica 34(1967)167.
6) Levi, M.W., Sapp, R.C. and Culvahouse, J.W., Phys.Rev. 121(1961)538.
7) Culvahouse, J.W., Unruh, W. and Sapp, R.C., Phys.Rev. 121(1961)1370.
8) Culvahouse, J.W., J.chem.Phys. 36(1962)2720.
9) Bijl, D. and Rose-Innes, A.C., Proc.Phys.Soc. (London) A66(1953)954.
10) Bleaney, B., Bowers, K.D. and Trenam, R.S., Proc.Roy.Soc. (London) A228(1955) 157.
11) Zalkin, A., Forrester, J.D. and Templeton, D.H., J.chem.Phys. 39(1963)2881.
12) De Vries, A.J. and Livius, J.W.M. Commun. Leiden No. 349a; Appl. sci. Res. 17(1967)31.
13) Daniels, J.M., Proc.Phys.Soc. (London) A66(1953)673.
14) Joenk, R.J., J.appl.Phys. 34(1963)1097.
15) Hornung, E.W., Brodale, G.E., Fisher, R.A. and Giauque, W.F., J.chem.Phys. 45(1966)614.
16) Lubbers, J. and Huiskamp, W.J., Commun. Leiden No.354b; Physica 34(1967)212.
17) Hoskins, R.H., Pastor, R.C. and Trigger, K.R., J.chem.Phys. 30(1959)1630.
18) Wielinga, R.F., Lubbers, J. and Huiskamp, W.J., Commun. Leiden No. 361b; Physica 37(1967)375.
19) Vilches, O.E. and Wheatley, J.C., Phys.Rev. 148(1966)509.
20) Mess, K.W., Lagendijk, E., Zimmerman, N.J., Van Duyneveldt, A.J., Giesen, J.J. and Huiskamp, W.J., Commun. Leiden No. 372a; Physica 43(1969)165.
21) Van Duyneveldt, A.J., et al., Physica to be published.
22) Van den Broek, J., Thesis, Leiden (1960).

23) Essam, J.W. and Garelick, H., Proc.Phys.Soc. (London) 92(1967)136.
24) Syozi, I., Progr. theoret. Phys. (Kyoto) 34(1965)189.
25) Rushbrooke, G.S. and Morgan, D.J., Mol.Phys. 4(1961)1.
26) Sapp, R.C. and Nelson, D.A., Bull.Amer.Phys.Soc. 11(1966)911.
27) Daniels, J.M., Giles, J.C. and LeBlanc, M.A.R., Canad.J.Phys. 39(1961)53.
28) Lubbers, J. and Huiskamp, W.J., Commun. Leiden No.353a; Physica 34(1967)166.
29) Leask, M.J.M. and Wolf, W.P., Proc.Phys.Soc. (London) 81(1963)252.
30) Culvahouse, J.M., Schinke, D.P. and Pfortmiller, L.G., Phys.Rev. 177(1969)454.
31) We are very much indebted to Prof. J.M. Culvahouse for discussions on the La-double nitrate results.
Culvahouse, J.M., to be published.
32. Van Ormondt, D., thesis Delft, 1968.

SAMENVATTING

In dit proefschrift worden onderzoekingen beschreven betreffende magnetische en calorische eigenschappen van magnetische kristallen bij zeer lage temperaturen, te weten in het temperatuurgebied tussen 1 K en 0.001 K. De metingen zijn verricht aan twee verschillende kristalsystemen, namelijk aan dubbelnitraat kristallen met de chemische formule $A_2B_3(NO_3)_{12}.24H_2O$, waarin A en B respektievelijk drie- en tweewaardig positief geladen ionen zijn welke zowel diamagnetisch als paramagnetisch kunnen zijn, en aan twee cobaltzouten met de formule $CoCs_3Hal_5$, waarin Hal achtereenvolgens het eenwaardig negatieve chloor en broom voorstelt. Vanuit theoretisch oogpunt bezien zijn deze laatste twee zouten het meest aantrekkelijk wegens hun eenvoudige kristalstruktuur en de eenvoudige vorm van de wisselwerking tussen de magnetische dipoolmomenten. De kristalstruktuur van de dubbelnitraten is goed bekend (trigonaal), echter de wisselwerkingen in deze zouten kunnen van voornamelijk dipolaire aard zijn of van het exchange type, in welk geval de ionen waartussen exchange wisselwerking bestaat, niet volgens een eenvoudig Bravaisrooster zijn gerangschikt.

Elke stof waarin zich magnetische momenten bevinden, zal zich ordenen indien de temperatuur voldoende wordt verlaagd. De interactie tussen de ionen kan worden gerepresenteerd door een effektief z.g. moleculair magnetisch veld H_{mol}. Magnetische ordening kan optreden als de interactie-energie van dezelfde grootte orde is als de thermische energie, d.w.z. als $\mu H_{mol} \approx kT$; μ is het magnetische moment, k de Boltzmann constante en T de temperatuur. Voor een magnetisch systeem dat een overgangstemperatuur heeft van $T_c \approx 1$ K, bedraagt het moleculaire veld ongeveer 10^4 Oe. Als een uitwendig magnetisch veld ter grootte van het moleculaire veld wordt aangelegd, zal de magnetische orde zeer worden beïnvloed. Als gevolg van deze beïnvloeding kunnen belangwekkende gegevens worden verkregen t.a.v. de aard en de sterkte van de wisselwerking tussen de ionen. Alle onderzochte preparaten welke in dit proefschrift worden besproken vertonen een magnetische fase-overgang beneden 1 K, zodat de benodigde magnetische velden ter verstoring van de magnetische orde gemakkelijk met de gebruikelijke laboratoriumapparatuur verkregen kunnen worden. Enige algemene beschouwingen over magnetische ordening en de verschijnselen welke zijn bestudeerd, worden besproken in hoofdstuk I.

Voor de bepaling van de temperatuur beneden 1 K wordt meestal gebruik gemaakt van de susceptibiliteit, χ, van een paramagnetisch zout. In het temperatuur-

gebied waar deze methode goed bruikbaar is, volgt de susceptibiliteit een Curie-Weiss wet, $\chi = C/(T-\theta)$, waarin C de Curie-constante is en θ de paramagnetische Curie-temperatuur. Bij het aanbrengen van een relatief sterk uitwendig magnetisch veld wordt χ echter zeer beïnvloed; grote en vaak onzekere correcties zijn nodig om de temperatuur te bepalen. Daarom werd bij alle in dit proefschrift beschreven experimenten gebruik gemaakt van een koolthermometer. De temperatuur kan dan worden bepaald met behulp van een betrekking tussen de weerstand, R, en de temperatuur, T, welke weinig wordt beïnvloed door een magnetisch veld. Deze R–T relatie kan worden verkregen door de weerstand van de koolthermometer te vergelijken met de susceptibiliteit van een paramagnetisch zout, dat de wet van Curie-Weiss goed volgt. Van groot belang is uiteraard, dat de betrekking tussen R en T gedurende langere tijd onveranderd blijft. De onderzoekingen, welke zijn verricht naar deze reproduceerbaarheid, de veldafhankelijkheid en het thermische contact met het preparaat, worden besproken in hoofdstuk II. Voorts wordt in dit hoofdstuk beknopt de gebruikte apparatuur beschreven.

In hoofdstuk III worden magnetische en calorische metingen aan cerium magnesium nitraat, $Ce_2Mg_3(NO_3)_{12}.24H_2O$, bij zeer lage temperaturen ($T < 0.01$ K) besproken. In dit zout zijn de wisselwerkingen tussen de ionen praktisch geheel van dipolaire aard. Voor een spinsysteem met alleen dipool-dipool koppeling is geen exakte berekening van de grondtoestand bekend en het is een open vraag of een dergelijk systeem lange-afstandsordening vertoont beneden een kritische temperatuur. De magnetische susceptibiliteit van cerium magnesium nitraat wordt veelvuldig gebruikt voor temperatuurmeting in het gebied van enige milligraden, waar echter meningsverschillen bestaan over de daarbij gebruikte temperatuurschaal.

Metingen aan de susceptibiliteit als funktie van de entropie, S/R, werden uitgevoerd aan een bolvormig en aan een ellipsoidaal éénkristal. Als resultaat werd gevonden dat bij een entropie die lager is dan 0.38 R de susceptibiliteit constant blijft binnen de meetnauwkeurigheid, en een waarde heeft, overeenkomende met de demagnetiserende faktor van het preparaat. Ook werd de susceptibiliteit in een parallel uitwendig veld gemeten en hieruit bleek dat χ sterk daalde in velden groter dan of gelijk aan het demagnetiserende veld. Metingen van de warmte-inhoud als funktie van de entropie werden uitgevoerd om een temperatuurschaal vast te stellen, d.w.z. de betrekking tussen absolute temperatuur en magnetische temperatuur, $T^* \equiv \chi/C$, van een bolvormig éénkristal. Uit de afhankelijkheid tussen S/R en T volgt het verloop van de soortelijke warmte als funktie van T. De soortelijke warmte bleek een maximum te vertonen bij een temperatuur $T_c = 1.9(\pm 0.1)$mK, ($1\text{mK} = 10^{-3}$K). Uit deze resultaten werd geconcludeerd dat cerium magnesium nitraat zich ferromagnetisch ordent bij deze T_c. Voorts mag men dan verwachten dat beneden T_c het preparaat zich opsplitst in domeinen. De laagst bereikte temperatuur bleek $1.0(\pm 0.3)$mK te zijn. Tenslotte werden metingen verricht aan de susceptibiliteit in relatief lage longitudinale en transversale magnetische velden, waaruit de soortelijke warmte bij relatief hoge temperaturen kon worden bepaald.

In hoofdstuk IV worden metingen besproken aan het warmtecontact tussen het spinsysteem en het rooster in cerium magnesium nitraat. Tevens worden enige aanvullende metingen besproken aan koper cesium tuttonzout, $CuCs_2(SO_4)_2.6H_2O$. Deze beide zouten werden gekozen om hun goed gedefiniëerde energieschema in een magnetisch veld van de orde van 1 kOe. Beide zouten blijven paramagnetisch tot temperaturen ver beneden 0.1 K. Hoewel het warmtecontact tussen magnetische spinsystemen en de roostergolven in velerlei magnetische verbindingen is bestudeerd, ontbreken metingen beneden 1 K nagenoeg geheel. Veelal wordt pas in dit temperatuurgebied het warmtecontact door een relatief eenvoudig mechanisme, het zogenaamde direkte relaxatieproces, beheerst. Het bleek echter dat in beide zouten het contact tussen het spinsysteem en het omringende bad niet wordt bepaald door het direkte relaxatieproces alleen, maar vooral door de z.g. fonon-bottleneck. Dit verschijnsel treedt op als de energiestroom uit het spinsysteem naar het omringende bad wordt bepaald door het warmtetransport tussen de fononen, waarmee het spinsysteem energie kan uitwisselen en de rest van het fononen-systeem. In het koperzout werd een afhankelijkheid van de energiestroom van de dikte waargenomen, hetgeen niet het geval was in het ceriumzout. De invloed van enige verontreinigingen op de relaxatie in cerium magnesium nitraat werd bestudeerd, evenals de gevolgen van verdunning van het cerium spinsysteem met het diamagnetische lanthaan. Uit de waargenomen afhankelijkheid van het energietransport tussen spinsysteem en bad van het veld en de hoek, θ, welke dat veld maakt met de kristallografische c as, werd het mogelijke optreden van het direkte proces voor kleine magnetische velden ($H \approx 1000$ Oe) voor $\theta \leq 20°$, geconcludeerd. Tenslotte worden enige metingen van het warmtecontact tussen spinsysteem en rooster bij zeer lage temperaturen ($0.02\ K < T < 0.1\ K$) en in lage velden ($H < 1000$ Oe) besproken. Deze metingen werden uitgevoerd door een cerium magnesium nitraat kristal te laten afkoelen door een metaalplaatje met een veel lagere temperatuur. Ook hier werd het optreden van een fonon-bottleneck geconstateerd.

Hoofdstuk V presenteert magnetische, calorische en relaxatiemetingen aan $CoCs_3Cl_5$ en $CoCs_3Br_5$. Op grond van paramagnetische resonantiemetingen aan Co-ionen is te voorspellen dat de magnetische wisselwerkingen tussen de Co-ionen in de grondtoestand zeer goed beantwoorden aan het door Lenz voorgestelde model van magnetische interacties (Ising model). In dit model treedt wisselwerking tussen slechts één ruimtelijke component van de spinvektoren op, hetgeen een zeer belangrijke vereenvoudiging betekent t.o.v. het door Heisenberg voorgestelde model met wisselwerking tussen de drie ruimtelijke componenten. Deze vereenvoudiging heeft ertoe geleid dat verscheidene eigenschappen van het Ising model exact kunnen worden berekend of althans met hoge nauwkeurigheid benaderd. Uit de metingen aan beide cobaltzouten kon worden besloten dat het chloride zich gedraagt als een zout waarin z.g. drie-dimensionale Ising exchange wisselwerking plaatsvindt, terwijl het bromide een goed voorbeeld lijkt van een twee-dimensionaal Ising model. Uit de susceptibiliteitsmetingen bleek dat beide zouten zich antiferromagnetisch ordenen be-

neden respektievelijk 0.527 K en 0.282 K voor het chloride en bromide. Metingen werden verricht aan de verlaging van deze overgangstemperaturen onder invloed van een uitwendig magneetveld. De resultaten voor $CoCs_3Cl_5$ en $CoCs_3Br_5$ bleken goed overeen te stemmen met theoretische voorspellingen voor respektievelijk een drie-dimensionale, enkelvoudig kubische en een twee-dimensionale, kwadratische Ising antiferromagneet. Voor beide zouten werd tevens het fasediagram in het H–T vlak onderzocht door de temperatuurvariatie waar te nemen als funktie van een variërend uitwendig veld. Deze metingen berusten op de toepassing van het magnetocalorische effect. De spin-rooster relaxatietijd, τ, werd bepaald en deze bleek evenredig te zijn met T^{-7} voor $T > T_N$ en vrijwel onafhankelijk van een uitwendig veld.

Tenslotte worden in hoofdstuk VI een aantal metingen beschreven aan vier dubbelnitraten $X_3La_2(NO_3)_{12}.24H_2O$, waarin achtereenvolgens X staat voor Cu, Ni, Mn en Co. De dubbelnitraten zijn weliswaar chemisch en kristallografisch geen eenvoudige verbindingen, maar vele eigenschappen van de tweewaardige ionen zijn door middel van allerlei metingen goed bepaald. De octaëdrische omringing van de tweewaardige ionen door zes watermoleculen vormt een geschikt uitgangspunt voor zowel experimentele als theoretische studie van de grootte van de magnetische wisselwerking tussen de ionen, d.w.z. van de zogenaamde superexchange interactie via tussengelegen watermoleculen. De genoemde zouten vertonen een maximum in de soortelijke warmte bij achtereenvolgens 0.089 K, 0.393 K, 0.230 K en 0.189 K. Beneden deze temperaturen gedragen het Cu, Mn en Co zout zich antiferromagnetisch, zoals uit de susceptibiliteit blijkt. Het Ni zout vertoont echter beneden de overgangstemperatuur een spontane magnetisatie, overeenkomend met 1/3 van de totale verzadigingsmagnetisatie bij het absolute nulpunt. Op grond van de kristalstruktuur en in het bijzonder op grond van de resultaten verkregen over het koperzout, wordt een model voorgesteld waarin 2/3 van de magnetische ionen op kristallografische X-plaatsen (onderlinge afstand 4.99 Å, terwijl de afstand tot de volgende magnetische buur 7.14 Å is) antiferromagnetisch in paren gekoppeld zijn met een exchange wisselwerking $H = -2J\ \vec{s}_1.\vec{s}_2$. Op grond van dit model kon voor het koperzout een exchange constante $J/k = -0.23$ K voor deze paarinteractie worden verkregen. Dit was mogelijk door een Schottky-curve boven T_N aan te passen aan de waargenomen soortelijke warmte bij relatief hoge temperatuur, waarbij een singlet-triplet energiesplitsing t.g.v. de isotrope exchange koppeling werd aangenomen. Voor alle vier zouten werden isentropen in het H–T vlak gemeten; de grootste temperatuurdaling werd waargenomen in het Ni zout. Kernoriëntatie van ^{54}Mn in het mangaanzout werd bestudeerd voor verschillende waarden van magnetisch veld en temperatuur. Als resultaat werd onder meer gevonden dat de kernspin-rooster relaxatietijd zeer kort is zelfs bij de laagst bereikte temperatuur ($\tau \approx 100$s bij $T \approx 0.05$ K), dit in tegenstelling tot de zeer lange relaxatietijden welke zijn waargenomen in diverse andere Mn zouten.

Ten einde te voldoen aan het verzoek van de faculteit der Wiskunde en Natuurwetenschappen, volgt hierbij een kort overzicht van mijn studie.

In 1959 legde ik het eindexamen H.B.S. B af aan de Willem de Zwijger H.B.S. te Rotterdam, waarna ik met mijn studie natuur- en wiskunde met bijvak sterrekunde, aan de Rijksuniversiteit te Leiden aanving. In april 1962 legde ik het kandidaatsexamen a' af. In september 1962 begon ik met mijn werkzaamheden op het Kamerlingh Onnes Laboratorium in de werkgroep F.O.M. KIV. Bij de voorbereiding van het doctoraal examen experimentele natuurkunde werden colleges gevolgd van Prof. dr S.R. de Groot, Prof. dr P. Mazur en Prof. dr J.A.M. Cox. Tevens volgde ik de colleges van Prof. dr J. Kistemaker en Prof. dr J.A. Goedkoop. Tijdens het eerste jaar van mijn werkzaamheden in de werkgroep assisteerde ik dr H. van Kempen. Prof. dr A.R. Miedema bracht mij de grondbeginselen van de experimentele natuurkunde op onnavolgbare wijze bij. Na zijn vertrek in 1965 werden mijn werkzaamheden geleid en gestimuleerd door dr W.J. Huiskamp. In juni 1965 werd het doctoraal examen afgelegd.

Sinds 1963 heb ik op het praktikum voor pre-kandidaten geassisteerd. De Stichting voor Fundamenteel Onderzoek der Materie (F.O.M.) verleende mij in 1963 een studietoelage. In november 1965 werd ik als wetenschappelijk medewerker aangesteld bij de Stichting F.O.M.

Tijdens mijn werkzaamheden heb ik van alle medewerkers van de werkgroep alle mogelijke medewerking gehad. Dr W.J. Huiskamp heeft vele waardevolle discussies en suggesties gegeven, zonder welke dit proefschrift onmogelijk in deze vorm tot stand zou zijn gekomen. Prof. dr C.J. Gorter heeft voortdurend belangstelling getoond voor het onderzoek en was altijd bereid tot het voeren van discussies en het geven van suggesties. Met veel genoegen denk ik terug aan de prettige samenwerking met drs. J.N. Haasbroek en dr R.F. Wielinga, met wie ik vele nuttige discussies had. Dr A.S. Edelstein stimuleerde het onderzoek naar de bruikbaarheid van de koolthermometer beneden 1 K. Dr H. Postma verleende zijn medewerking bij enkele experimenten gedaan in Petten. De suggesties van dr J. Lubbers en zijn steun bij de experimenten beschreven in hoofdstuk III, waren zeer waardevol. Bijzonder plezierige ervaringen deed ik op tijdens de samenwerking met drs. E. Lagendijk. Met drs. L. Niesen heb ik vele nuttige en vaak uitputtende discussies gehad. Drs. H.W.J. Blöte verschafte de cobalt preparaten, beschreven in hoofdstuk V en berekende dipoolsommen, vermeld in hoofdstuk VI. De contacten met Prof. dr P.W. Kasteleijn zijn van belang geweest bij de tot stand koming van dit proefschrift.

Voor het welslagen van de experimenten was de steun van de heer J. van Weesel onmisbaar. De heren J. van der Waals en T. Nieboer waren altijd bereid hun medewerking te verlenen. De glazen apparatuur werd vervaardigd door de heren A.R.B. Gerritse, B. Kret en C.J. van Klink. De heer R. Hulstman ontwikkelde en verzorgde de benodigde elektronika. De heer W.F. Tegelaar maakte de tekeningen van dit proefschrift en de administratieve staf verzorgde een groot deel van het benodigde typewerk.